February 2012 EPA 530-R-10-003

Conceptual Model Scenarios for the Vapor Intrusion Pathway

Office of Solid Waste and Emergency Response
U.S. Environmental Protection Agency
Washington, DC 20460

[This page intentionally left blank.]

DISCLAIMER

This document presents technical information on the phenomenon of subsurface vapor intrusion, based upon EPA's current understanding. This document does not confer legal rights, impose legal obligations, or implement any statutory or regulatory provisions. This document does not change or substitute for any statutory or regulatory provisions. Interested parties are free to raise questions and objections about the appropriateness of the application of the examples presented in this document to a particular situation. Finally, this is a living document and may be revised periodically without public notice. EPA welcomes public comments on this document at any time and will consider those comments in any future revisions. Mention of trade names or commercial products does not constitute endorsement or recommendation for use.

AUTHORS AND CONTRIBUTORS

The U.S. Environmental Protection Agency (EPA), Office of Resource Conservation and Recovery (ORCR), Washington, DC, was responsible for the preparation of EPA's *Conceptual Model Scenarios for the Vapor Intrusion Pathway*. Dr. Lilian Abreu, ARCADIS Inc., was the primary author, with Dr. Henry Schuver, ORCR, as supporting author.

The authors wish to acknowledge the important contributions of Dr. William Wertz and Todd McAlary, Geosyntec Consultants, Dr. Ian Hers, Golder Associates, and Dr. Paul Johnson, Arizona State University, who provided review and suggestions for this technical report, as well as RTI International who managed document reviews, editing, and preparation. Robert Truesdale was the RTI Project Leader and Anne Lutes was the RTI technical editor. SRA International, Inc., managed the external peer reviews.

Table of Contents

Executive Summary ES-1
ES.1 Purpose and Objectives ES-1
ES.2 Methodology, Assumptions, and Limitations ES-2
ES.3 Summary of Results ES-2
1.0 Introduction 1
1.1 Background 1
1.2 Objectives 3
1.3 Methodology 3
1.4 Simulation Inputs, Assumptions, and Limitations 4
1.5 Document Development and Peer Review 7
1.6 Document Organization 7
2.0 Sources of Contaminated Vapors in the Subsurface 9
3.0 Vapor Transport and Fate in the Subsurface 11
3.1 Diffusive Transport of Vapors in the Unsaturated Zone 12
3.2 Advective Transport of Vapors Near Building Foundations 15
4.0 Factors Affecting Vapor Migration and Indoor Air Concentrations of Recalcitrant VOCs 21
4.1 Source Concentration 22
4.2 Source Depth and Lateral Distance from Building 25
4.3 Other Conditions Simulated for Scenarios with Homogeneous Subsurface 31
4.3.1 Multiple Buildings 31
4.3.2 Permeable Fill and Building Pressurization 35
4.3.3 Building Conditions 37
4.3.4 Multiple Sources 40
4.4 Subsurface Heterogeneities and Ground Cover 42
4.4.1 Moisture Content in Layered Soils 42
4.4.2 Lower Moisture Content Below the Building 47
4.4.3 Heterogeneous Subsurface, Finite Sources, and Ground Cover 49
4.4.4 Geologic Barrier 60
5.0 Factors Affecting Vapor Migration and Indoor Air Concentrations of Biodegradable VOCs 65
5.1 Source Concentration 66
5.2 Source Depth 72
5.3 Source Lateral Distance from Building 76
5.4 Moisture Content in Layered Soil 79
5.5 Geologic Barrier 82
6.0 Temporal and Spatial Variability in Subsurface and Indoor Air Concentrations 85
6.1 Transient Transport Following Source Release 85
6.1.1 Effect of Moisture Content on Transient Transport 87
6.1.2 Effect of Sorption on Transient Transport 92
6.2 Wind Load on Buildings 94
6.3 Atmospheric and Indoor Air Pressure Fluctuations 97
6.4 Seasonal Phenomena 101
6.4.1 Fluctuations in Water Table Elevation 101

6.4.2 Rainfall Events and Water Infiltration 103
7.0 Examples Comparing Soil Gas Concentration at Different Locations 105
8.0 Summary of Results 109
9.0 References 111

Appendix A Model Equations
Appendix B Model Inputs and Assumptions
Appendix C Document Development and Peer-Review Process
Appendix D Variables Index

List of Figures

GENERAL VAPOR FATE AND TRANSPORT (SECTIONS 1.0 to 3.0)

1. Conceptualized illustration of the vapor intrusion pathway. 3

GENERAL SOIL VAPOR FLOW

2. Direction of the vapor migration (due to diffusion) and resulting soil vapor concentration distribution for a groundwater vapor source (or NAPL at groundwater level). 13
3. Direction of vapor migration (due to diffusion) and resulting soil vapor concentration distribution for a source in unsaturated soil (vadose zone).....14

PRESSURE & VAPORS NEAR BUILDING FOUNDATIONS

4. Change in pressure field distribution and soil gas flow rate (Qs) due to slab crack position and groundwater depth.....16
5. Soil vapor concentration distribution influenced by building pressurization and slab crack position. 18
6. Relationship between normalized indoor air concentration (α) and soil gas flow rate (Qs) into or out of the building. 19

RECALCITRANT HYDROCARBONS (SECTION 4.0)

SOURCE CONCENTRATION AND FOUNDATION TYPE

7a. Effect of source vapor concentration and foundation type on soil vapor distribution and indoor air concentration. 23
7b. Soil vapor concentration distribution and indoor air concentration from 7a presented as normalized values (i.e., the absolute values in 7a were divided by the source vapor concentration). 24

SOURCE DEPTH AND LATERAL DISTANCE TO BUILDING (HOMOGENEOUS SUBSURFACE)

8. Effect of groundwater source depth on soil vapor distribution and normalized indoor air concentration (α) for two foundation types. 26
9. Soil vapor distribution and normalized indoor air concentration (α) for a spatially finite vapor source laterally separated from building at two groundwater depths. 27
10. Soil vapor distribution and normalized indoor air concentration (α) for a spatially finite vapor source directly under a building at two groundwater depths. 28
11. Relationship between source-building lateral separation distance and normalized indoor air concentration (α). 29
12. Soil vapor distribution and normalized indoor air concentration (α) for two spatially finite source types (unsaturated soil and groundwater) laterally separated from building. 30

MULTIPLE BUILDINGS (HOMOGENOUS SUBSURFACE)

13. Soil vapor distribution and normalized indoor air concentration (α) for a scenario with two identical buildings separated by 10 m overlying a plume. 32
14. Soil vapor distribution and normalized indoor air concentration (α) for a scenario with two identical adjacent buildings overlying a plume. 33
15. Soil vapor distribution and normalized indoor air concentration (α) for a scenario with two adjacent buildings with different foundation types overlying a plume. 34
16. Soil vapor distribution for a scenario with two adjacent buildings under opposite pressurization, and with permeable backfill. 36
17. Normalized indoor air concentration (α) for different combinations of building conditions (e.g., pressurization, AER) and sub-slab vapor concentration. 39
18. Soil vapor distribution and indoor air (IA) concentration for a scenario with two buildings and two vapor sources. 41

HETEROGENEOUS SUBSURFACE

19a. Full view of the soil layers used in the simulations presented in Figures 19b and 19c. 43
19b. Effect of soil layers (19a) on pressure field, soil vapor distribution, and normalized indoor air concentration (α) for building under-pressurized by 5 Pa. 44
19c. Effect of soil layers (19a) on pressure field, soil vapor distribution, and normalized indoor air concentration (α) for buildings over-pressurized by 5 Pa. 45
20. Soil vapor distribution and normalized indoor air concentration (α) for scenarios with different soil moisture content in the subsurface and below building. 48
21a. Soil layers and ground cover scenarios used in the simulations presented in 21b with a shallow laterally separated vapor source. 50
21b. Effect of soil layers and ground covers (21a) on soil vapor distribution and normalized indoor air concentration (α) for a shallow laterally separated vapor source. 51
22a. Soil layer scenarios used in the simulations presented in 22b with a deep laterally separated vapor source. 52

22b. Effect of soil layers (22a) on soil vapor distribution and normalized indoor air concentration (α) for a deep laterally separated vapor source. 53
23a. Discontinuous soil layers and ground cover scenarios used in the simulations presented in 23b for two buildings separated by 10 m overlying a plume. 55
23b. Effect of discontinuous soil layers and ground cover (23a) on soil vapor distribution and normalized indoor air concentration (α) for two buildings separated by 10 m. 56
24a. Discontinuous soil layers and ground cover scenarios used in the simulations presented in 24b for two adjacent buildings near a plume.....58
24b. Effect of discontinuous soil layers and ground cover (24a) on soil vapor concentration distribution and normalized indoor air concentration (α) for two adjacent buildings. 59

GEOLOGIC BARRIERS

25. Effect of geologic vapor barriers on soil vapor distribution and normalized indoor air concentration (α). 61
26. Effect of a geologic vapor barrier on soil vapor distribution and normalized indoor air concentration (α) for two buildings separated by 10 m. 62
27. Effect of a geologic vapor barrier on soil vapor distribution and normalized indoor air concentration (α) for two adjacent buildings. 63

PETROLEUM AND OTHER AEROBICALLY BIODEGRADABLE HYDROCARBONS (SECTION 5.0)

SOURCE CONCENTRATION AND FOUNDATION TYPE

28. Effect of source vapor concentration on hydrocarbon and oxygen distribution in soil gas and normalized indoor air concentration (α) for a building with basement. 68
29. Effect of source vapor concentration on hydrocarbon and oxygen distribution in soil gas and normalized indoor air concentration (α) for a slab-on-grade building. 69
30. Relationship between source vapor concentration and normalized indoor air concentration (α) for three biodegradation rates (λ), two source depths and a building with basement. 70
31. Relationship between source vapor concentration and normalized indoor air concentration (α) for three biodegradation rates (λ), two source depths and a slab-on-grade building. 71

SOURCE DEPTH AND LATERAL DISTANCE TO BUILDING

32. Effect of source depth and vapor concentration on hydrocarbon and oxygen distribution in soil gas and normalized indoor air concentration (α) for a slab-on-grade building. 73
33. Relationship between source depth and normalized indoor air concentration (α) for a building with basement, two source vapor concentrations, and three biodegradation rates (λ) 74

34. Relationship between source depth and normalized indoor air concentration (α) for a slab-on-grade building, two source vapor concentrations, and three biodegradation rates (λ). 75
35. Effect of source depth and source-building lateral separation distance on the distribution of hydrocarbon and oxygen in soil gas for a NAPL source 77
36. Relationship between source-building lateral separation distance and normalized indoor air concentration (α) for a NAPL source, two source depths, and three biodegradation rates (λ). 78

HETEROGENEOUS SUBSURFACE

37. Effect of layered soils (rows A–D) on hydrocarbon and oxygen distribution in soil gas and normalized indoor air concentration (α) for two building pressures (basement scenario). 80
38. Effect of source vapor concentration on hydrocarbon and oxygen distribution in soil gas and normalized indoor air concentration (α) for scenarios with low permeability soils at the ground surface (e.g., soil layer scenario on row D of 37). 81

GEOLOGIC BARRIERS

39. Effect of geologic barriers on hydrocarbon and oxygen distribution in soil gas and normalized indoor air concentration (α) for a NAPL source at 5m bgs. 83
40. Effect of geologic barriers on hydrocarbon and oxygen distribution in soil gas and normalized indoor air concentration for a dissolved groundwater source at 5m bgs. 84

TEMPORAL AND SPATIAL VARIABILITY (SECTION 6.0)

41. Estimated time (y-axis, d=days) for chemicals to reach near-steady vapor concentrations (τ_{ss}) as a function of the distance from a source. Time on the plot is normalized by the retardation factor (Rv). 86
42. Effect of transport time on soil vapor distribution and normalized indoor air concentration (α) for different soil pore water saturation (deep source, 8 m bgs). 88
43. Effect of transport time on soil vapor distribution and normalized indoor air concentration (α) for different soil pore water saturation (shallow source, 3 m bgs). 89
44. Effect of transport times on soil vapor distribution for scenarios with homogeneous lithology and layered soils, and multiple buildings over spatially finite vapor source. 91
45. Effect of transport time on soil vapor distribution and normalized indoor air concentrations (α) for scenarios with varying koc and foc. 93

WIND LOAD

46a. Effect of building wind load on ground surface and sub-slab gauge pressure distribution. 95
46b. Effect of building wind load on sub-slab soil vapor distribution for recalcitrant and aerobically biodegradable VOCs. 96

ATMOSPHERIC AND INDOOR AIR PRESSURE FLUCTUATIONS

47. Barometric pressure fluctuations used in the simulations presented in Figures 48 through 51. 98
48. Temporal variation in the pressure difference between indoor air and sub-slab air resulting from fluctuations in barometric pressure (47) for two soil types. 99
49. Temporal reversal of the air flow direction resulting from fluctuations in indoor-sub-slab pressure difference (48). 99
50. Temporal variation of the indoor air VOC concentration (y-axis) resulting from fluctuations in indoor sub-slab pressure difference and reversals of air flow direction (Figures 48 and 49). 100
51. Temporal variation of the sub-slab VOC concentration (y-axis) resulting from fluctuations in indoor-sub-slab pressure difference and reversals of air flow direction (Figures 48 and 49). Concentration measured at location below slab crack. 100

WATER TABLE FLUCTUATIONS

52. Schematic illustration of water table fluctuations and the increase of VOC-impacted area from a groundwater source. 101
53. Schematic illustration of water table fluctuations and the increase of VOC-impacted area from a vadose zone (unsaturated soil) source. 102

EXAMPLE SCENARIOS COMPARING SOIL GAS CONCENTRATIONS AT DIFFERENT LOCATIONS (SECTION 7.0)

54. Scenarios with extensive groundwater source directly below a building. The symbols highlight areas for comparing soil vapor concentrations. 106
55. Scenarios with a groundwater source at different lateral distances from a building. The symbols highlight areas for comparing soil vapor concentrations. 107
56. Scenario with multiple buildings and multiple sources. The symbols highlight areas for comparing soil vapor concentrations. 108

EXECUTIVE SUMMARY

Vapor intrusion occurs when volatile organic compounds (VOCs) from contaminated soil or groundwater migrate upwards toward the ground surface and into overlying buildings through gaps and cracks in foundation slabs or basement walls. The route VOCs take from a subsurface source to the air inside a building is referred to as the vapor intrusion pathway.

Since the U.S. Environmental Protection Agency (EPA) published the 2002 EPA draft vapor intrusion guidance (*Draft Guidance for Evaluating the Vapor Intrusion to Indoor Air Pathway from Groundwater and Soils*; EPA530-D-02-004, U.S. EPA, 2002), the understanding of the vapor intrusion pathway has grown substantially. This *Conceptual Model Scenarios for the Vapor Intrusion Pathway* technical document expands on the understanding and conceptualizations presented in that draft guidance document and those appearing subsequently in the Interstate Technology and Regulatory Council's 2007 practical guideline (ITRC, 2007).

ES.1 Purpose and Objectives

The simulation results presented in this document are intended to illustrate how different site and building conditions might influence both the distribution of VOCs in the subsurface and the indoor air quality of structures in the vicinity of a soil or groundwater VOC source. Simulation results are presented for a range of simplified scenarios to help vapor intrusion practitioners visualize potential subsurface distributions of VOCs in soil gas and the relationship between them; indoor air concentrations; and characteristics of the vapor source, chemicals of concern, soils, and buildings, including their lateral and vertical (depth) position with respect to the contaminant source or sources. In addition, the simulation results provide some insight into spatial and temporal variability of soil gas and indoor air concentrations. This information can help practitioners develop more accurate conceptual site models, design better sampling plans, and better interpret the results of site investigations.

VOC concentrations in soil gas attenuate, or decrease, as the VOCs move from the source through the soil and into indoor air. The extent of attenuation is related to site conditions, building properties, and chemical properties, and is typically quantified in terms of an attenuation factor defined as the ratio of indoor air concentration to source vapor concentration. The primary objective of this document is to provide simplified simulation examples of how several factors (e.g., subsurface and building conditions) work together to determine (1) the distribution of VOC contaminants in the subsurface and (2) the indoor air concentration relative to a source concentration. Factors addressed in this document include vapor source characteristics (e.g., concentration, size, location, depth), subsurface conditions (e.g., soil layers, moisture conditions, oxygen levels for biodegradation), and building characteristics (e.g., foundation type and condition, pressurization, air exchange rates), as well as general site conditions (e.g., wind, ground cover), and the range of simulations included here covers common conditions encountered at sites where vapor intrusion is a concern. Both aerobically biodegradable petroleum hydrocarbons and other, more recalcitrant, contaminants that do not readily biodegrade in the soil gas under natural aerobic conditions (i.e., chlorinated solvents) are modeled, and the simulations include both single- and multiple-building scenarios, as well as

transient conditions to investigate how soil gas and indoor air concentrations might vary with time.

ES.2 Methodology, Assumptions, and Limitations

The work presented in this technical document features three-dimensional (3-D) mathematical model simulations for a range of conceptual model scenarios. Although the model visualizations presented in this document are based on a sound theoretical framework (Abreu, 2005; Abreu and Johnson, 2005; 2006), they are by necessity generated for simplified scenario inputs that may or may not adequately represent the complexities found at real sites. Thus, these simulations (or any use of the model described herein) are not intended to replace site-specific investigations. Rather, the simulated visualizations should enable practitioners to plan better investigations of vapor intrusion sites and to better interpret their results.

ES.3 Summary of Results

This document was prepared to help environmental practitioners gain insight into the processes and variables involved in the vapor intrusion pathway and to provide a theoretical framework with which to better understand the complex vapor fate and transport conditions typically encountered at actual contaminated sites. Actual site-specific conditions may lead to more complex VOC distributions than shown for the simplified conceptual model scenarios used in this technical document. Nevertheless, the following general observations can be made from these theoretical analyses and may be useful when considering the vapor intrusion pathway at a particular site. Report sections are provided so the reader can review examples and understand the basis and limitations for each observation:

- The horizontal and vertical distance over which vapors may migrate in the subsurface (primarily by diffusion) depends on the concentration of the source (**Sections 4.1** and **5.1**), the source depth (**Sections 4.2** and **5.2**), the soil matrix properties (e.g., porosity and moisture content, **Sections 4.4** and **5.4**), and the time since the release occurred (**Section 6.1**).
- Subsurface heterogeneities in site geology (e.g., layering, moisture content; see **Sections 4.4**, **5.4**, and **5.5**) influence the extent of vapor transport from a contaminant source to overlying or adjacent buildings.
- Advective flow occurs predominantly near cracks and openings in the building foundation slab and may affect the distribution of VOCs directly beneath the structure (**Section 3.2**). Heterogeneities in the permeability of geologic materials and backfill (**Section 4.3.2**), along with wind effects and building and atmospheric pressure temporal variation, may contribute to spatial and temporal variability of VOC concentrations in sub-slab soil gas and indoor air (**Section 6**).
- The distribution of VOCs in soil gas beneath a building is not the only factor that determines the indoor air concentration. The indoor air VOC concentration is also influenced by building conditions, including the existence of cracks in the foundation, building pressurization, and air exchange rate, which in turn can be related to other factors such as temperature, wind, barometric pressure, occupant behavior, and building operations (**Section 4.3**).

- In cases where the subsurface is homogeneous, building conditions are the same (e.g., air exchange rate, pressurization), and the source vapor concentration extends evenly beneath each building, the presence of multiple single-family residences at typical spacing can have little or no effect on the predicted indoor air VOC concentration for a single building (**Section 4.3**).
- Simulations assuming an impermeable ground cover suggest that VOC concentrations in shallow soil gas can be higher under the low permeability ground covers than under open soil (**Section 4.4.3**).
- The soil gas concentration distribution of aerobically biodegradable petroleum hydrocarbons can be significantly different from that of chlorinated solvents, which are comparatively more recalcitrant and do not readily biodegrade in the soil gas under natural aerobic conditions (**Section 5**).
- The simulations presented in this document illustrate that VOC concentrations may not be uniform beneath a building slab and in the subsurface. Section 7 shows, for some different scenarios, how exterior soil gas samples may be similar to or different from the sub-slab concentration, depending on site-specific conditions and the location and depth of the soil gas sample.

The conceptual scenarios simulated in this document illustrate that there are several factors influencing the distribution of VOC concentrations in soil gas and in indoor air, and suggest that assessment of the distribution of VOC concentrations in soil gas at sites and in indoor air can be supported by characterization of the site geology, building conditions, source extent, biodegradation, and other site-specific factors that can influence the distribution of VOCs in the subsurface and their migration into the indoor air of overlying buildings.

One of the key expected benefits of this document is to help practitioners visualize what to expect under various site conditions so they can select samples judiciously in order to minimize both the uncertainty and costs associated with vapor intrusion assessment.

[This page intentionally left blank.]

1.0 Introduction

This chapter provides context for the simulations that are included in the following chapters. It includes a discussion on the objectives and methodology used when developing the simulations and a discussion on the inputs, assumptions, and limitations of the simulations. There are no simulations in this chapter.

In November 2002, the U.S. Environmental Protection Agency (EPA) issued draft vapor intrusion guidance (*Draft Guidance for Evaluating the Vapor Intrusion to Indoor Air Pathway from Groundwater and Soils*; U.S. EPA, 2002) that was based on the understanding of vapor intrusion at that time. Since then, the understanding of the vapor intrusion pathway has grown substantially. This *Conceptual Model Scenarios for the Vapor Intrusion Pathway* document expands on the understanding and conceptualizations presented in that November 2002 draft guidance document and those appearing subsequently in the Interstate Technology and Regulatory Council's (ITRC's) 2007 practical guideline (ITRC, 2007).[1] Simulation results presented in this document are intended to illustrate how different site and building conditions might influence the distribution of VOCs in the subsurface and the indoor air quality of structures in the vicinity of a soil or groundwater contaminant source. Simulation results are presented for a range of simplified scenarios to help vapor intrusion practitioners visualize potential subsurface soil gas distributions of VOCs and the relationship between them, indoor air concentrations, and characteristics of the vapor source, chemicals of concern, soils, and buildings, including their lateral and vertical (depth) position with respect to the contaminant source or sources. In addition, the simulation results provide some insight to spatial and temporal variability of soil gas and indoor air concentration. This information can help practitioners develop more accurate conceptual site models, design better sampling plans, and better interpret the results of site investigations. The materials and analyses presented in this document are based on complex mathematical simulations of contaminant fate and transport and intrusion into buildings for simplified sets of model inputs. Care must be taken in interpreting and acting on the simulation results presented in this technical document, as some aspects of this work have yet to be studied in actual field settings (e.g., high frequency transient measurement studies are still needed). Therefore, the intent in presenting the simulation results is to aid in conceptualization and interpretation, not to replace appropriate site investigation.

1.1 Background

Vapor intrusion occurs when VOCs from contaminated soils or groundwater migrate upwards toward the ground surface and into overlying buildings through gaps and cracks in foundation slabs or basement walls. This contaminant migration is driven naturally by differences in concentrations and air pressure between the subsurface contaminated areas and the affected buildings. The route VOCs take from a subsurface source to the air inside a building is referred to as the vapor intrusion pathway. When VOCs present in soil gas migrate to the interior of a building and reach concentrations that could pose a potentially unacceptable health risk, the pathway is considered "complete."

[1] This report was developed by EPA's vapor intrusion guidance development team for the Office of Solid Waste and Emergency Response. The primary investigator and author of the report was Dr. Lilian D.V. Abreu (ARCADIS U.S., Inc., San Francisco, CA) under contract to EPA.

The term "VOC" is used throughout this document because volatile organics are usually the chemicals of concern at vapor intrusion sites, but semi-volatile organic compounds (SVOCs) and elemental mercury can also volatilize and contaminate soil gas and indoor air by vapor intrusion. Although the simulations presented in this document are based on representative VOC properties, they are useful to qualitatively understand the vapor fate and transport of other vapor-forming compounds. The terms "soil gas" and "soil vapor" are used interchangeably in this document to refer to the medium through which VOC vapors move by diffusion from higher to lower concentrations; soil gas also carries contaminants wherever it moves, by advection (i.e., soil gas flow), in particular from the sub-slab region into buildings. Finally, the term "soil" is used in this document to mean both the agricultural soil zone and the zone of unconsolidated, unsaturated material beneath it, but above the water table.

VOC concentrations in soil gas attenuate, or decrease, as the VOCs move from the source through the soil and into indoor air. This reduction in VOC concentration from a measurement point in the subsurface to indoor air is referred to as attenuation and occurs because the VOC emissions into a building are mixed with the natural flow of ambient air through the building. The extent of attenuation depends on the emission rate into the building, and the emission rate can be affected by the following:

- Subsurface features (e.g., fine-grained soils, high-moisture soil layers) that may hinder the diffusion and advection of VOCs
- Biodegradation of contaminants, which leads to a decrease in the emissions along the vapor migration pathway
- The integrity of the foundation and sub-grade walls
- Changes with time in groundwater level, source strength, and infiltration rates
- Pressurization of the building (under-pressurization draws soil gas into a building)
- Air exchange into a building, which brings fresh air into the enclosed space and dilutes the concentration of VOCs that enter through the vapor intrusion pathway.

Johnson and Ettinger (1991) defined a parameter to relate the vapor concentration of a chemical inside the building to its vapor concentration at the subsurface source and called it the "vapor intrusion attenuation factor," or "alpha" (α). It is defined as the concentration in indoor air divided by the concentration in soil gas at some depth. In this document, the vapor intrusion attenuation factor (α) is always defined as the indoor air concentration (C_{indoor}) divided by the soil vapor concentration immediately above the VOC source (C_{source}); as such, α is a source-normalized indoor air concentration (i.e., actual indoor air concentration divided by the source concentration), as follows:

$$\alpha = \frac{C_{indoor}}{C_{source}}$$

In this document, the source is defined as the region of highest vapor concentration; therefore, the normalized indoor air concentration (α) is always less than one. Throughout this document, we use the term "normalized indoor air concentration" in the text (periodically with α in parentheses following), and α in the figures for brevity.

1.2 Objectives

Vapor intrusion is an evolving field of science, and there is a need to expand the understanding of this pathway beyond the simple conceptual model presented in **Figure 1** (U.S. EPA, 2002), which illustrates a source of contamination in soil and groundwater and indicates the upward movement of VOCs from this source toward and into buildings. The work presented in this technical document features three-dimensional (3-D) mathematical model simulations for a wide range of conceptual model scenarios, with the objective of providing a theoretical basis for vapor intrusion practitioners to better understand the processes and variables involved in the vapor intrusion pathway and how they affect the distribution of soil vapor concentrations and soil vapor intrusion into buildings. Although the model visualizations presented in this document are based on a sound theoretical framework, they are by necessity generated for simplified inputs that may or may not adequately represent the complexities found at real sites. Thus, these simulations (or any use of the model described herein) are not intended to replace site-specific investigations. Rather, the simulated visualizations presented in this document should enable practitioners to plan better investigations of vapor intrusion sites and to better interpret their results.

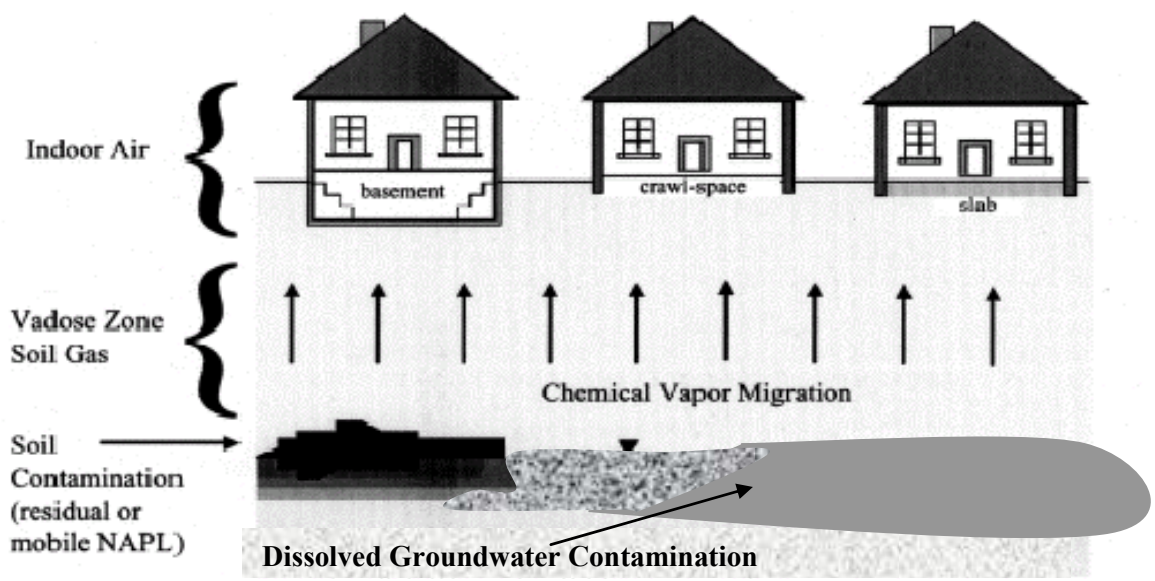

Figure 1. Conceptualized illustration of the vapor intrusion pathway.
(U.S. EPA, 2002)

1.3 Methodology

Most of the discussion and figures presented in this document were generated using a 3-D numerical model that simulates the fate and transport of contaminants in the subsurface and intrusion into buildings. The model was developed by Dr. Lilian D.V. Abreu and Dr. Paul C. Johnson at Arizona State University (Abreu and Johnson, 2005, 2006; Abreu, 2005). Details of the mathematical model development are presented in the cited publications and are not repeated here. Briefly, the numerical model simultaneously solves equations for the soil gas pressure field (from which the advective flow field is computed), advective and diffusive transport and reaction of multiple chemicals in the subsurface, flow and chemical transport through foundation cracks,

and chemical mixing indoors. The model's equations are summarized in **Appendix A.** The numerical accuracy of the code has been demonstrated through comparison of model predictions with other analytical and numerical model results (Abreu and Johnson, 2005; Abreu, 2005; Pennell et al., 2009; Bozkurt et al., 2009). The model predictions for assumed recalcitrant chemicals (i.e., chemicals with no or slow biodegradation in soil gas under natural aerobic conditions) are consistent with field measurements summarized by Hers et al. (2003). Also, the model predictions for aerobic biodegradation scenarios anticipate the key features of the field data of sites presented in the literature (Abreu and Johnson, 2006; Davis, 2009). The model was altered slightly from what is described in the sources cited above (see **Appendix A**): the indoor air is still considered to be well mixed, but the mixing is no longer limited to steady-state conditions as presented in Abreu and Johnson (2005, 2006) and Abreu (2005).

The Abreu and Johnson 3-D model is more complex than the one-dimensional (1-D) Johnson and Ettinger model, which has traditionally been applied for prediction of vapor intrusion (Johnson and Ettinger, 1991; U.S. EPA, 2004). Johnson (2002; 2005) used the Johnson and Ettinger model to provide insights on the effects of a variety of vapor intrusion pathway variables on indoor air concentrations and on functional relationships between critical parameters (e.g., soil conditions, building cracks, the vertical separation between the source and the building) and vapor intrusion attenuation factors. The current document uses the Abreu and Johnson 3-D model to simulate several processes that cannot be simulated with the 1-D Johnson and Ettinger model, such as effects of lateral source-building separation, finite sources, laterally discontinuous soil layers, and coupled oxygen and chemical transport and biodegradation.

The Abreu and Johnson 3-D model calculates the chemical vapor concentration in the subsurface, the mass flow rates into the building(s), and the indoor air concentration due to vapor intrusion. To facilitate the discussion and the presentation of results, the model output has been normalized using the source concentration (i.e., the maximum vapor concentration in the subsurface). When the output is an indoor air concentration, we call this source-normalized value the "normalized indoor air concentration" or just "α" in the figures. When the output is soil vapor concentrations, these are also presented as source-normalized values, called "normalized soil vapor concentrations." In either case, the normalized concentrations shown in the figures can be multiplied by the source concentration to convert them into absolute concentration values. The contour lines in most of the figures (2-D contour plots on vertical cross-sections through the center of the building and horizontal plan views at a specified depth below ground surface [bgs]) show these normalized soil vapor concentrations, which are always dimensionless and range from 0 to 1, with 1 being equal to the concentration at the source.

1.4 Simulation Inputs, Assumptions, and Limitations

Unless specified in the text and figures, the model input values common to all simulations (i.e., baseline conditions) are the same ones used in the published work of Abreu and Johnson (2005, 2006). Detailed baseline inputs and assumptions are presented in **Appendix B**, along with the conditions that are varied in the simulations to show the influence of selected building, source, and soil conditions. The physical-chemical properties of benzene were used in the simulations because they are similar to those for several compounds of interest in vapor intrusion.

The baseline conditions were selected to represent a typical size single-family home. Because this technical document is intended to provide the practitioner with insight as to how key site characteristics might affect vapor transport in the subsurface and vapor intrusion into buildings, the homogeneous subsurface case was selected as the baseline to introduce the simplest case first, before incorporating the complexities of layered and heterogeneous soils. The effects of these more complex conditions are also presented in this document (primarily in **Section 4.4**).

The baseline inputs used for the simulations in this document can be summarized as follows:

- A small residential building with a 1,000 ft^2 (or about 100 m^2) footprint with a basement or slab-on-grade foundation that is cracked around the perimeter and has a steady under-pressurization of 5 pascals (Pa) relative to the atmosphere
- If the building is a multi-floor building, vapor intrusion and mixing in the lowest level
- Sandy homogeneous soils
- A constant strength and spatially extensive vapor source, and steady-state pressure and vapor transport conditions
- Contaminants that do not readily biodegrade aerobically in the subsurface (i.e., assumed to be recalcitrant compounds in model simulations)
- A single vapor source located on top of the capillary fringe (from either a dissolved groundwater source or a non-aqueous–phase liquid [NAPL] plume source).

Appendix B presents detailed input values. Examples of conditions simulated that differ from the baseline include the following:

- Cracks located at the centerline of the foundation
- Continuous and discontinuous soil layers
- Multiple buildings
- Finite-sized sources, multiple sources, and unsaturated zone sources
- Transient transport conditions
- Biodegradable contaminants.

Although the majority of the simulations examine the effects of different subsurface conditions, simulations were also performed to examine the effects of different building conditions.

The 3-D model used in this work simulates the transport of contaminant vapors in the unsaturated soil zone; it does not model the transport of dissolved contaminants via groundwater flow in the saturated soil zone, and for these model runs, there was no net flow up or down of soil moisture in the unsaturated zone (e.g., from infiltration or a rising water table). The foundation floor and walls are treated as being impermeable barriers to the transport of vapors from the subsurface to the indoors, except where there are cracks or openings in the foundation. In actual foundations, the ability of concrete to hinder the transport of soil gas depends on the physical integrity of the concrete and characteristics determined by cement mixtures, cement/water ratios, and production processes (e.g., poured concrete vs. concrete block). Intact

concrete is virtually impermeable to air flow; nevertheless, volatile compounds from soil gas may diffuse through a concrete slab at relatively low rates (Nielson et al., 1997; Renken and Rosenberg, 1995; Rogers et al., 1994). The baseline conditions for most simulations presented in this document assume a full-length perimeter crack, a building with a steady under-pressurization of 5 Pa, relatively dry sandy soils, and a constant source concentration (i.e., no depletion of the source). These inputs result in upper-bound diffusion coefficients and steady flows into the building and so are thought to be conservative. To help put the results in context, for simulations not involving aerobic biodegradation, the model-predicted normalized indoor air concentrations (α) are consistent with site-specific measurements reported in the literature (Hers et al., 2003; Johnson et al., 2002).

The current version of the 3-D model simulates buildings with basement or slab-on-grade foundations; it does not simulate buildings with a crawl space. A crawl space is a space between the ground and the first floor of a building, but it is usually not high enough for a person to stand upright. According to the U.S. Census Bureau (2006), about 26% of U.S. single-family housing units have a crawl space. Soil vapor can also intrude into buildings with a crawl space. According to Nazaroff and Nero (1988), the building substructure influences the degree of pressure coupling between the indoor air and the soil vapor: the interior of a slab-on-grade building or a basement is potentially well coupled to the nearby soil. A building with a crawl space substructure may be well coupled or not, depending on (1) whether the crawl space is vented and the extent of that ventilation, and (2) the presence and condition of any water vapor barrier between the lowest floor in a building and the crawl-space. The contaminant transport processes in the subsurface and the building factors affecting vapor intrusion that are described in this technical document also apply to scenarios including buildings with crawl spaces; nevertheless, the vapor concentration distribution in the subsurface below the building and the contaminant emission rates into the crawl space can differ if there is no foundation concrete slab acting as a cap and a barrier for upward contaminant transport. Although the vapor concentrations in the subsurface below a crawl space could be lower than the ones below a slab-floored basement or a slab-on-grade foundation, the contaminant emissions into the crawl spaces could be higher. The ventilation rate of the crawl space and the nature and condition of the crawl space floor (e.g., concrete slab, concrete skim-coat, plastic water-vapor barrier, dirt) are key parameters affecting the air concentration that may eventually intrude into the building above.

It should be emphasized that actual site conditions will vary from the simplified inputs used to define the conceptual model scenarios discussed in this document. As a result, actual VOC distributions at field sites may be more complex (i.e., spatially and temporally variable) than those shown in this document. These simulations are presented as an aid to visualizing the behavior of VOCs during vapor intrusion, which should improve a practitioner's ability to plan effective vapor intrusion investigations and properly interpret their results. Subsurface and building heterogeneities, spatial and temporal variability, and possible interactions of subsurface and building conditions are examples of site-specific information that should be considered along with these simulations in the evaluation of the potential for vapor intrusion for any given site.

In a site assessment for vapor intrusion, any relevant background VOC levels (i.e., contaminants in indoor air that come from either indoor sources or from ambient [outdoor] air) should be taken into consideration. As a simplifying assumption, this work assumes that all VOCs in indoor air are the result of vapor intrusion (i.e., all VOCs in indoor air come from a source in the

subsurface) and that there are no background VOC contributions from indoor sources or outdoor air. In addition, indoor air concentrations are not assumed to be influenced by sorption (or desorption) to building materials. The EPA document *Background Indoor Air Concentrations of Volatile Organic Compounds in North American Residences: A Compilation and Implications for Vapor Intrusion* (U.S. EPA, 2011) presents an evaluation of measured background VOC levels in published indoor air studies.

The conceptual scenarios simulated in this document illustrate that many factors influence the distribution of contaminant concentrations in soil gas and suggest that selecting soil gas sampling locations is a site-specific decision that should be supported by characterization of the extent, location, and concentration of the source, as well as site geology, biodegradation, building conditions, and other site-specific factors that can influence the distribution of VOCs in the soil gas.

1.5 Document Development and Peer Review

This document was developed by EPA's Office of Solid Waste and Emergency Response (OSWER). This document has undergone extensive internal agency review and has been subjected to EPA's external peer review process. Details on the review stages and process may be found in **Appendix C** to this document.

1.6 Document Organization

This technical document provides a series of simulations showing how different building and subsurface conditions might influence vapor migration and VOC concentrations in soil gas and indoor air as VOCs move from a source into indoor air. The document is divided into sections that include basic discussions of subsurface vapor sources (**Section 2**) and vapor migration processes (**Section 3**). The remaining simulation results are organized according to the conditions and processes they illustrate:

- **Section 4:** Factors Affecting Vapor Migration and Indoor Air Concentrations of Recalcitrant VOCs
- **Section 5:** Factors Affecting Vapor Migration and Indoor Air Concentrations of Biodegradable VOCs
- **Section 6:** Temporal and Spatial Variability in Subsurface and Indoor Air Concentrations.

Section 7 provides example scenarios illustrating that soil gas concentrations at exterior locations may be similar to or different from sub-slab concentrations. **Section 8** summarizes the results of the simulations presented in this technical document, and **Section 9** provides the references cited.

At the beginning of each section or subsection, text boxes are provided to guide the reader through the simulations and results and help identify scenarios of interest.

Appendices A and **B** provide the model equations and the model inputs and assumptions, respectively. **Appendix C** describes the development of this document and the peer-review

process. **Appendix D** contains the Variables Index, which lists the major variables in each simulation, grouped into source conditions, subsurface conditions, and building characteristics, to help the reader identify scenarios of interest.

As discussed in **Section 1.4**, the homogeneous subsurface scenario was selected as a baseline to introduce the simplest case first, before incorporating the complexities of layered and heterogeneous soils. Therefore, in each section of this technical document, the factors affecting vapor migration and indoor air concentrations are presented first for homogeneous soils with single or multiple buildings; then the effects of complexities in subsurface conditions are gradually introduced with layered and heterogeneous soils for single- and multiple-building scenarios. The factors discussed in **Section 4** for recalcitrant chemicals are also discussed in **Section 5** for aerobically biodegradable petroleum hydrocarbons to illustrate effects of biodegradation on the distribution of VOCs in subsurface soil and indoor air.

2.0 Sources of Contaminated Vapors in the Subsurface

This chapter includes a discussion on how sources are defined for the purposes of the simulations and a basic discussion of the transport and distribution of VOCs as they move from the source. There are no simulations in this chapter.

Many factors or activities may create a vapor source in the subsurface, including leaking gas pipes, leaking underground storage tanks, aboveground spills, aboveground facilities that use VOCs during operations, historical subsurface disposal of industrial wastes, and landfills. Groundwater flowing through these primary source zones can be impacted and migrate away and in turn be a source of contaminant vapors downgradient of the primary release area. In the context of the vapor intrusion pathway, a source of contaminated vapors may be defined as the presence of chemicals of sufficient volatility (and toxicity) that they are likely to volatilize under normal temperature and pressure conditions and migrate through the porous media in the soil matrix and into indoor air and present a potential risk to human health. Such sources may exist in the form of contaminated soil gas and pore water in the unsaturated zone, residual or mobile non-aqueous phase liquids (NAPLs) in the subsurface soil or on top of the groundwater table, or dissolved-phase contaminants in groundwater. NAPL sources can be of particular concern because they typically create higher unsaturated zone vapor concentrations and mass flux than those above dissolved groundwater plumes of the same chemicals. Most of the simulations in this technical document assume a vapor source in soil gas above the groundwater table; the vapors may originate from either dissolved VOCs in groundwater at the top of the capillary fringe or NAPL sources on top of the water table. A few simulations (e.g., Figures 3 and 18) address the presence of vapor sources in the vadose zone, above the groundwater table, which could be either lighter-than-water NAPL or denser-than-water NAPL trapped in pore spaces.

The capillary fringe is a zone immediately above the water table that acts like a sponge sucking water up from the underlying groundwater. At the base of the capillary fringe, most of the soil pores are completely filled with water. Above this zone, water content decreases with increasing distance above the water table. The grain size of the soil particles influences the height of the capillary fringe: fine-grained soils exert greater suction on the groundwater table, resulting in a thicker capillary fringe that may be irregular across the upper surface, while coarse-grained soils exert less suction, resulting in a thinner capillary fringe that tends to be flatter along the top. The capillary fringe may reduce the emission of vapors from a dissolved groundwater source because its elevated water content limits the vapor migration (VOCs migrate much more slowly through water than through air). In the case of a NAPL source floating above the water table, the capillary fringe may also contain residual NAPL, and as a result, the emissions of vapors are less restricted by the capillary fringe.

If the vapor source is in the vadose zone, the vapors migrate radially in all directions from the source (i.e., upward toward the atmosphere, laterally outward, and downward toward the water table, which may eventually lead to groundwater contamination). For all source types, soil vapor concentrations decrease as distance from the source increases. If soil vapor monitoring data at a given site are not consistent with this trend, there may be multiple VOC sources, such as NAPL source(s) in the vadose zone and a dissolved groundwater source.

Soil sources can be small and groundwater sources can be long and narrow due to site hydrogeology; nevertheless, the soil gas plume associated with such sources can be large. When interpreting the nature and extent of soil gas contamination, it is important to discern the origins of VOCs in soil gas. The potential presence of multiple sources and the sparseness of groundwater data at sites usually make this process difficult (Rivett, 1995).

VOCs in a vapor source may be classified by their potential for degradation during vapor transport:

- **Recalcitrant** chemicals have a slow rate of biodegradation in natural aerobic settings. These chemicals tend to persist in the environment for a long time. In this document, recalcitrant chemicals are assumed to represent the chlorinated solvents, such as tetrachloroethene (PCE) and trichloroethene (TCE).
- **Aerobically biodegradable** chemicals readily degrade in the presence of oxygen due to microbiological processes. Many of the petroleum hydrocarbons and methane fall in this category.

A VOC's potential for degradation during vapor migration will influence its vapor distribution in the subsurface and consequently its potential for vapor intrusion into buildings. **Sections 3** and **4** discuss vapor intrusion processes and variables assuming that the chemicals are recalcitrant. **Section 5** shows the effect of aerobic biodegradation on vapor intrusion processes and variables. Other types of chemical degradation are not addressed in this document, including anaerobic degradation, hydrolysis, and catalyzed reduction reactions. Some chemicals, such as the chlorinated solvents, may produce more toxic compounds when they undergo degradation (e.g., PCE and TCE may produce vinyl chloride through anaerobic degradation). Production of such toxic degradation products is not addressed in this document but should be considered in a site-specific investigation.

3.0 Vapor Transport and Fate in the Subsurface

The simulations in this chapter address the role of diffusion and advection in shaping the migration and distribution of VOC vapors in subsurface soils and in indoor air. The VOC distributions are depicted as "normalized" values (i.e., the values are the vapor concentration at a given location divided by the source vapor concentration) rather than as absolute values. The use of normalized values makes it easier to envision the VOC distribution and its applicability to any source concentration.
In this chapter, the VOCs depicted in the simulations are "recalcitrant," that is, they are not subject to aerobic biodegradation. Depictions that include aerobic biodegradation are covered in Section 5.

Vapor transport in the subsurface may be controlled by four primary processes:

- **Diffusion** occurs when there are spatial differences in VOC concentrations in the subsurface; vapors diffuse in the direction of lower concentrations.
- **Advection** occurs when there is bulk movement of soil gas induced by spatial differences in soil gas pressure.
- **Phase partitioning** refers to the processes leading to VOC distribution between the soil gas, the dissolved phase in soil pore water, and the sorbed phase on soil particle surfaces. Phase partitioning will retard contaminant vapor transport in the subsurface under transient conditions, but not under steady-state transport conditions, when the mass transfer between phases approaches equilibrium.
- **Degradation** is usually associated with biodegradation, in which VOCs are converted to other chemicals by microorganisms in the subsurface.

Vapor transport may occur under transient or steady-state conditions. Under transient conditions, concentrations are changing with time. Under steady-state conditions, concentrations and pressures are constant with time, although they may vary spatially. For example, if the conditions are at steady state, the source concentration is constant with time (it does not increase or decrease), the VOC concentration distribution is fully developed, and the concentration in each location is constant with time; also, all contaminant fluxes and emission rates are constant with time. For steady-state transport conditions, the parameters that influence the transport by diffusion and advection are soil porosity and moisture content, chemical diffusion coefficients in air and water, soil gas permeability, and building pressurization. The Henry's law constant (which quantifies chemical partitioning between air and water) may also influence transport when moisture content is high and Henry's law constant is very low. For transient transport conditions, VOC transport may also be influenced by phase transfer to the aqueous and solid phases, which depend on the VOC-specific Henry's law constant and sorption coefficient to soil organic carbon (Koc), and on the mass fraction of organic carbon in soil (foc).

Most simulations presented in this technical document represent steady-state transport conditions; only a few transient transport scenarios are illustrated and discussed. Because the 3-D Abreu and Johnson model is a transient solution of the transport equations, the steady-state scenarios presented in this document were obtained by running the model long enough to achieve essentially steady-state conditions.

This section discusses the mechanisms of diffusion and advection under steady-state conditions with no degradation. Biodegradation is introduced in **Section 5,** and the effect of transient state conditions is introduced in **Section 6**.

3.1 Diffusive Transport of Vapors in the Unsaturated Zone

The objective of this section is to introduce the general concept of diffusion and the direction of vapor migration for different source locations. This section shows how recalcitrant contaminants migrate by diffusion through homogeneous soils from a source that is either at the groundwater table (**Figure 2**) or at the unsaturated soil zone (**Figure 3**). The contaminant vapor distribution reflects the location and geometry of the vapor source "footprint." To clearly show how concentration changes away from the source, the sources are limited in size and laterally separated from the building.

Vapor transport (or migration) by diffusion occurs when VOC concentrations vary spatially: vapors migrate from an area of higher concentration (the source) to an area of lower concentration (the surrounding area), as illustrated by the arrows in **Figure 2** (groundwater source) and in **Figure 3** (vadose zone source). In the subsurface away from a building, the dominant process for vapor transport is typically diffusion, but in the subsurface near a building, both diffusion and advection processes may be important, as discussed in **Section 3.2**. Diffusion occurs through the soil gas and water present in the soil pores. Air (vapor-phase) diffusion coefficients are about 10,000 times greater than water diffusion coefficients, so vapor diffusion through the air-filled pores of the soil matrix is usually the dominant diffusion transport mechanism for VOCs in the unsaturated zone, except in cases of high moisture content and very low Henry's law constant. Consequently, for similar concentration gradients, as soil moisture content increases, the vapor diffusion rate decreases.

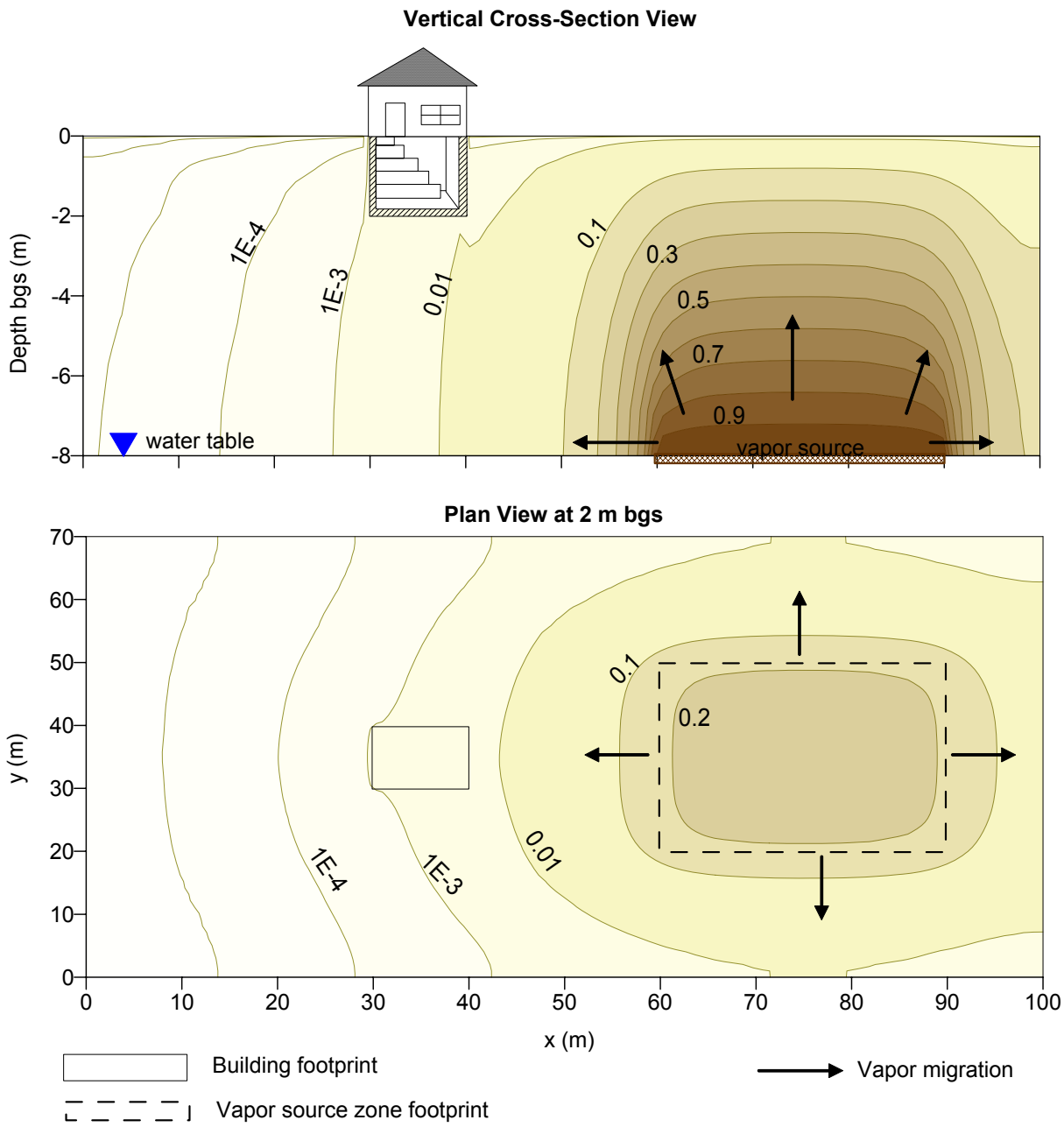

Figure 2. Direction of the vapor migration (due to diffusion) and resulting soil vapor concentration distribution for a groundwater vapor source (or NAPL at groundwater level).
The soil vapor concentration contour lines are normalized by the source vapor concentration.

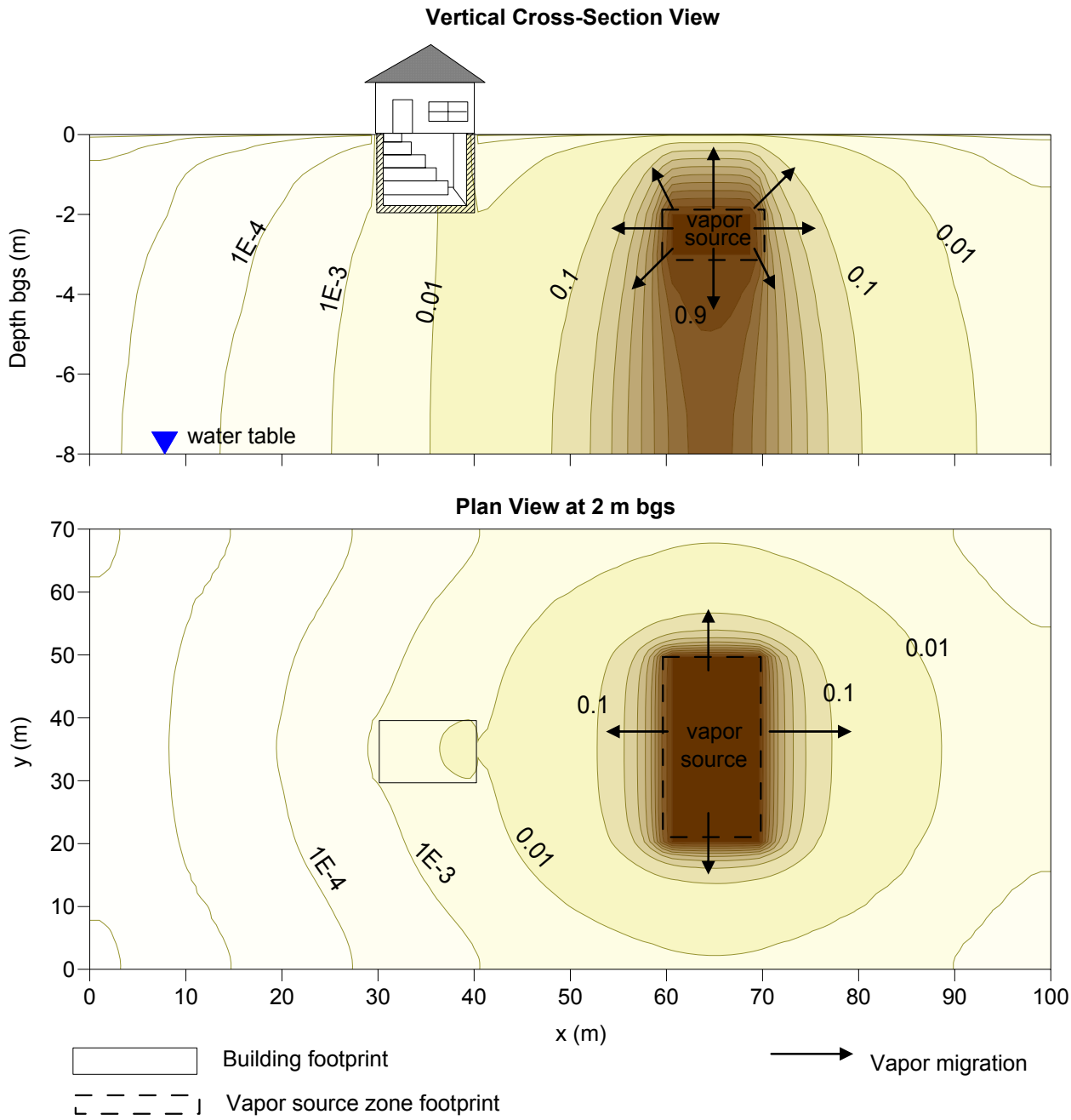

Figure 3. Direction of vapor migration (due to diffusion) and resulting soil vapor concentration distribution for a source in unsaturated soil (vadose zone).

The soil vapor concentration contour lines are normalized by the source vapor concentration.

3.2 Advective Transport of Vapors Near Building Foundations

The figures in this section illustrate how the pressure difference between a building and the underlying soil impacts advective flow (**Figure 4**) and VOC concentrations (**Figure 5**) under different foundation crack and building pressure conditions. The lower the indoor air pressure relative to the sub-slab soil gas pressure (i.e., the more under-pressurized a building is), the larger the soil gas flow rate into the building (Q_{soil}) and the larger the concentrations of contaminants in the indoor air due to vapor intrusion, provided the soil type is permeable to soil gas flow. The plots in **Figure 6** illustrate that when the soil gas flow rate into the building (Q_{soil}) exceeds about 5 to10 L/min, the rate of contaminant diffusion from the source to the sub-slab may limit the amount of contaminants available to flow into the building.

Advective soil gas transport occurs when soil gas containing VOCs moves due to spatial pressure differences, which occur, for example, whenever there is a difference between the air pressure within a building and the soil gas pressure. The air pressure within a building can be lower or higher than the soil gas pressure, and even small pressure differences may cause advective flow of gas into or out of the building through pores, cracks, or openings in the building floor or basement walls. The pressure difference may be caused by temperature differences (i.e., the "stack effect," when hot air inside the building rises), wind load on the building walls, the operation of mechanical devices (e.g., exhaust fans, air conditioners, heating units), or the operation of combustion devices that vent exhaust gases to the outside (e.g., fireplaces, furnaces).

The pressure difference between a house-sized building and the surrounding soil is usually most significant within 1 to 2 m of the structure, but measurable effects have been reported up to 5 m from the structure (Nazaroff et al., 1987). Temperature differences or unbalanced mechanical ventilation are likely to induce a symmetrical pressure distribution in the subsurface, but the wind load on a building adds an asymmetrical component to the pressure distribution in the subsurface and thus to the distribution of contaminants in soil gas.

In this technical document, the building and soil air pressures are reported as gauge pressure, which is defined as the pressure difference relative to atmospheric conditions. If the building's absolute pressure is lower than the atmospheric pressure (pressure differential is a negative number), the building is under-pressurized; if it is higher than the atmospheric pressure (pressure differential is a positive number), the building is over-pressurized.

Examples of the predicted soil gas pressure distribution around buildings, as well as the resultant advective soil gas flow rates into the building (Qs), are presented in **Figure 4** for two soil gas entry points consisting of (1) a crack along the perimeter of the foundation slab and (2) cracks at the center of the floor slab. The cracks have the same total length and width; only the location of the cracks is different. The pressure distribution is symmetrical to the center of the building foundation because the subsurface is homogeneous and wind load was not included in these simulations.

Soil gas flows perpendicularly to the pressure field contour lines illustrated in Figure 4, and for the case of perimeter cracks, the calculated pressure fields suggest that air primarily travels down from the ground surface to the foundation crack located along the perimeter, with the flow lines beneath the building extending to greater depths in areas where the depth to the water table is greater. For the center-of-foundation crack scenario, the calculated flow is primarily horizontal beneath the foundation, and the uniformity of the flow increases as the depth to groundwater

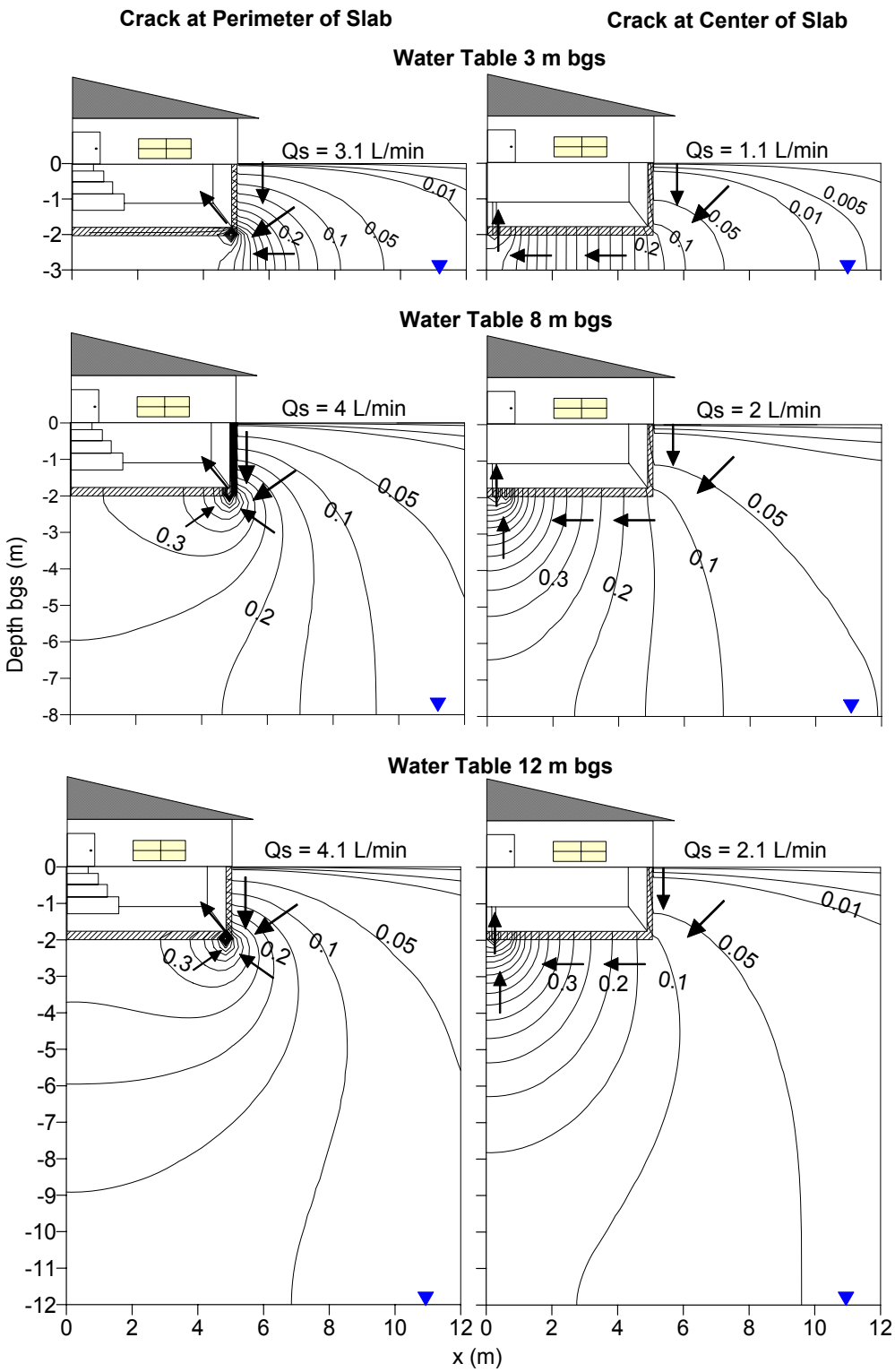

Figure 4. Change in pressure field distribution and soil gas flow rate (Qs) due to slab crack position and groundwater depth.

The soil gas gauge pressure contour lines are normalized by indoor air gauge pressure (5 Pa, under-pressurization). The arrows indicate soil gas flow direction.
(Abreu, 2005)

decreases. The predicted soil gas flow rates are relatively insensitive to water table depth when the depth is greater than 5 m bgs.

It should be noted that the simulations presented in Figure 4 represent homogeneous, sandy soils. Under the homogeneous conditions simulated, the flow to a perimeter crack is larger than the flow to a center-of-foundation crack because of the shorter flow path length from ground surface to a perimeter crack. Heterogeneities in the subsurface at real sites will affect the pressure gradient field and result in spatially more complex flow rates and patterns than those shown in Figure 4.

In scenarios with coarser soils (sands and gravels), the soil gas permeability is high, and changes in building pressurization may affect the air flow field and the resultant soil vapor concentration profiles near buildings, as illustrated in **Figure 5** for two soil gas entry points consisting of cracks at the perimeter and at the center of the foundation slab. These simulations assume a homogeneous subsurface (sand) and no wind load, resulting in a symmetrical soil gas distribution beneath the building foundation. Figure 5 shows that under-pressurized buildings may have higher soil vapor concentrations beneath the foundation when compared with over-pressurized buildings where clean indoor air (i.e., no indoor VOC sources) flows outward to the soil through the foundation cracks and dilutes soil vapor concentrations in the region around the crack and, to some extent, beneath the slab. The profiles in Figure 5 also illustrate spatial variability in sub-slab soil vapor concentration distribution. Although not presented in Figure 5, scenarios with a building at atmospheric conditions (i.e., not pressurized) could still exhibit some concentration buildup below the foundation due to the capping effect of the concrete slab.

In scenarios with fine-grained soils (silts and clays), the soil gas permeability is low. Therefore, in these scenarios, building pressurization may not affect the soil vapor concentration profile because the airflow field and soil gas flow rates (Qs) may be negligible. Nevertheless, over-pressurization of the building can reduce the indoor air concentration by driving the soil gas flow direction from the building to the soil, as presented in **Figure 6** and discussed below.

The soil gas flow rate into and out of a building also affects the indoor air concentration. Figure 6 shows the influence of soil gas flow rate (Q_s) on normalized indoor air concentration (α) predicted by the model for basement and slab-on-grade foundations with full-length perimeter cracks and a homogeneous subsurface for a range of soil properties that represent gravel, sand, silt, and clays (Abreu and Johnson, 2005, Table 2). The results in Figure 6 suggest that the normalized indoor air concentrations (α) decrease rapidly for lower soil gas flow rates (e.g., less than 1 L/min) and are relatively constant for higher soil gas flow rates (e.g., greater than 5 L/min), because at those higher rates, the VOC transport into the building becomes limited by the rate at which VOC mass diffuses from the source to the soil below the building. Figure 6 also illustrates the effect that building pressurization may have in reducing vapor intrusion, as shown by the reductions in the normalized indoor air concentrations for negative soil gas flow rates (Qs) corresponding to building over-pressurization.

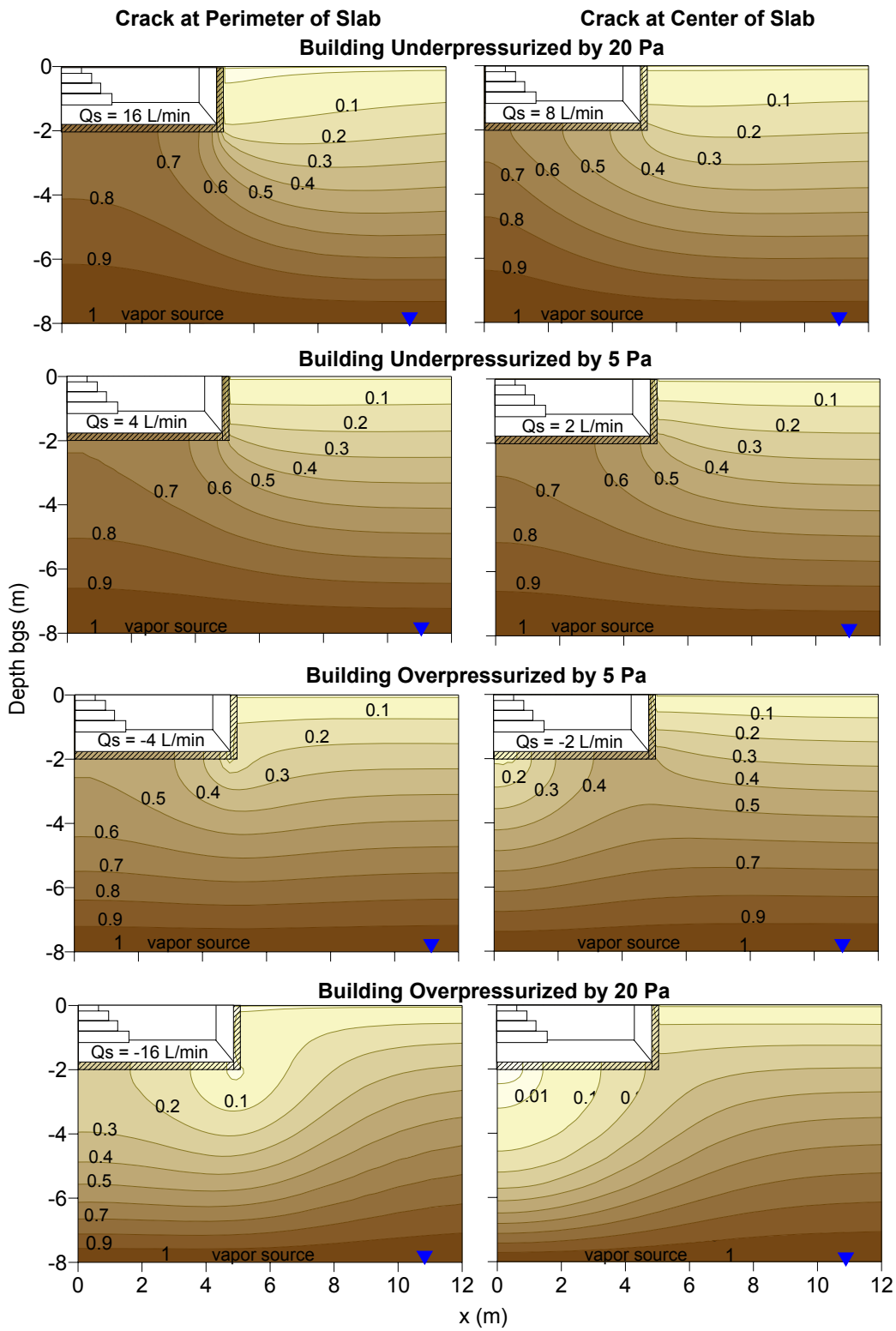

Figure 5. Soil vapor concentration distribution influenced by building pressurization and slab crack position.

The soil vapor concentration contour lines are normalized by the source vapor concentration at 8 m bgs. Positive values of the soil gas flow rate (Qs) reflect gas flow into the building, and negative values reflect flow out of the building.

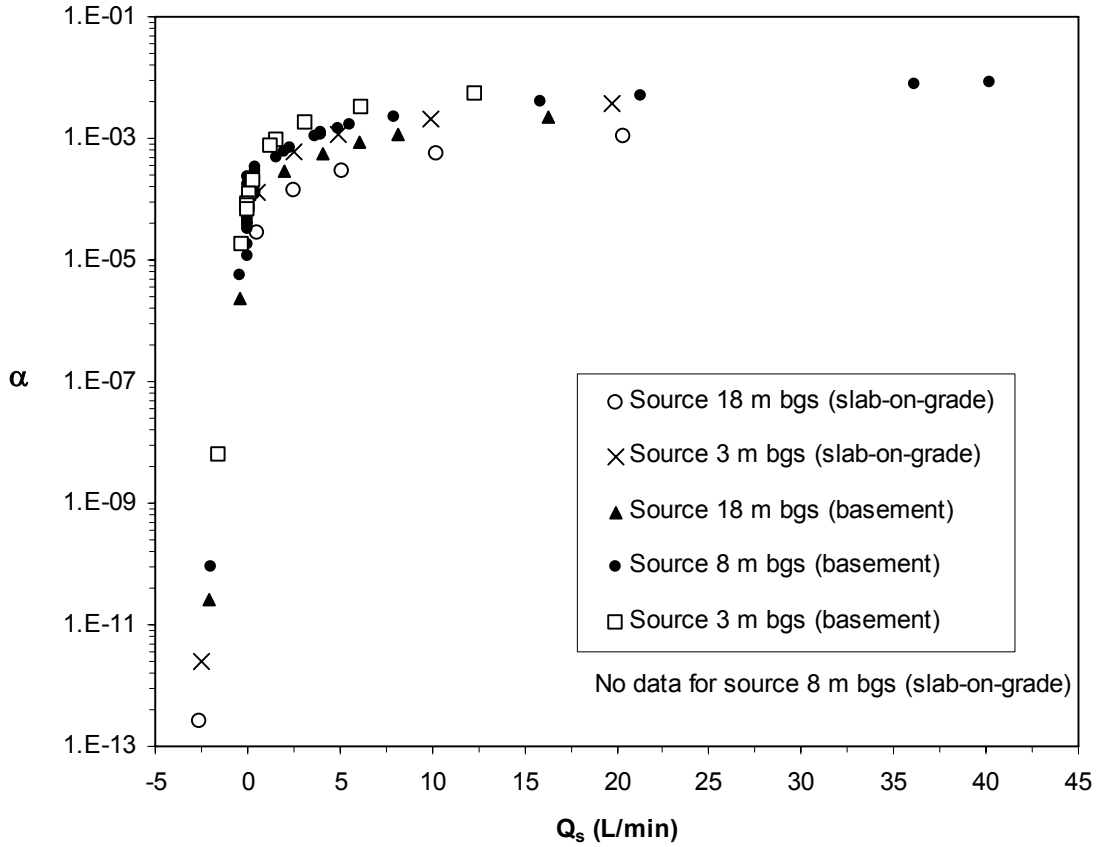

Figure 6. Relationship between normalized indoor air concentration (α) and soil gas flow rate (Qs) into or out of the building.

Positive values of Qs reflect soil gas flow from the subsurface into the building; negative values reflect flow out of the building and into the subsurface. (Abreu and Johnson, 2005)

The simulations presented in this technical document account for pressure-driven advective flow near the foundation, but no density-driven advective flow in soil gas in the subsurface environment. Although density-driven advective flow of soil gas has been discussed in the literature (e.g., Falta et al., 1989; Mendoza and Frind, 1990; Johnson et al., 1992; Hughes et al., 1996), only in extremely high permeability materials could density-driven advection occur, and it would be limited to the close proximity of a NAPL source in the unsaturated zone (Johnson et al., 1992; Hughes et al., 1996). This extreme scenario (for density-driven advective flow in soil gas in the subsurface environment) was not simulated here, because this document focuses on more typical scenarios, where diffusion is the dominant transport mechanism for VOCs in the unsaturated zone away from the building, as discussed in **Section 3.1**.

[This page intentionally left blank.]

4.0 Factors Affecting Vapor Migration and Indoor Air Concentrations of Recalcitrant VOCs

The simulations in this chapter cover a broad range of factors (source concentration and location, subsurface characteristics, building conditions) that can affect the migration and distribution of VOC vapors in subsurface soils and in indoor air. In this chapter, the VOCs depicted in the simulations are recalcitrant and not subject to aerobic biodegradation. Depictions that include aerobic biodegradation are covered in Section 5. The simulations in Section 4 are applicable to chlorinated hydrocarbons.

Several factors may affect subsurface vapor migration and the indoor air concentration due to vapor intrusion into buildings. Although the main factors discussed in this section can affect both recalcitrant and biodegradable contaminants, this section focuses on the behavior of recalcitrant contaminants. In this document, recalcitrant compounds are assumed to represent the contaminants that do not readily biodegrade in the subsurface under natural aerobic conditions (e.g., chlorinated hydrocarbons). The additional factors and responses unique to biodegradable contaminants are discussed in **Section 5.0**. The factors discussed here include the following:

- Source concentration (**Section 4.1**)
- Source depth and lateral distance from a building (**Section 4.2**)
- Other factors in scenarios with a homogeneous subsurface, including multiple buildings, permeable fill and building pressurization, building conditions, and multiple sources (**Section 4.3**)
- Subsurface heterogeneities, including soil moisture distribution and ground cover (**Section 4.4**).

The simulations presented below show the effect of varying one variable at a time (e.g., source depth) while the other variables (e.g., building pressurization, air exchange rate) are held constant at the baseline values (described in **Appendix B**), unless otherwise specified in the text and figures. The results and discussions in each subsection are specifically related to the conditions simulated and are intended to show general trends and provide a basic understanding of expected soil vapor concentration profiles and indoor air concentration for the conditions simulated.

Many simulations in this technical document were performed for the baseline homogeneous subsurface condition, which assumes sandy soils with a pore water saturation of 20% of the total pore space. The predicted normalized indoor air concentrations for those simulations are representative of relatively dry, high-permeability soil conditions. For soils typically having a higher moisture content (e.g., silt, clay), which results in less vapor migration by diffusion and advection, less vapor intrusion is expected to occur (and the normalized indoor air concentrations are expected to be smaller).

4.1 Source Concentration

The figures in this section illustrate the relationship between the source vapor concentration (1,000 and 100,000 μg/m^3) and the concentration of VOCs in the soil gas and indoor air for basement and slab-on-grade foundation types (**Figure 7a**). Because concentrations are primary variable in these scenarios, the results are illustrated both in absolute and normalized concentrations. These simulations illustrate how the foundation slab inhibits upward diffusion when compared with the open surface areas beside the buildings so that the VOC concentrations beneath a building are higher than they are at an equivalent depth beside it (if the soil is homogeneous and the source is under the building). **Figure 7b** depicts the same scenarios that are depicted in **Figure 7a** but presents the VOC distributions as "normalized" values.

For recalcitrant VOCs the effect of the source concentration on vapor migration and indoor air concentration due to vapor intrusion is illustrated in **Figures 7a** and **7b**. Figure 7a presents the soil vapor concentration profiles and the indoor air concentrations in units of μg/m^3. Figure 7b is a normalized version of Figure 7a, where the soil vapor concentration profile and the indoor air concentration are normalized (divided) by the source vapor concentration. These figures present two vapor source strengths, 1,000 and 100,000 μg/m^3, and two building foundation types, basement and slab-on-grade. The source is located beneath the building at a depth of 8 m bgs, which is 6 m below the foundation slab for the basement scenario and about 8 m below the foundation for the slab-on-grade scenario.

As illustrated in Figure 7a, the higher source concentrations result in higher concentrations in the subsurface gas and in the indoor air (if there is a vapor intrusion pathway). Figure 7b shows that, for recalcitrant chemicals, normalized soil vapor concentration distributions and normalized indoor air concentrations (α) are independent of the source vapor concentration (when all other factors are held constant).

The chemical concentration is higher beneath the foundation slab compared with concentrations at similar depths away from the building. This effect is common for all simulations in which the soil is homogeneous and the source is under the building. This effect is more pronounced for basement foundations than for slab-on-grade foundations because of the shorter distance between a basement foundation and the source and because the soil beneath a basement foundation is further from the surface. In the open surface areas far from the building, transport is dominated by diffusion, and the vertical concentration distribution changes linearly with upward distance from the source and is the same for both basement and slab-on-grade constructions.

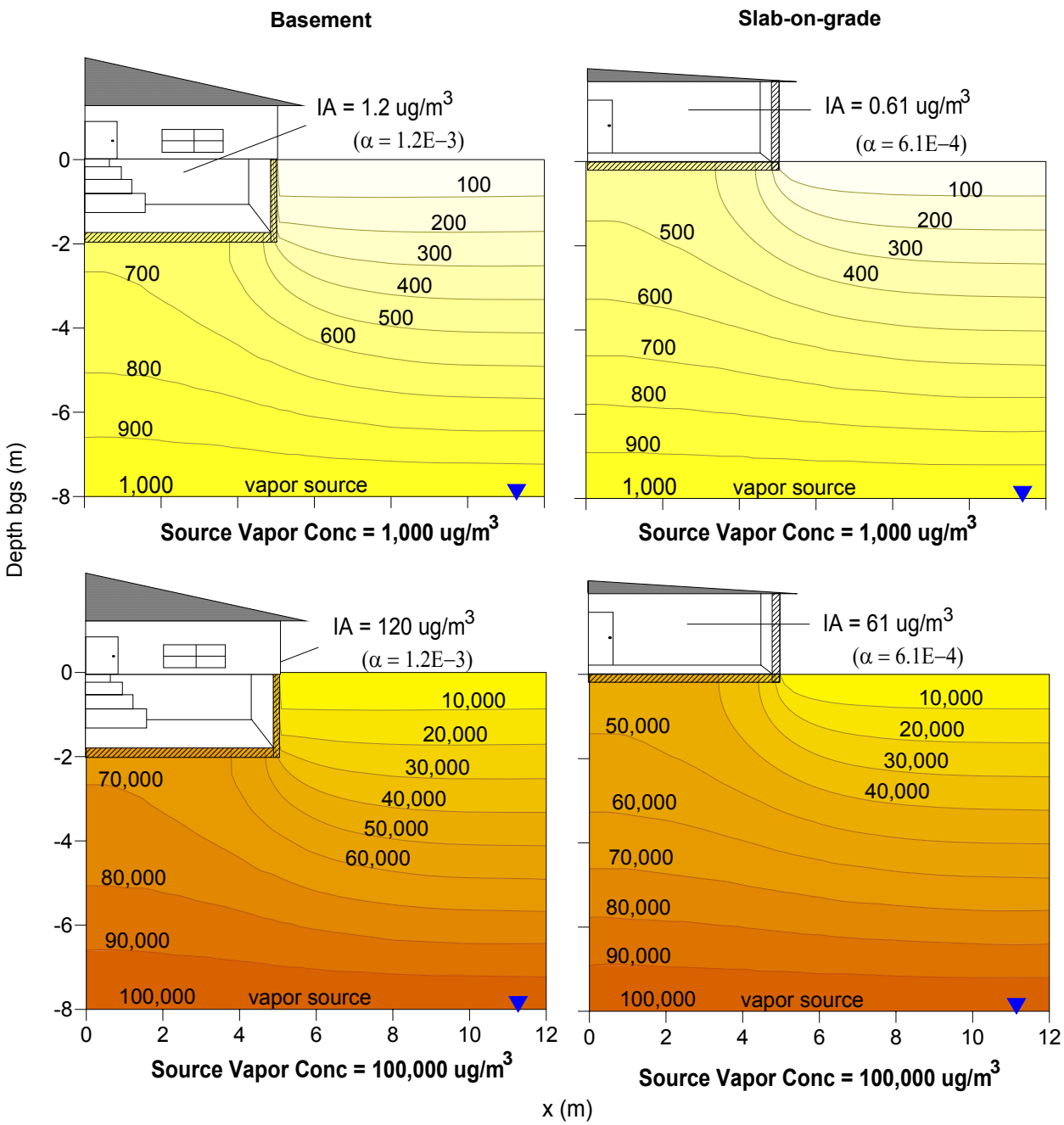

Figure 7a. Effect of source vapor concentration and foundation type on soil vapor distribution and indoor air concentration.

Soil vapor concentration contour lines are in units of $\mu g/m^3$. IA is the indoor air concentration in units of $\mu g/m^3$ and α is the normalized indoor air concentration (dimensionless). The source is located at 8 m bgs.

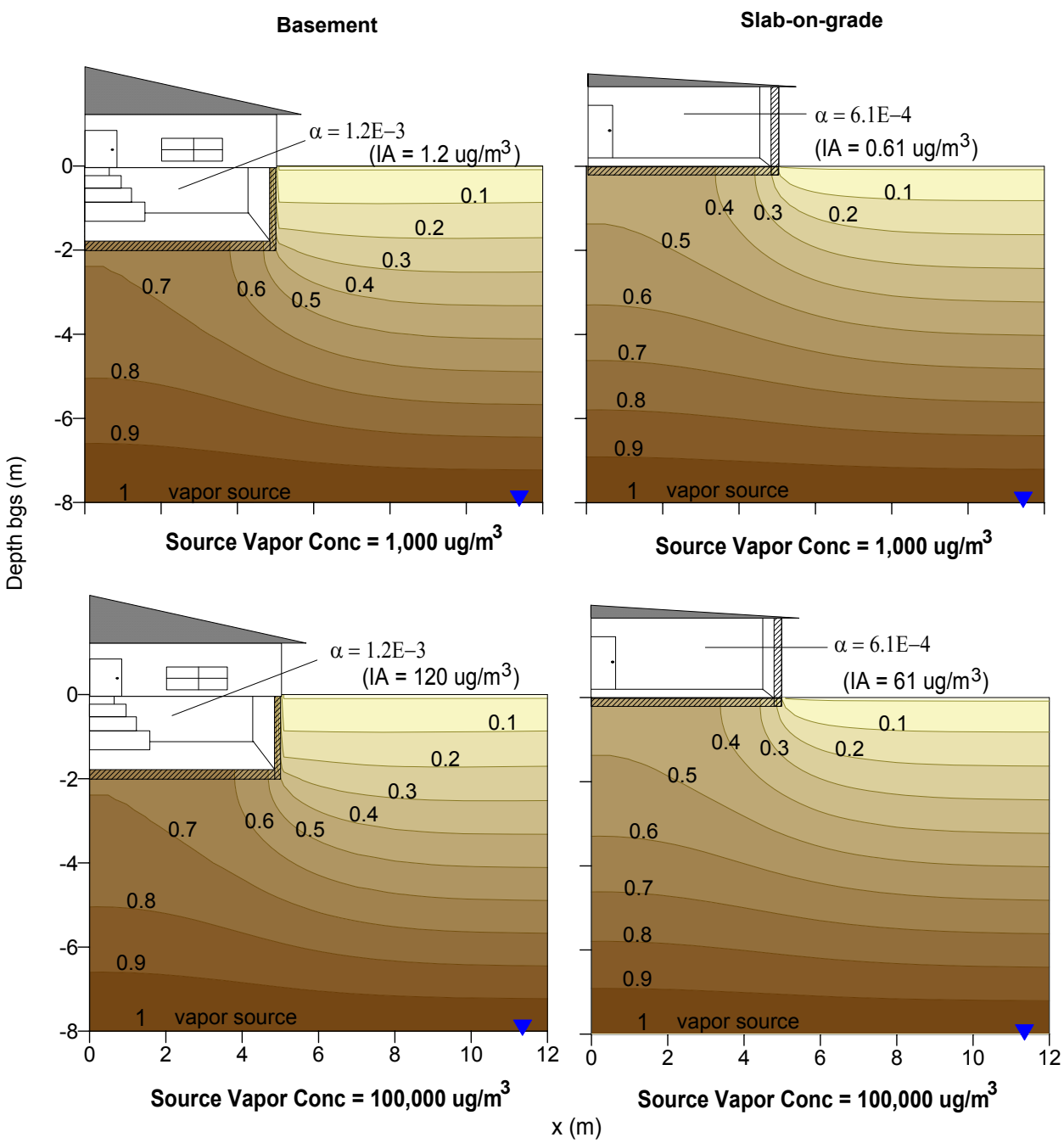

Figure 7b. Soil vapor concentration distribution and indoor air concentration from Figure 7a presented as normalized values (i.e., the absolute values in Figure 7a were divided by the source vapor concentration).

The source is located at 8 m bgs.

4.2 Source Depth and Lateral Distance from Building

The figures in this section illustrate how the depth and location of the source influence soil vapor and indoor air contaminant concentrations. In settings with homogeneous soils and a vapor source at the groundwater table directly beneath the building, the soil gas and indoor air concentrations of VOCs are inversely related to the distance between the source and the building (**Figure 8** and **Figure 10**). In settings where the vapor source at the groundwater table is not directly under the base of the building (i.e., it is laterally offset from it), the indoor air concentrations increase with the source depth as a result of greater lateral diffusion from the source (**Figure 9**). **Figure 11** is a plot that depicts how those relationships vary depending on the groundwater vapor source depth and its lateral separation from the building. **Figure 12** illustrates how lateral diffusion can create similar normalized indoor air concentrations for two sources at different depths but at similar lateral distances from the building: one source is at a shallow unsaturated soil zone, and the other source is at a deeper groundwater table.

The effect of source depth on the soil vapor concentration distribution of recalcitrant chemicals is illustrated in **Figure 8**. The figure presents normalized soil vapor concentration profiles for a uniform groundwater vapor source located beneath the building at three different depths (3, 8, and 18 m bgs) and for two building foundation types (basement and slab-on-grade). The source depth measured from the building foundation is 1, 6, and 16 m for the basement scenario and approximately 3, 8, and 18 m for the slab-on-grade scenario.

For the shallowest source (3 m bgs), the concentration below the foundation is about 90% of the source concentration for the basement scenario and about 30–80% of the source concentration for the slab-on-grade scenario. For a deep source located 18 m bgs, the predicted concentration below the foundation is about 20–30% of the source concentration for the basement scenario and about 10–20% of the source concentration for the slab-on-grade scenario. The normalized indoor air concentrations (α) presented in Figure 8 show that as the source depth increases by a factor of six, the normalized indoor air concentration decreases by a factor of three. For the basement scenario, the normalized indoor air concentrations are similar as the source depth increases from 3 to 8 m bgs because the increased soil gas flow beneath the building predicted for the water table at 8 m bgs offsets the difference in near-crack soil gas concentrations. The normalized indoor air concentrations of comparable basement and slab-on-grade scenarios differ by at most about a factor of two; the difference is due to the larger source-slab separation and air flow pathway in the slab-on-grade scenario.

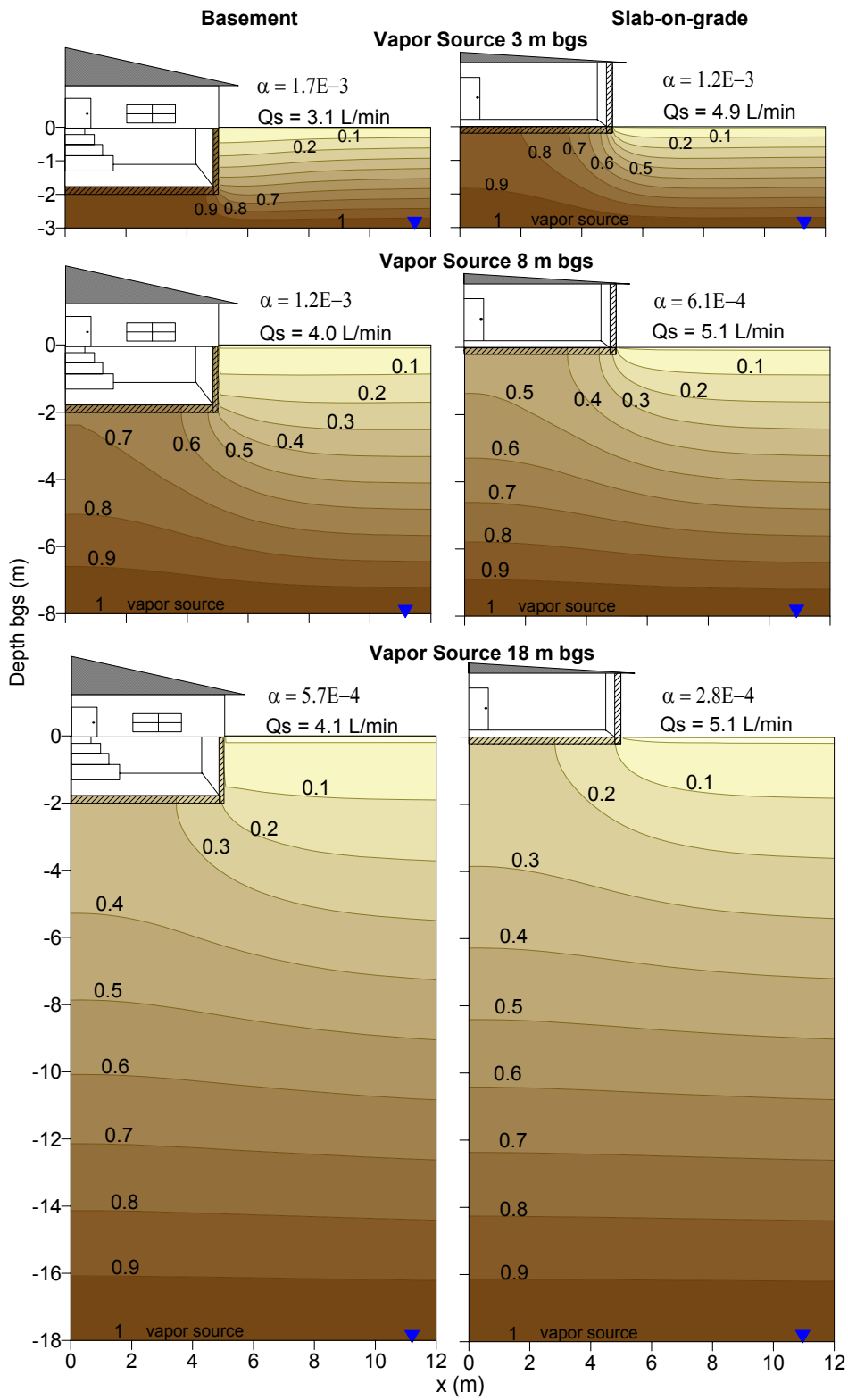

Figure 8. Effect of groundwater source depth on soil vapor distribution and normalized indoor air concentration (α) for two foundation types.

The soil vapor concentration contour lines are normalized by the source vapor concentration. Qs is the soil gas flow rate predicted for building under-pressurized by 5 Pa.

(Abreu, 2005)

As discussed previously, for a source located at the water table, vapors migrate upward and laterally outward from the source. **Figure 9** presents predicted normalized soil vapor concentration distributions and normalized indoor air concentrations for a vapor source located at a lateral distance from a building with a basement. This figure illustrates the upward and lateral vapor migration for a vapor source of recalcitrant chemicals at groundwater level in a homogeneous subsurface. If the groundwater is shallow and the ground surface is open to the atmosphere, vapor migration is predominantly upwards toward the atmosphere and lateral migration is less significant. If the groundwater is deeper, lateral vapor migration becomes more significant compared with upward migration. In the conceptual site scenarios represented in Figure 9, the normalized indoor air concentration for the scenario with deep groundwater is three orders of magnitude greater than the value with shallow groundwater; therefore, under the simulated conditions, vapor intrusion may be of greater potential concern if a laterally displaced source is deeper rather than shallower for recalcitrant compounds.

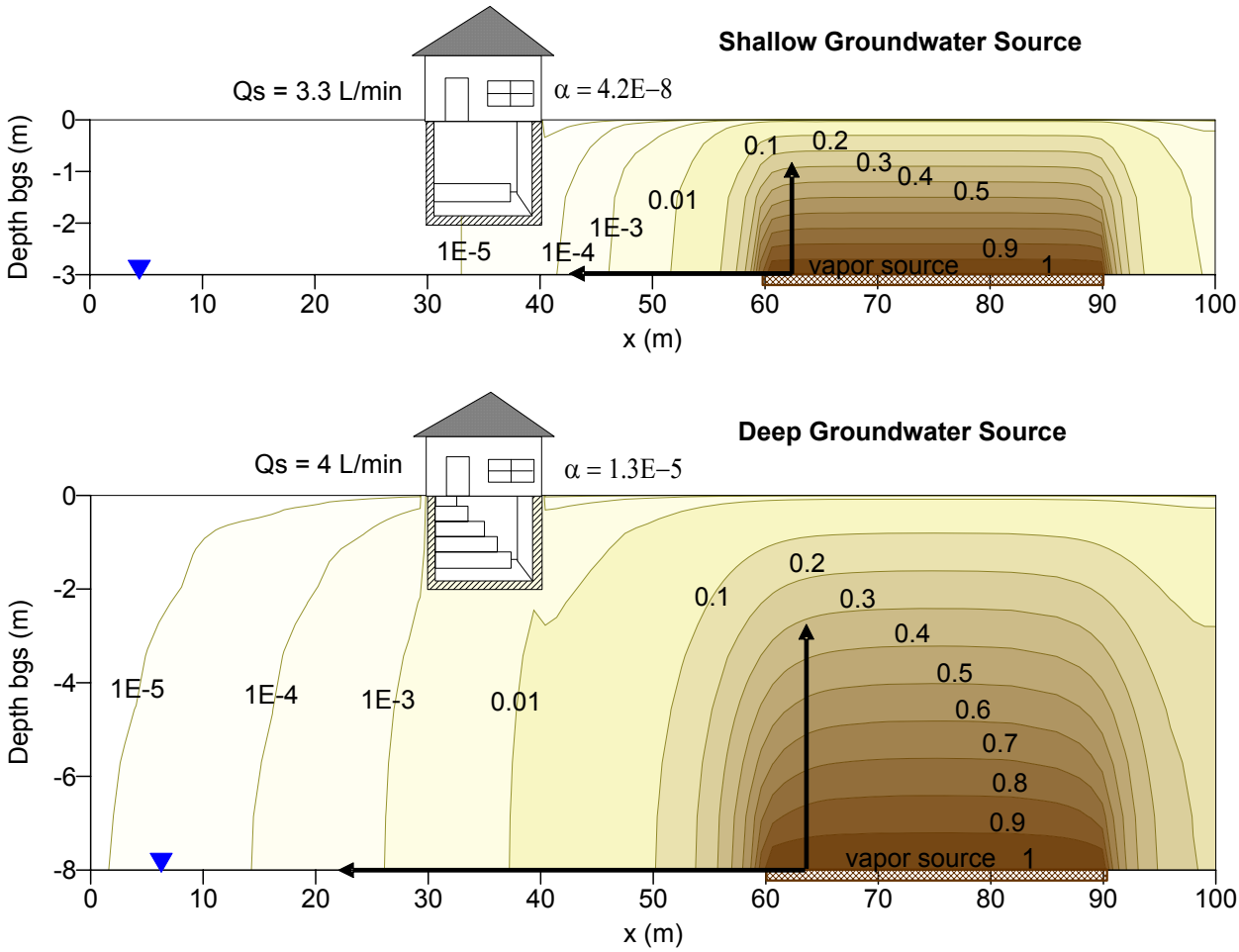

Figure 9. Soil vapor distribution and normalized indoor air concentration (α) for a spatially finite vapor source laterally separated from building at two groundwater depths.

The soil vapor concentration contour lines are normalized by the source vapor concentration. Qs is the soil gas flow rate predicted for building under-pressurized by 5 Pa.

(Abreu, 2005)

If the vapor source is underneath the building, as illustrated in **Figure 10**, the normalized indoor air concentration decreases with increasing source depth, with a difference between the normalized indoor air concentrations of the shallow source (3 m bgs) and the deep source (8 m bgs) of about 40%. Comparison of the normalized indoor air concentrations between Figures 9 and 10 illustrates the effect of source location on the contaminant indoor air concentrations (i.e., comparing a source below the building with a source at 20 m lateral distance from the building, with both sources at the same depth below ground surface). The difference between the normalized indoor air concentrations for the source beneath the building and the source to the side is about two orders of magnitude for the deep source and about five orders of magnitude for the shallow source with an open ground surface.

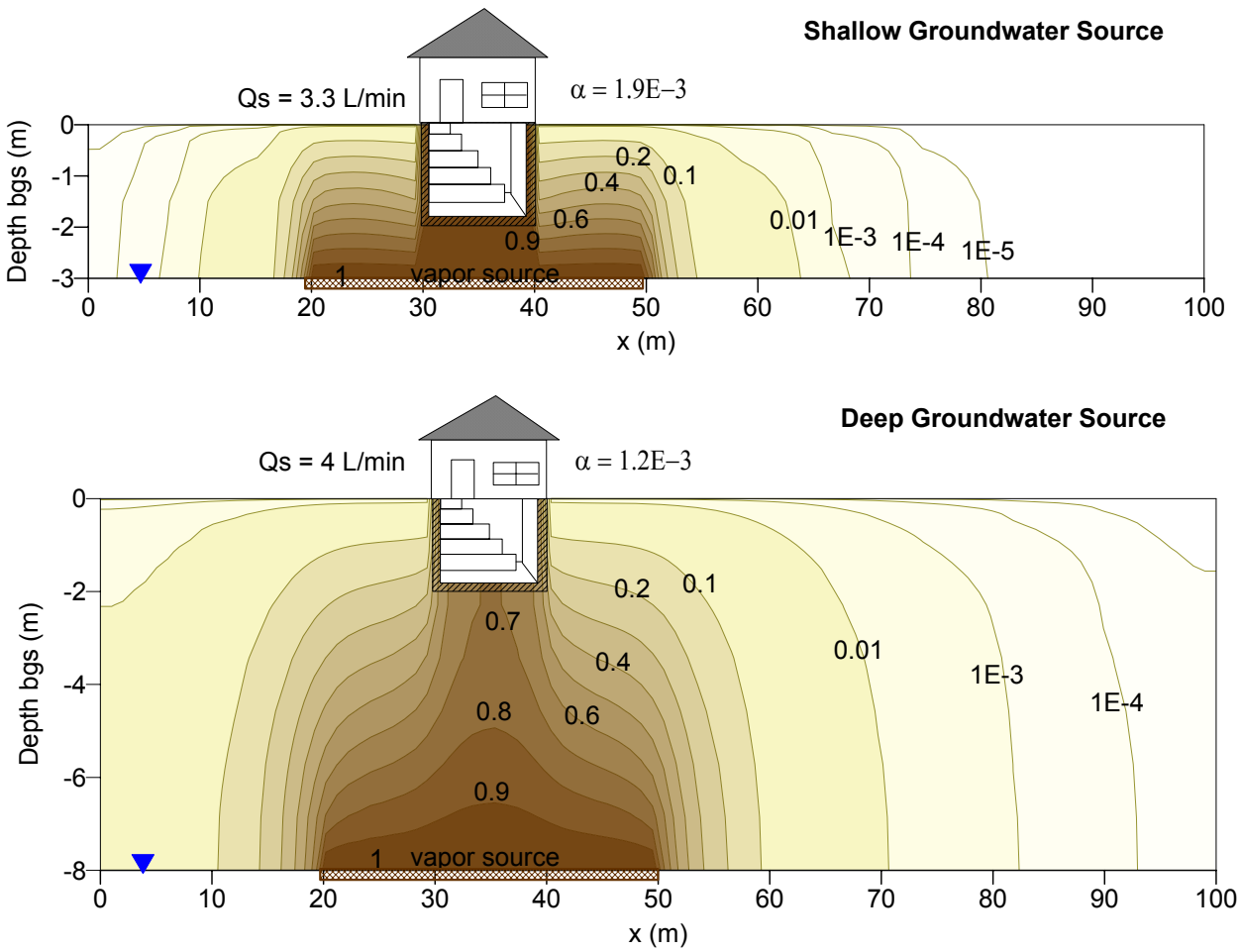

Figure 10. Soil vapor distribution and normalized indoor air concentration (α) for a spatially finite vapor source directly under a building at two groundwater depths.

The soil vapor concentration contour lines are normalized by the source vapor concentration. Qs is the soil gas flow rate predicted for building under-pressurized by 5 Pa.

(Abreu, 2005)

The relationship between the normalized indoor air concentration and the lateral separation between the source and the building is plotted in **Figure 11** (from Abreu and Johnson, 2006) for the basement and slab-on-grade scenarios with the source at two groundwater depths (3 and 8 m bgs). The results show that the dependence of indoor air concentrations on lateral distance between the source and the building is more influenced by the source depth and less influenced by the foundation type (basement, slab-on-grade). With increasing lateral distance from the building, the normalized indoor air concentration decreases more rapidly for shallow sources than for deeper ones. For laterally displaced sources, normalized indoor air concentrations are higher for deeper sources than for shallow ones if the subsurface is homogeneous and open to the atmosphere. These results are in general agreement with the work of Lowell and Eklund (2004).

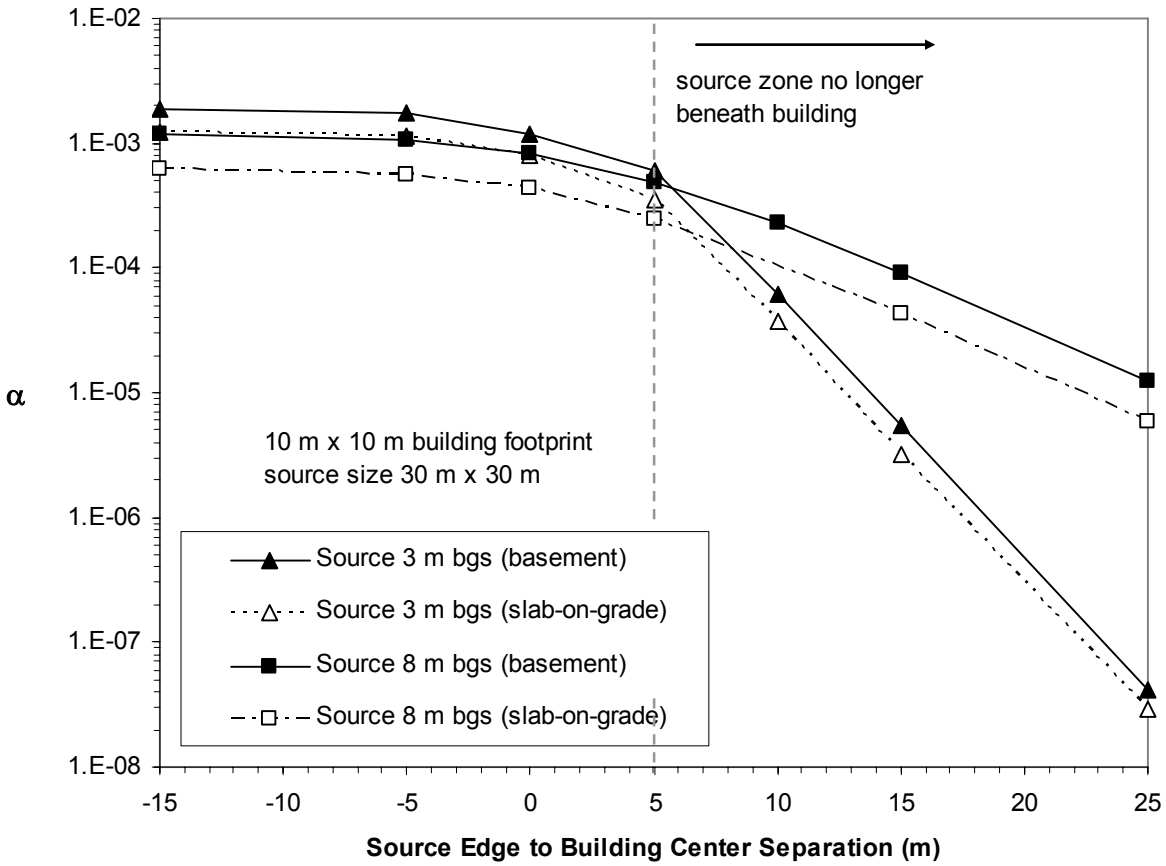

Figure 11. Relationship between source-building lateral separation distance and normalized indoor air concentration (α).

The separation is measured from the edge of the source zone to the center of the building; negative values and values <5 m indicate that the source is to some extent beneath the building.

Basement and slab-on-grade scenarios. Source located at groundwater table at depths 3 m and 8 m bgs. (Abreu and Johnson, 2006)

The results and discussion presented in Figures 9 to 11 are specific to groundwater vapor sources at the top of the capillary fringe and where there is homogeneous sandy soil; variations from these assumptions will affect the results and conclusions. For example, **Figure 12** shows the predicted results for a scenario with a vapor source in the vadose zone and a scenario with a vapor source located at groundwater level. Both sources are at a 20 m lateral distance from the edge of a building, and the groundwater depth is 8 m bgs in both scenarios; the source located in the vadose zone extends from 2 to 3 m bgs. The normalized indoor air concentrations calculated for these scenarios are similar (1.3E-5 and 1.7E-5), although the source at the vadose zone is shallower (2–3 m bgs). The vertical extension of the vadose zone source (1 m) and its distance to the water table (5 m) allowed the vapors to migrate in all directions and not just preferentially upwards. Other scenarios with a layered and heterogeneous subsurface are presented in **Section 4.4**.

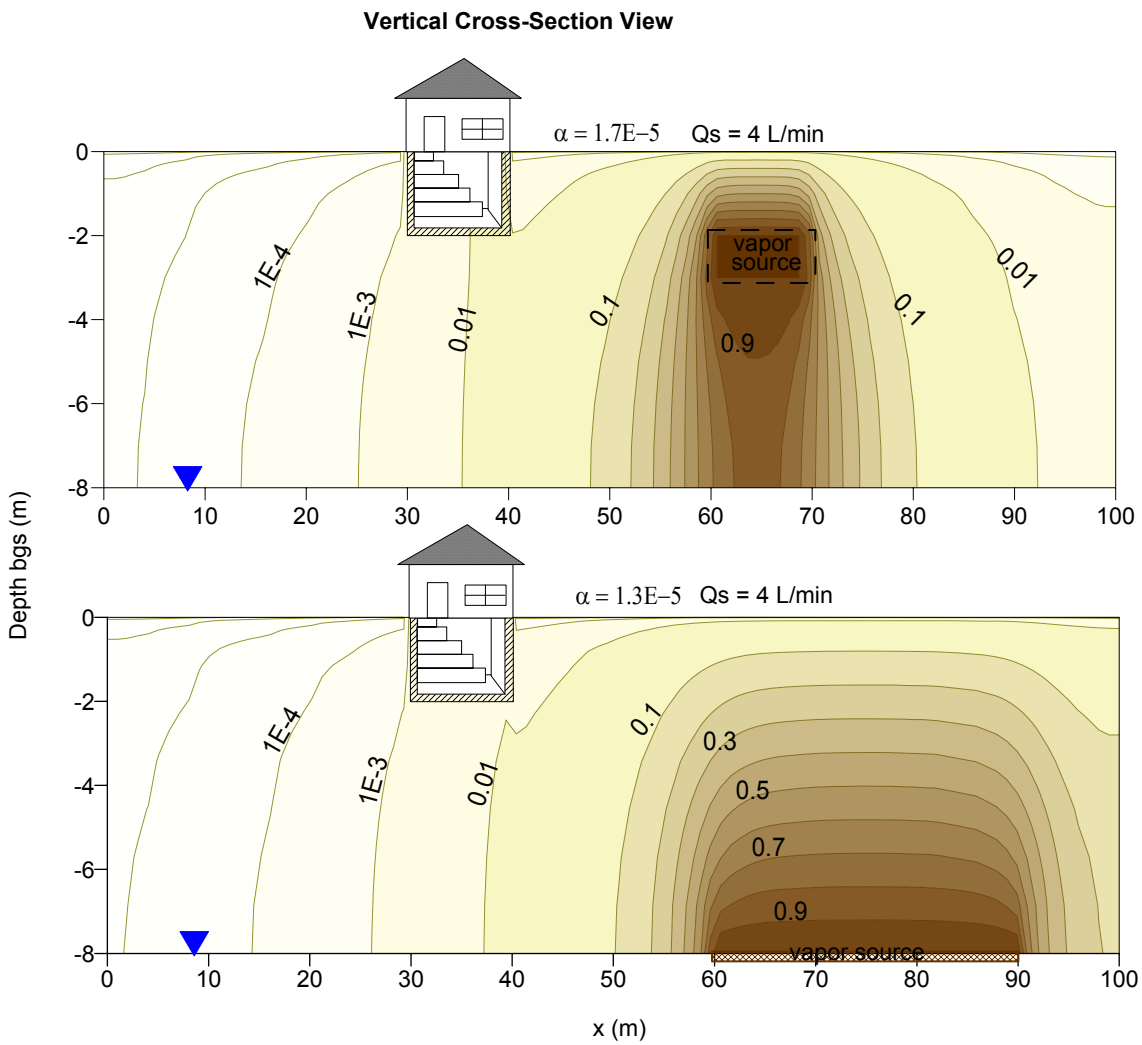

Figure 12. Soil vapor distribution and normalized indoor air concentration (α) for two spatially finite source types (unsaturated soil and groundwater) laterally separated from building.
The soil vapor concentration contour lines are normalized by the source vapor concentration. Qs is the soil gas flow rate predicted for building under-pressurized by 5 Pa. The groundwater table is at 8 m bgs.

4.3 Other Conditions Simulated for Scenarios with Homogeneous Subsurface

This section presents soil vapor concentration profiles from a large vapor source of recalcitrant VOCs that extends beneath two or more buildings and illustrates how a variety of building variables, such as foundation condition or building pressurization, affect the distribution of soil vapor concentration and the indoor air concentration. For many of these simulations, the soil vapor concentration distribution is illustrated as one vertical cross-section through the center of the building and horizontal plan views at two depths.

4.3.1 Multiple Buildings

The figures in this section illustrate that the presence of multiple single-family residences at typical spacing and construction styles may have little or no effect on vapor intrusion when compared with a single-building scenario (compare **Figure 13** through **Figure 15** with **Figure 7b**). They also illustrate the potential capping effect of the foundation slab, resulting in higher concentrations below the building compared with the concentrations at similar depths at exterior locations.

The effect of multiple buildings on the soil vapor concentration distribution and the indoor air concentration for homogeneous subsurface scenarios are illustrated in the next three figures. The vapor source is located at a depth of 8 m bgs and extends beneath each building. **Figure 13** shows two buildings with basements that are 10 m apart, **Figure 14** shows two adjacent buildings with basements, and **Figure 15** shows two adjacent buildings, one with a basement and one with a slab-on-grade foundation. The buildings are all under the baseline conditions reported in **Appendix B** (e.g., constant under-pressurization, air exchange rate, perimeter cracks).

Figures 13 through 15 illustrate that under homogeneous conditions and for under-pressurized buildings, soil vapor concentrations are higher beneath the building footprints than at the same depth in adjacent open areas. These figures show that the presence of multiple buildings has little or no effect on the normalized indoor air concentration (α) for a single building (see Figure 10) if the building conditions are the same, the subsurface is homogeneous, and the source vapor concentration extends evenly beneath each building. The scenario in Figure 15 also illustrates the effect of an impermeable surface adjacent to a building, with the impermeable surface represented by the slab-on-grade foundation slab of the second building. The vapor concentration in the subsurface adjacent to the basement below the impermeable surface is higher than the concentration at a comparable depth below an open-ground surface, which is consistent with scenarios modeled by Pennell et al. (2009). Other conceptual model scenarios are presented in **Section 4.4** to illustrate the effect if the subsurface is heterogeneous, as well as the effect of natural or anthropogenic barriers to contaminant migration.

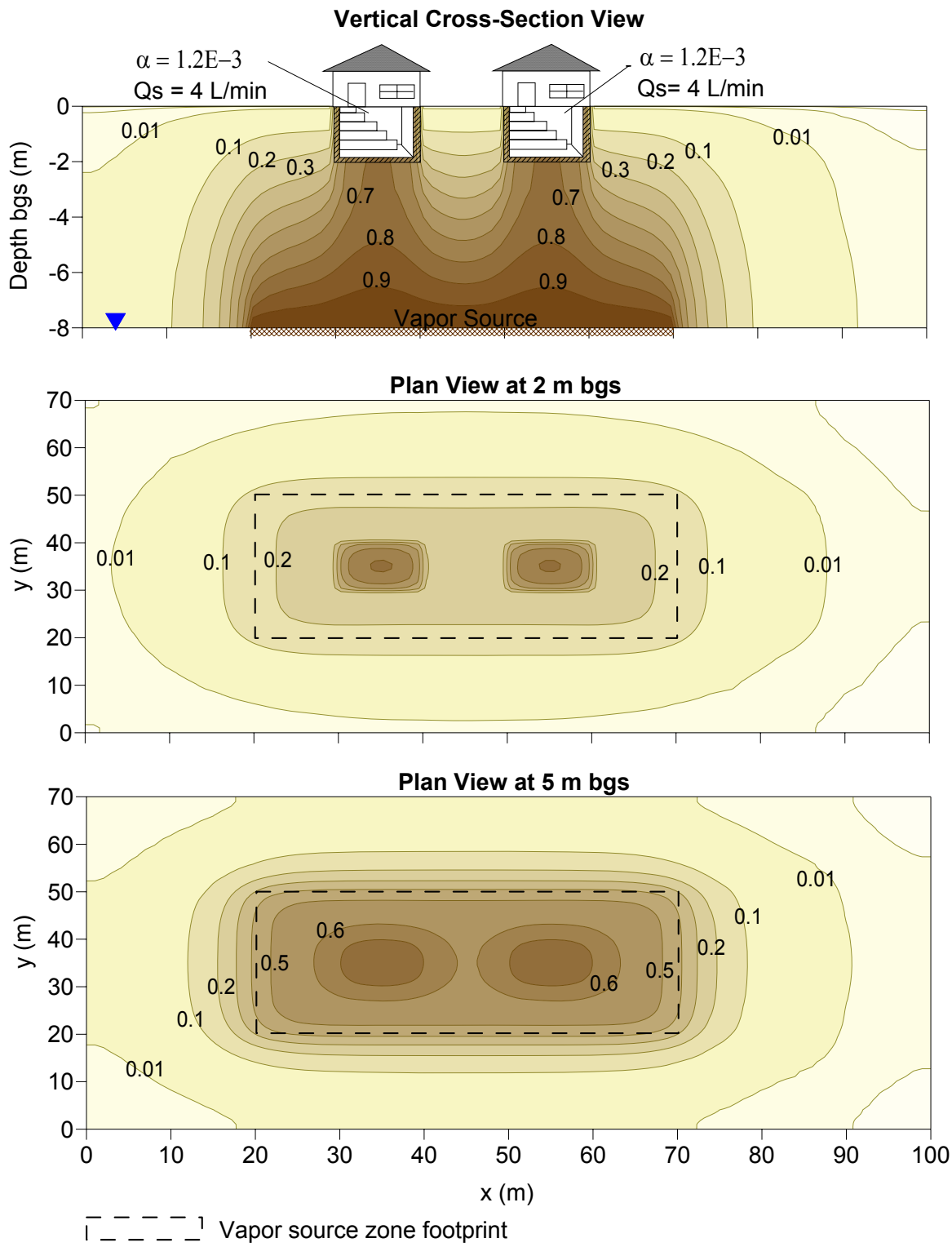

Figure 13. Soil vapor distribution and normalized indoor air concentration (α) for a scenario with two identical buildings separated by 10 m overlying a plume.

The soil vapor concentration contour lines are normalized by the source vapor concentration. The source is at 8 m bgs. Qs is the soil gas flow rate predicted for building under-pressurized by 5 Pa.

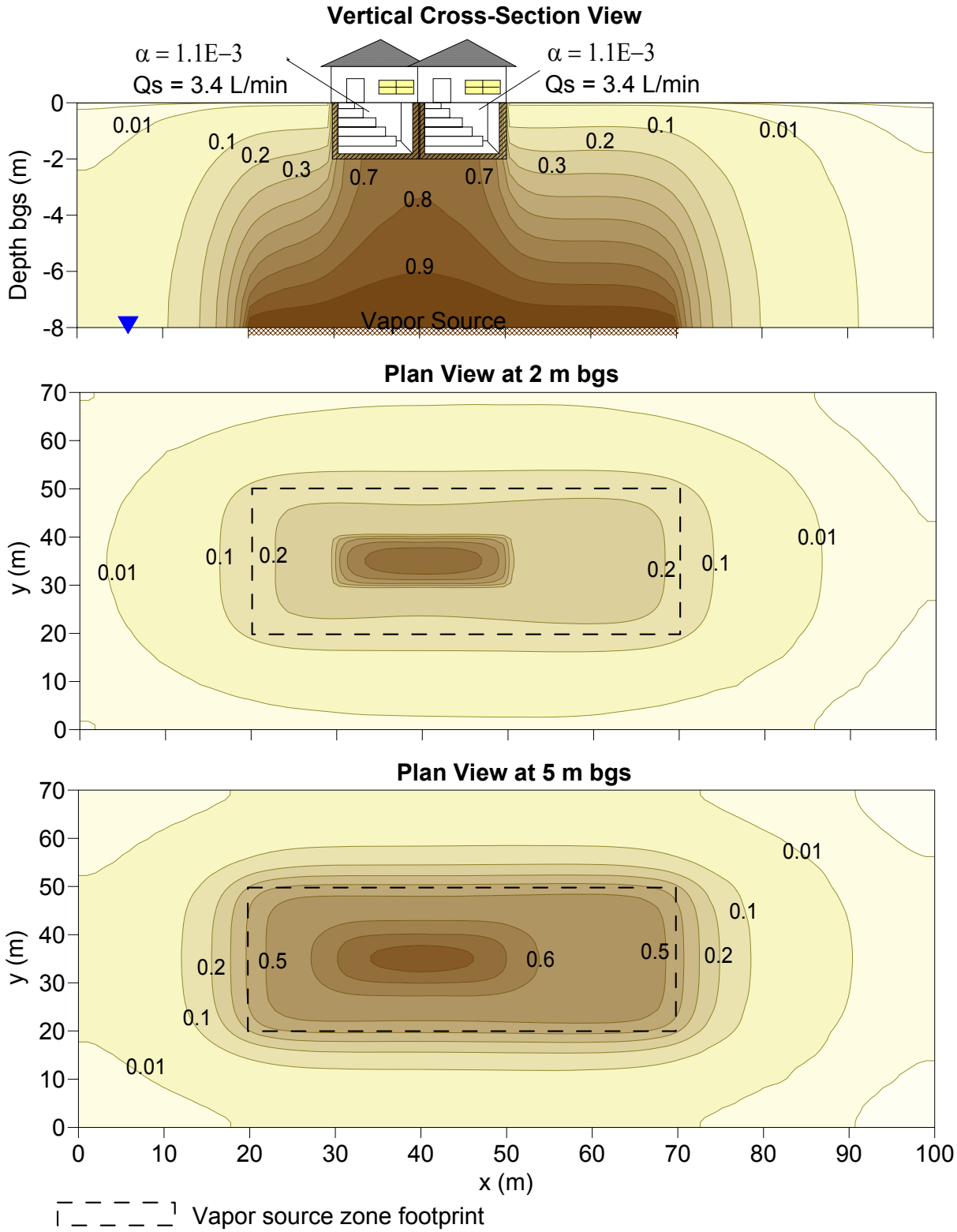

Figure 14. Soil vapor distribution and normalized indoor air concentration (α) for a scenario with two identical adjacent buildings overlying a plume.

The soil vapor concentration contour lines are normalized by the source vapor concentration. The source is at 8 m bgs. Qs is the soil gas flow rate predicted for building under-pressurized by 5 Pa.

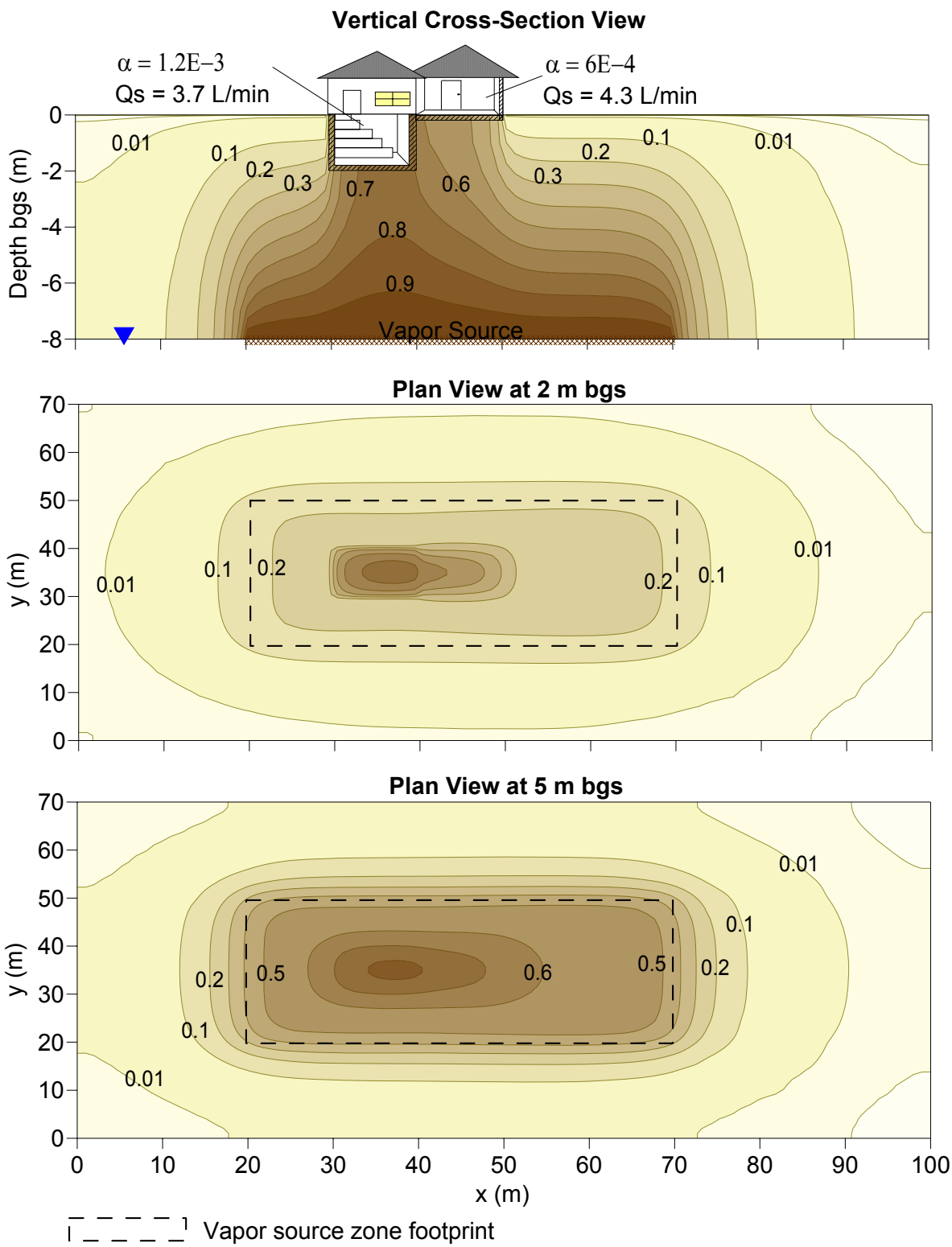

Figure 15. Soil vapor distribution and normalized indoor air concentration (α) for a scenario with two adjacent buildings with different foundation types overlying a plume.

The soil vapor concentration contour lines are normalized by the source vapor concentration. The source is at 8 m bgs. Qs is the soil gas flow rate predicted for building under-pressurized by 5 Pa.

4.3.2 Permeable Fill and Building Pressurization

Figure 16 compares building over-pressurization with building under-pressurization for two adjacent buildings with permeable backfill around the building foundations. With permeable sub-foundation conditions, over-pressurization leads to flow out of the building, lower subslab VOCs, and very low indoor air VOC concentrations, while under-pressurization leads to soil gas flow into the building and elevated subslab and indoor air VOCs.

A common construction practice is to backfill around and beneath a concrete foundation with construction aggregate (various mixtures of gravel and sand). Granular fill may also exist along utility conduits below the floor (e.g., floor drains, sanitary sewer lines, water mains). This can create a region adjacent to the foundation slab and walls that is more permeable than the surrounding native soils. To gain some insight on the possible effect of a more permeable region adjacent to the foundation associated with building pressurization, a simulation was performed assuming two adjacent buildings with a 50 cm thick permeable fill around the foundation slab and walls. The fill was assumed to have a soil gas permeability of 5E-11 m^2 (coarse sand), a total porosity of 0.5 (cm^3_{voids}/cm^3_{soil}), and a moisture content of 0.01 ($cm^3_{water}/cm^3_{voids}$).[2] The native soil properties are for the baseline homogeneous sand presented in **Appendix B**, and the two buildings are under baseline conditions, except that one building is assumed to be under-pressurized by 2 Pa (gauge pressure) and the second building is assumed to be over-pressurized by 2 Pa.

The predicted normalized soil vapor concentration distribution, normalized indoor air concentration (α), and soil gas flow rates (Qs) are presented in **Figure 16**. The predicted soil gas flow rates in and out of the buildings are about +7 L/min and –7 L/min at pressurization of 2 Pa and are higher than the soil gas flow rates predicted for buildings pressurized by 5 Pa without permeable fill (see Figure 5). The normalized indoor air concentrations fall in the same range of values found for the homogenous soil scenario with equivalent soil gas flow rates (see Figure 6). The reduction in indoor air concentration for the over-pressurized building is due to the air flow from indoors to the subsurface. For under-pressurized buildings with a permeable fill, Pennell et al. (2009) reported a similar increasing trend in soil gas flow rates, as well as a decrease in soil gas concentrations immediately near the building foundation.

Figure 16 illustrates that the presence of a permeable fill may increase the dilution of the sub-slab concentration if the air flow reverses direction in and out of the building (assuming that the source of VOCs is in the soil gas and not inside the building). Research is still needed, however, to determine to what extent the presence of granular fill and utility conduits facilitate the flow of air into the subsurface and ultimately, beneath the slab.

[2] Actual drainage layers may have different properties; these conditions were selected for modeling purposes to show the general effect of a layer that is relatively more permeable against the building foundation.

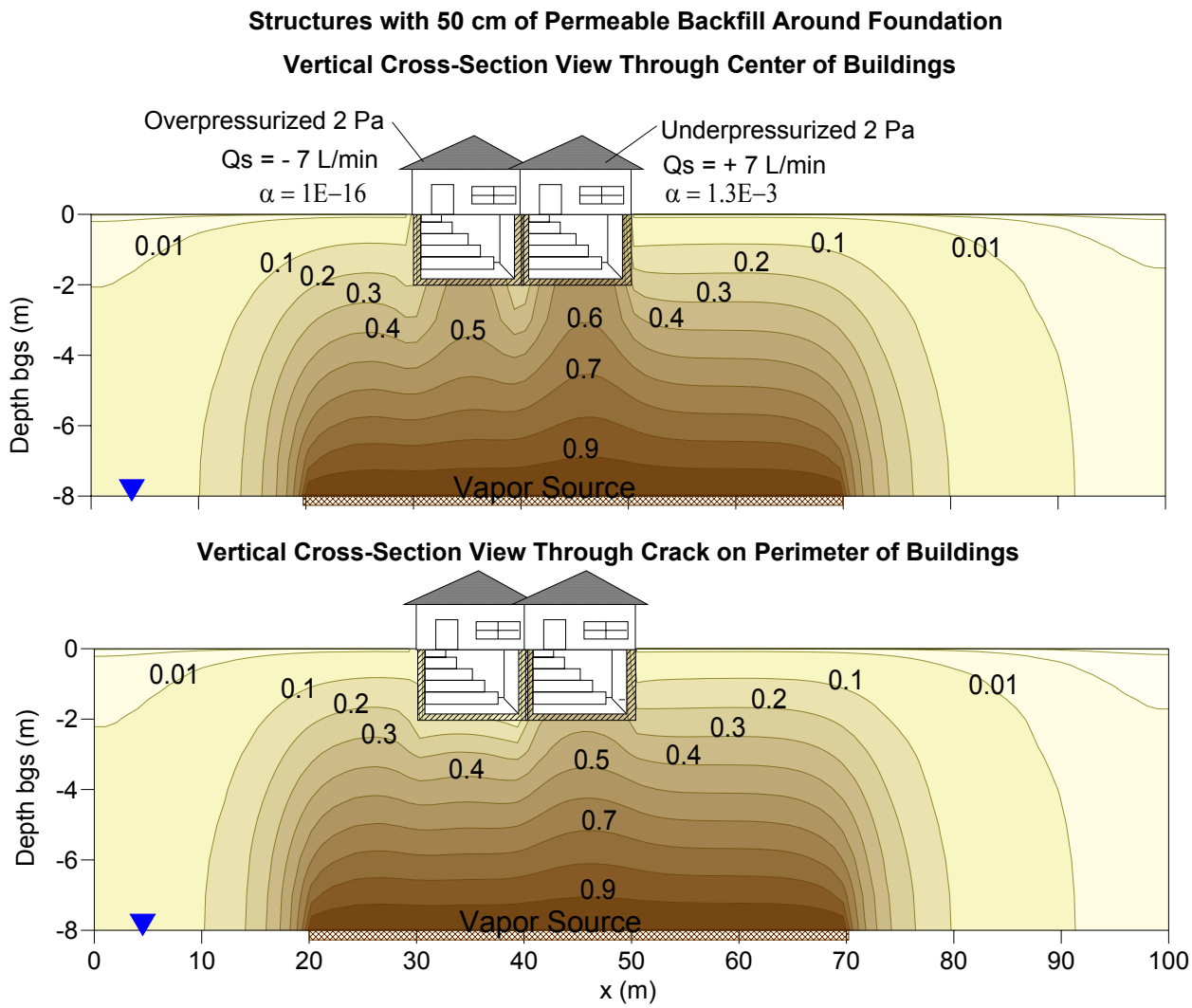

Figure 16. Soil vapor distribution for a scenario with two adjacent buildings under opposite pressurization, and with permeable backfill.

The soil vapor concentration contour lines are normalized by the source vapor concentration. The source is at 8 m bgs. α is the normalized indoor air concentration and Qs is the predicted soil gas flow rate.

4.3.3 Building Conditions

Figure 17 illustrates that building conditions play a major role in determining the degree to which contaminated vapors enter a structure (building pressurization and the nature of foundation cracks) and the degree to which indoor air is mixed with and diluted by outdoor air (building air exchange rate and building size: volume). The depicted scenarios include a building that is perfectly sealed and buildings with a range of under-pressurizations and air exchange rates. The depictions also include differing source conditions.

Most of the simulations presented so far address the effect of subsurface factors and building conditions assuming either one building at the site or the same set of conditions for each building. However, subsurface conditions and the vapor concentration distribution beneath buildings are not the only factors that determine the indoor air concentration due to vapor intrusion. Indoor air concentration is also influenced by building conditions, which may vary from building to building and may also vary seasonally (e.g., building air exchange rates may be higher in summer than in winter; the stack effect may be greater in the winter). Therefore, building conditions may explain some of the variability in indoor air concentrations found between buildings at the same site and may also explain the variability in indoor air concentration for the same building in different seasons (or at different times).

Variability of indoor air concentration between buildings in similar settings may be the result of variability in and interactions among the following building factors:

- Existence and extent of openings or cracks in the foundation
- Building pressurization and resultant soil gas flow rate (Qs) into (under-pressurized) or out of (over-pressurized) the building
- Building air exchange rate (AER), which is the number of times the indoor air is exchanged with outdoor atmospheric air over a specified period of time
- Building air flow rate (Qbdg), which is the rate at which the volume of contaminated indoor air is exchanged with outdoor atmospheric air; this volume is based on the height at which the contaminated indoor air is considered to be fully mixed.

For a given building, AER and Qbdg are not independent of each other, as AER is defined to be the Qbdg divided by the building volume; however, buildings of different size can have identical AERs but different values of Qbdg. In theory, the indoor air concentration is inversely proportional to AER and Qbdg, with indoor air concentration decreasing whenever AER and Qbdg increase (assuming other conditions remain constant). Two buildings at the same site may have the same sub-slab concentrations, the same AER values, but different Qbdg values because of different indoor air volumes; therefore, their normalized indoor air concentrations (α) may be different, as illustrated in the scenarios below.

Variations in the building pressurization and resulting Qs were discussed in previous sections (**Sections 3.2**), assuming that AER and Qbdg were constant. This section presents simulations that address the variability in AER and Qbdg between buildings, as well as the incomplete pathway case (i.e., no soil gas entry points or cracks in the foundation). **Figure 17** presents the conceptual models, based on specific scenarios and conditions simulated, and shows the

predicted normalized soil vapor concentration distribution and indoor air concentrations for three slab-on-grade buildings under several building conditions and source scenarios:

- **Building A** has no openings or cracks and the foundation is perfectly sealed; therefore, the vapor intrusion pathway for this building is incomplete and there is no indoor air contamination due to vapor intrusion. This example emphasizes the importance of building conditions, but it should be noted that this theoretical assumption is unlikely to be found under actual site conditions, because foundations may "leak" to some extent, as most foundations have some openings that will be conduits to soil gas flow and diffusive transport.
- **Buildings B** and **C** have full-length perimeter cracks in the foundation, are constantly under-pressurized, and have different AERs. The vapor intrusion pathway for these buildings is complete.
- In Scenario 1, the vapor source is large and extends beneath the three buildings; in Scenarios 2 and 3, a finite source extends below only Building A. Building B is 5 m away from the source edge, and Building C is 25 m away from the source edge.

The building conditions for each scenario are presented in Figure 17, from which we note the following:

- In Scenarios 1, 2 and 3, Building A has no indoor air contamination ($\alpha = 0$) because the foundation is perfectly sealed; therefore, the subsurface vapors do not intrude into the building regardless of the subsurface vapor concentration. As discussed above, a perfectly sealed foundation is very unlikely to be found under actual site conditions but is included here to illustrate the magnitude of change from sealed to cracked condition.
- In Scenario 1, Buildings B and C have similar vapor concentrations beneath the slab and the same derived soil gas flow rates (Qs), but the normalized indoor air concentrations (α) differ by about a factor of four. The difference in indoor air concentrations results from a lower assumed AER and Qbdg for Building B, resulting in less dilution of the contaminants in indoor air resulting from vapor intrusion.
- In Scenario 2, Buildings B and C have similar indoor air concentrations (α), although the concentration beneath Building C is about two orders of magnitude lower than the concentration beneath Building B. The similarity in indoor air concentrations results from the higher pressure differential (i.e., a higher Qs) and the lower AER and lower Qbdg values assumed for Building C.
- In Scenarios 2 and 3, the normalized indoor air concentrations for Building B differ by about one order of magnitude, although the buildings have similar vapor concentrations beneath the slab. The difference in indoor air concentrations is due to the combinations of Qs, AER, and Qbdg values, which result in greater vapor intrusion and less dilution of indoor air for Building B in Scenario 3.
- In all scenarios, there is spatial variability of the vapor concentration distribution below the slab for the three buildings.

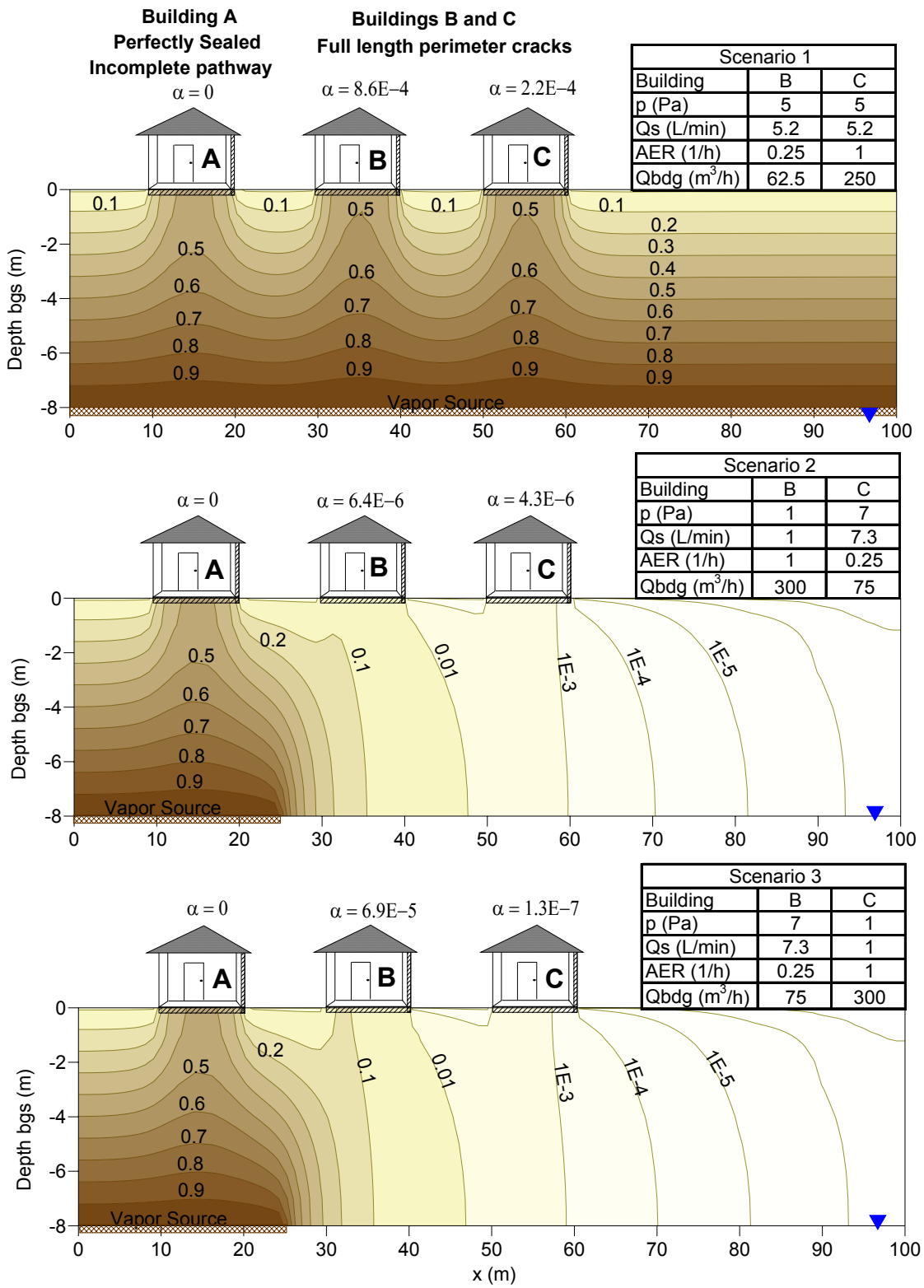

Figure 17. Normalized indoor air concentration (α) for different combinations of building conditions (e.g., pressurization, AER) and sub-slab vapor concentration.

The soil vapor concentration contour lines are normalized by the source vapor concentration. The source is at 8 m bgs. Qs is the soil gas flow rate predicted for building pressurization (p), AER is building air exchange rate, and Qbdg is building air flow rate.

4.3.4 Multiple Sources

Figure 18 illustrates that multiple sources will produce contaminant distribution patterns that differ from those associated with a single source. Thus, if field evidence indicates that soil gas concentrations increase with distance from the presumed source, the presence of an additional source should be considered.

As previously illustrated, the soil vapor concentration tends to decrease as the distance from the source increases, and it should not be higher than the concentration at the source. If the vapor concentration at a sampling point away from the source is higher than the concentration at the source, and assuming there is no bias in the sampling technique, this may indicate the existence of other sources that were not previously identified, or that the size, location, and strength of the identified source may not have been well characterized. An example of a concentration distribution for a site with multiple sources is presented in **Figure 18**, which illustrates a site with two buildings (basement and slab-on-grade) and two vapor sources: a groundwater source near the building with a basement and another source at the vadose zone closer to the slab-on-grade building. Both sources are recalcitrant VOCs and have the same vapor concentration of 10,000 $\mu g/m^3$, both buildings have the same characteristics (e.g., size, AER, cracks), and the subsurface is homogeneous. Although the slab-on-grade structure is located 30 m away from the groundwater source, its indoor air concentration is higher than the indoor air concentration in the building with a basement located only 10 m from the groundwater source, because of vapor intrusion from the vadose zone source adjacent to the slab-on-grade building.

Characterization of the source concentration distribution and multiple source locations is key to understanding contaminant distributions and identifying buildings with higher vapor intrusion risks.

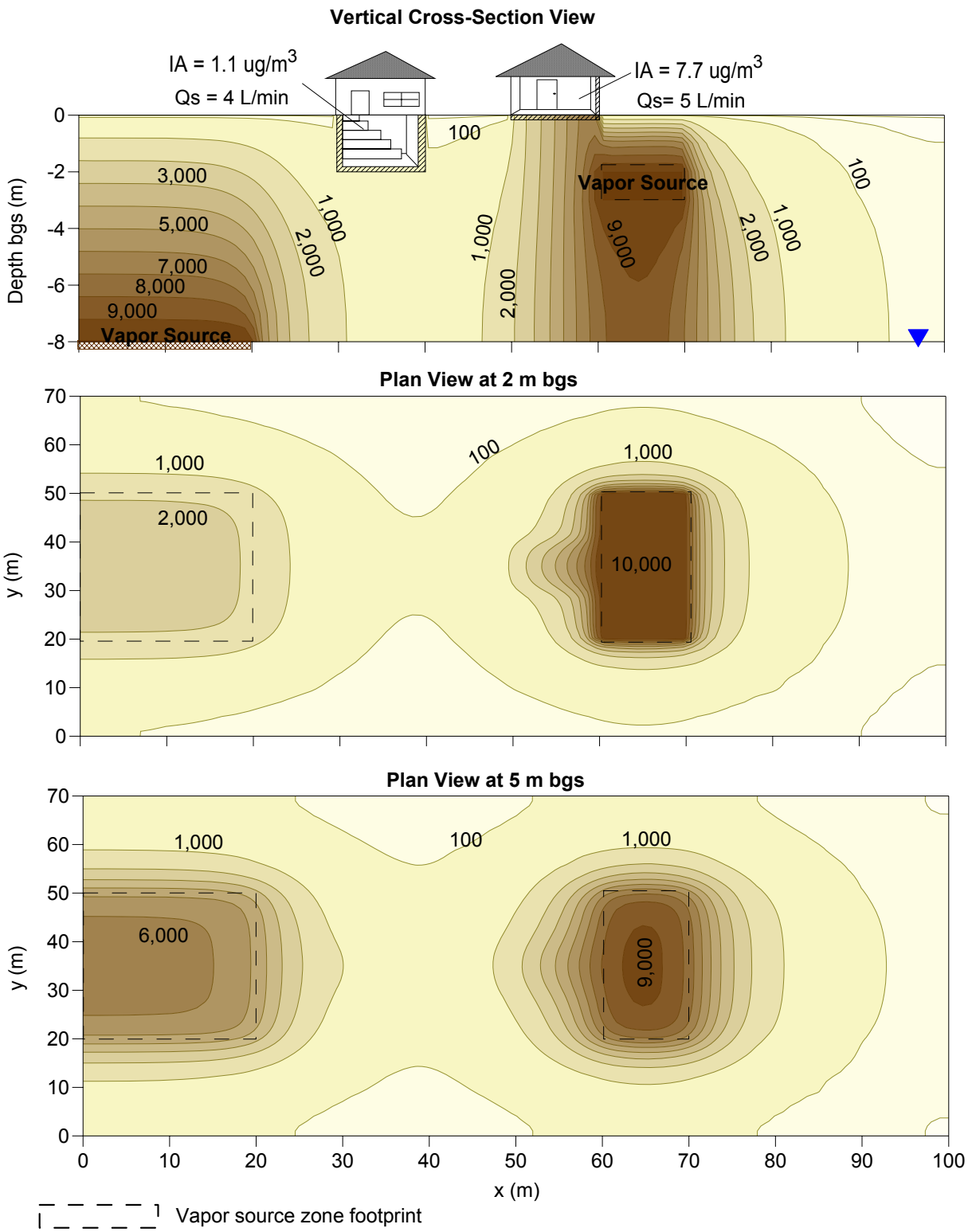

Figure 18. Soil vapor distribution and indoor air (IA) concentration for a scenario with two buildings and two vapor sources.

Concentrations are in units of $\mu g/m^3$. Qs is the soil gas flow rate predicted for building under-pressurized by 5 Pa.

4.4 Subsurface Heterogeneities and Ground Cover

Most simulations in this document model an open ground surface and homogeneous, low moisture content sandy soils with uniform transport properties in all directions. In reality, soils are rarely (if ever) homogeneous and are often horizontally layered, and these layers can be discontinuous and have different moisture conditions depending on how fine grained they are (e.g., silts and clays hold more moisture than sand and gravel). This has particular importance for vapor intrusion, because upward and lateral soil vapor migration may be limited by layers with higher moisture content. In addition, the ground surface may not be open to vapor transport where there are other buildings or impermeable covers.

The scenarios presented in this section assume several different configurations that combine the effects of a layered or heterogeneous subsurface with single or multiple buildings and open ground or impermeable ground cover.

4.4.1 Moisture Content in Layered Soils

The figures in this section use a single-building scenario to illustrate how non-homogeneous soils (i.e., soils with layers of higher and lower moisture and associated soil gas permeability, which varies inversely with soil moisture) can impact the pressure field distribution, soil gas flow patterns, and VOC concentrations in soil gas in the vicinity of a building. The impact of the layers depends on their location relative to the source and the building foundation. The locations of the soil layers are depicted in **Figure 19a**. The effects of those soil layer geometries on under-pressurized buildings are depicted in **Figure 19b**. The effects of those soil layer geometries on over-pressurized buildings are depicted in **Figure 19c**.

As discussed previously, the moisture content of the soil affects vapor transport by diffusion and may also affect advective transport, because higher moisture content decreases soil gas permeability. The simulations in this section illustrate how moisture content distribution in layered soils can affect vapor concentrations in soil gas for a simplified scenario of a single building with laterally continuous soil layers and a uniform groundwater vapor source directly beneath the building. The conceptual model scenarios are illustrated in **Figure 19a**. Scenario A is homogeneous sandy soil at baseline conditions, used for comparison. Scenario B includes four layers, with two layers of higher moisture content beneath the foundation. Scenario C includes six layers, with two layers of higher moisture content beneath the foundation and a third layer at the ground surface. Scenario D includes two soil layers, with the higher moisture content layer at ground surface. The layers with higher moisture content have a saturation (S) of 60% (percentage of water in soil pores relative to total pore space) and a soil gas permeability (K_g) of 1E-13 m^2. The layers with lower moisture content have an S of 20% and a K_g of 1E-11 m^2 (i.e., the baseline soil condition). Note that the impact of even higher moisture content (and lower permeability) layers (i.e., geologic barriers modeled assuming 95% saturation) is discussed in **Section 4.4.4**.

The simulations were performed for under- and over-pressurized buildings to evaluate the predicted effect of steady air flow into and out of the building. The predicted soil gas pressure field, the induced soil gas flow rate (Qs), and the predicted normalized indoor air concentration (α) and normalized soil vapor concentration distribution are presented in **Figures 19b** and **19c**.

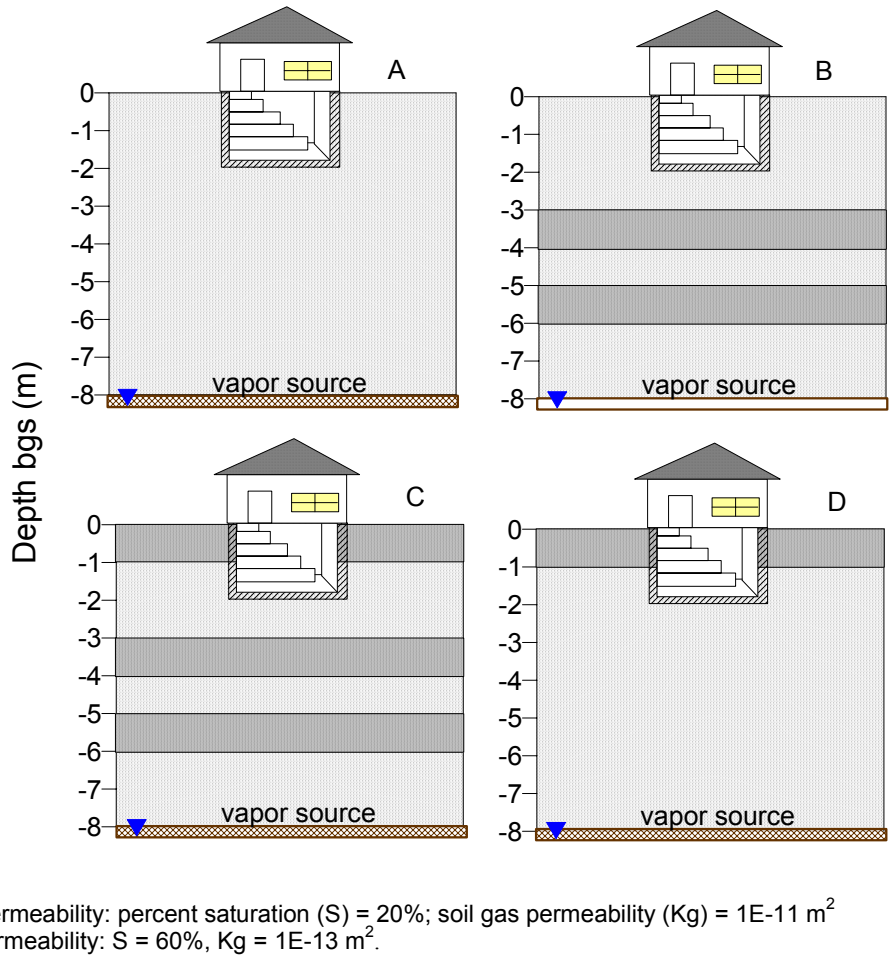

Figure 19a. Full view of the soil layers used in the simulations presented in Figures 19b and 19c.

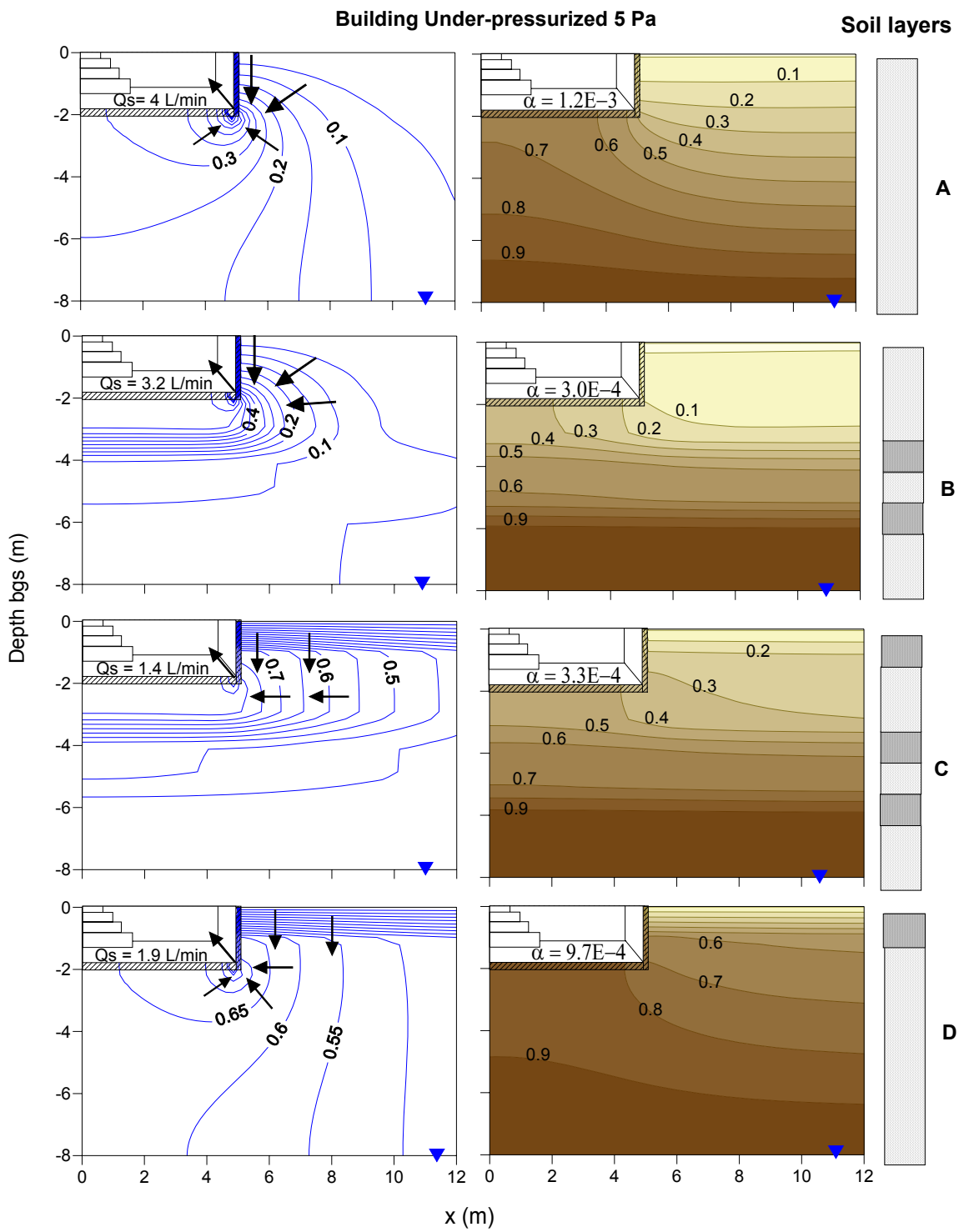

High permeability: percent saturation (S) = 20%; soil gas permeability (Kg) = 1E-11 m^2
Low permeability: S = 60%, Kg = 1E-13 m^2
The arrows indicate soil gas flow direction.

Figure 19b. Effect of soil layers (Figure 19a) on pressure field, soil vapor distribution, and normalized indoor air concentration (α) for building under-pressurized by 5 Pa.

The soil gas gauge pressure contour lines are normalized by indoor air gauge pressure. Qs is the predicted soil gas flow rate. The soil vapor concentration contour lines are normalized by the source vapor concentration. The source is at 8 m bgs.

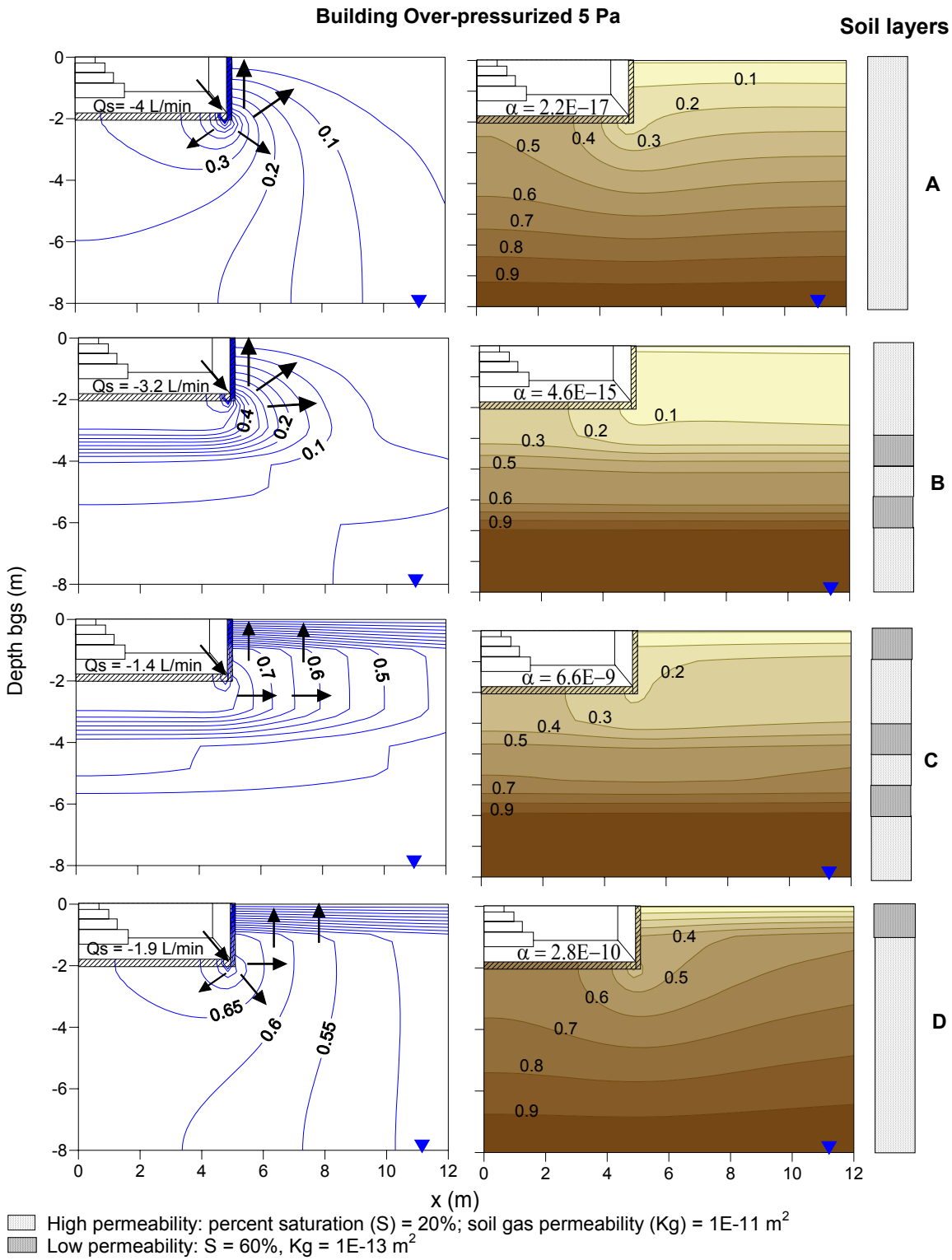

Figure 19c. Effect of soil layers (Figure 19a) on pressure field, soil vapor distribution, and normalized indoor air concentration (α) for buildings over-pressurized by 5 Pa.

The soil gas gauge pressure contour lines are normalized by indoor air gauge pressure. Qs is the predicted soil gas flow rate. The soil vapor concentration contour lines are normalized by the source vapor concentration. The source is at 8 m bgs.

The presence and position of different soil layers can affect the subsurface pressure field and the soil vapor concentration distribution. The pressure profiles presented in Figures 19b and 19c show how the position of layers with higher moisture content and lower gas permeability influence soil gas flow. Relative to Scenario A (homogeneous lower moisture content case), the soil gas flow rate (Qs) is reduced by more than 50% in the scenarios with a high moisture content layer on the ground surface (Scenarios C and D). In Scenario B, the higher moisture content layers below the building reduce the soil gas flow rate (Qs) by 20% relative to Scenario A. In general, the soil moisture condition close to the building affects the air permeability and flow; as the soil moisture content increases, the predicted flow of soil gas (into and out of the building) decreases.

The soil vapor concentration profiles presented in Figures 19b and 19c show that if the layers with higher moisture content are between the source and the foundation, then contaminant migration toward the foundation is reduced, the foundation has less influence on the concentration profile, and the sub-slab soil vapor concentration is lower compared with the homogeneous scenario. In the scenarios with high soil moisture content near the ground surface, the migration of contaminant vapors from soils to the atmosphere is reduced, resulting in higher soil vapor concentrations near the surface and beside the foundation wall. For Scenarios B and C with steady building under-pressurization (Figure 19b), the normalized indoor air concentrations (α) are similar (3.0E-4 and 3.3E-4, respectively) because the higher soil gas flow rate (Qs) in Scenario B is offset by the lower soil gas concentration near the crack. In these scenarios, the layered soils with higher moisture content layers between the source and the foundation reduced the normalized indoor air concentrations by about a factor of four compared with the homogeneous Scenario A, with a normalized indoor air concentration of 1.2E-3. Although Scenario D has a higher vapor concentration around the foundation, the normalized indoor air concentration for this scenario (9.7E-4) is about 20% less than the normalized indoor air concentration for the homogeneous scenario (Scenario A). The reduced soil gas flow rate (Qs) under the conditions simulated in Scenario D (due to higher moisture content layer on the ground surface) reduces vapor emissions into the building.

For the scenarios with steady building over-pressurization (Figure 19c), the normalized indoor air concentrations are several orders of magnitude smaller than the ones predicted for a steady under-pressurized building (Figure 19b).

4.4.2 Lower Moisture Content Below the Building

The simulations in this section further illustrate how nonhomogeneous soil conditions can impact the soil gas flow into the building and VOC concentrations in soil gas in the vicinity of a building and in the indoor air. These simulations expand on the concepts in Section 4.4.1 by varying the moisture content, and thus soil gas permeability, laterally as well as vertically. They simulate conditions that might be encountered when the presence of the building results in reduced soil moisture immediately beneath it. The impact of the layers depends on their location relative to the source and the foundation (**Figures 20a** through **d**).

The simulations in this section illustrate conditions where moisture content is lower below the building than in the subsurface beside the building (Tillman and Weaver, 2007) or lower than in the layer on top of the source. The conceptual model scenarios illustrated in **Figure 20** represent a single building with a finite vapor source directly under the building at a groundwater level of 8 m bgs. The building is at baseline conditions (under-pressurized by 5 Pa, perimeter crack). Scenario A is the homogeneous baseline soil condition, used for comparison. In Scenario B, the pore water saturation (S) is 15% below the building and 40% in the subsurface next to the building. In Scenario C, S is 60% in a 3 m thick layer directly above the vapor source and 20% in the overlaying subsurface. Scenario D is a combination of Scenarios B and C. The permeability is not uniform and decreases with increasing moisture content in these simulations, as noted in the legend beneath each figure.

The normalized soil vapor concentration distribution, the soil gas flow rates (Qs), and the normalized indoor air concentration (α) for each scenario are presented in Figure 20. In Scenario B, the higher moisture content next to the building creates a barrier to vapor transport toward the ground, slightly increasing the vapor concentration below the building compared with the homogeneous scenario (Scenario A). The predicted soil gas flow rate (Qs) and the normalized indoor air concentration (α) in Scenario B are about 30% lower than those in Scenario A. In Scenario C, the higher moisture content layer right on top of the vapor source decreases the concentration of vapors below the building and the normalized indoor air concentration by about a factor of five compared with the ones in Scenario A. In Scenario D, the higher moisture content next to the building slightly changes the results from Scenario C, with Qs decreasing by 30%, the normalized soil vapor concentration increasing by a factor of two, and a similar normalized indoor air concentration. For the conditions simulated, higher moisture content on top of the vapor source affects the soil vapor concentration distribution and the indoor air concentrations more than higher moisture conditions next to the building do.

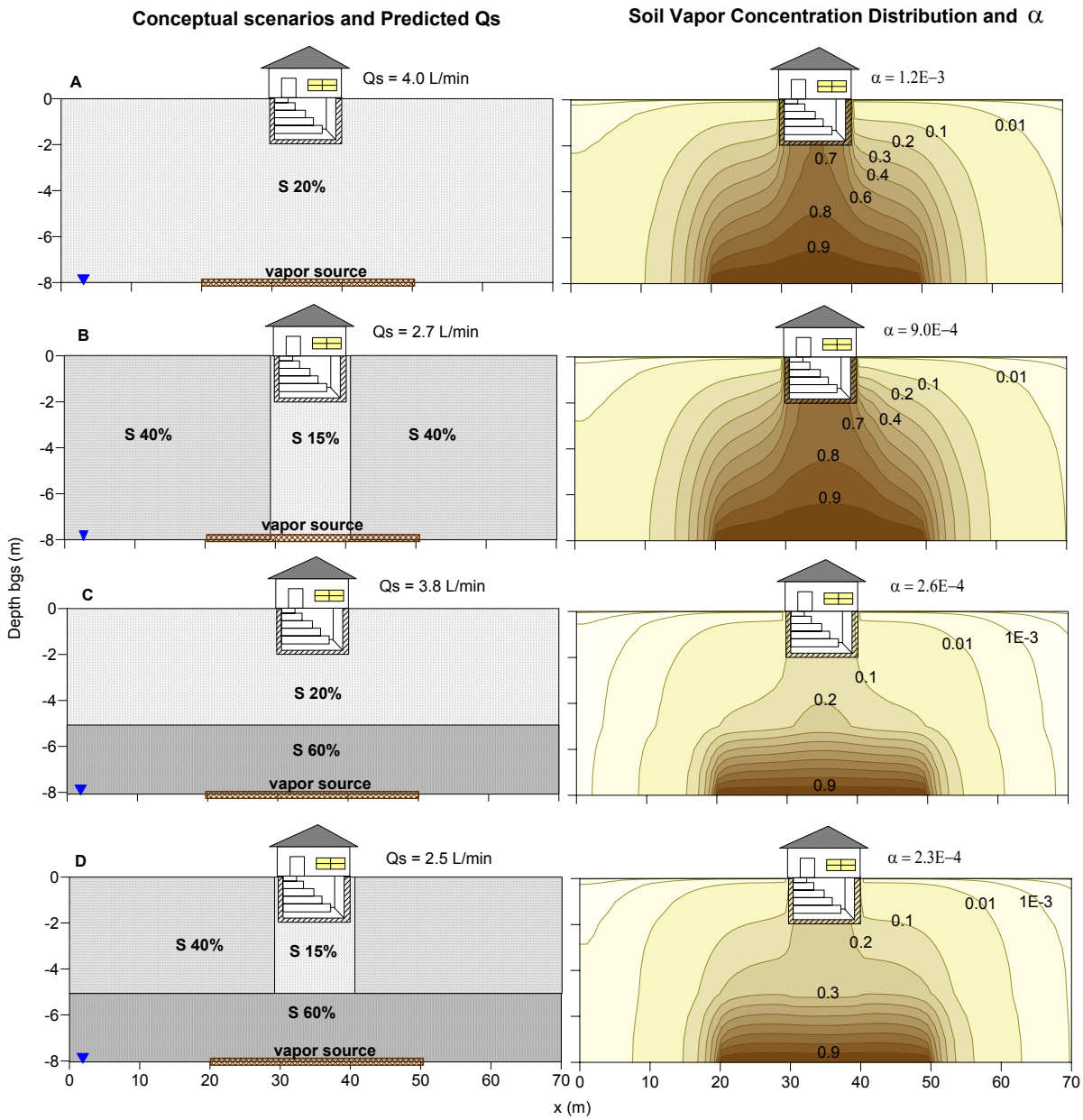

S = Percent saturation (percentage of soil pores filled with water)
For S = 15% and 20%, gas permeability (Kg) = 1E-11 m^2; for S = 40% and 60%, Kg = 1E-13 m^2.

Figure 20. Soil vapor distribution and normalized indoor air concentration (α) for scenarios with different soil moisture content in the subsurface and below building.

The soil vapor concentration contour lines are normalized by the source vapor concentration. The source is at 8 m bgs. Qs is the soil gas flow rate predicted for building under-pressurized by 5 Pa.

4.4.3 Heterogeneous Subsurface, Finite Sources, and Ground Cover

The simulations in this section further illustrate how non-homogeneous soil conditions can impact the soil gas flow into the building and VOC concentrations in soil gas in the vicinity of a building and in the indoor air. These simulations expand on the concepts in **Sections 4.4.1** and **4.4.2** by depicting a broad range of soil moisture distributions, source depths and locations, and ground cover scenarios for the same building conditions at scenarios with single or multiple buildings (with basement or slab-on-grade foundations). The simulations illustrate how high moisture content layers & impermeable ground cover can influence vapor intrusion differently for shallow (**Figures 21a** and **b**), and deep (**Figures 22a** and **b**) water table sources where the building is laterally separated from a finite source. They also depict the influence of discontinuous layers in settings where multiple buildings overlie a finite water table vapor source (**Figures 23a** and **b**) and where the source is laterally offset from one or more buildings (**Figures 24a** and **b**). The simulations illustrate that the indoor air concentrations can vary by many orders of magnitude depending on the configuration of the layers, the buildings, and the source.

This section presents a variety of scenarios with single or multiple buildings, finite sources, continuous or discontinuous soil layers, and an impermeable cover on the ground surface. The set of scenarios presented illustrates the effect of layers on the lateral migration for scenarios with a single building and the effect of heterogeneous conditions for scenarios with multiple buildings. These scenarios may help illustrate the spatial variability in the sub-slab concentration of the same building or between buildings at the same site. Note that the impermeability to vapor flow through a ground cover is a theoretical assumption intended to represent a very low permeability layer, such as a concrete pad; at actual sites, the permeability of such a barrier to vapor flow can be much higher due to cracks and other imperfections.

Figure 21a presents a set of simplified model scenarios that illustrate the effect of laterally continuous layers, impermeable ground cover for shallow groundwater (3 m bgs), and a finite vapor source located at a lateral distance of 20 m from a building. Scenario A is the homogeneous baseline soil condition, used for comparison. In Scenario B, a layer of higher moisture content (1 m thick) is on top of the vapor source at groundwater level (3 m depth). In Scenario C, a layer of higher moisture content is at the ground surface. In Scenario D, there is an impermeable cover at the ground surface extending from the building and partially over the source. **Figure 21b** presents the predicted normalized soil vapor concentration distribution, soil gas flow rate (Qs), and the indoor air concentration for the scenarios described in Figure 21a. In Scenario B, the high moisture content layer on top of the source reduces the vapor concentrations in the subsurface close to the building and in the indoor air by about two orders of magnitude compared with the homogeneous scenario (Scenario A). In Scenario C, the high moisture content layer on the ground surface promotes the migration of vapors to further lateral distances and increases the vapor concentrations in the subsurface and in the indoor air by about two orders of magnitude compared with Scenario A. Likewise, the impermeable surface in Scenario D increases the lateral migration of vapors and increases the vapor concentrations close to the building and in the indoor air by about three orders of magnitude compared with Scenario A. Also of note are the differences in concentration beneath the slab; for example, in each scenario, the sub-slab soil gas concentration declines by about an order of magnitude from one side of the building to the other.

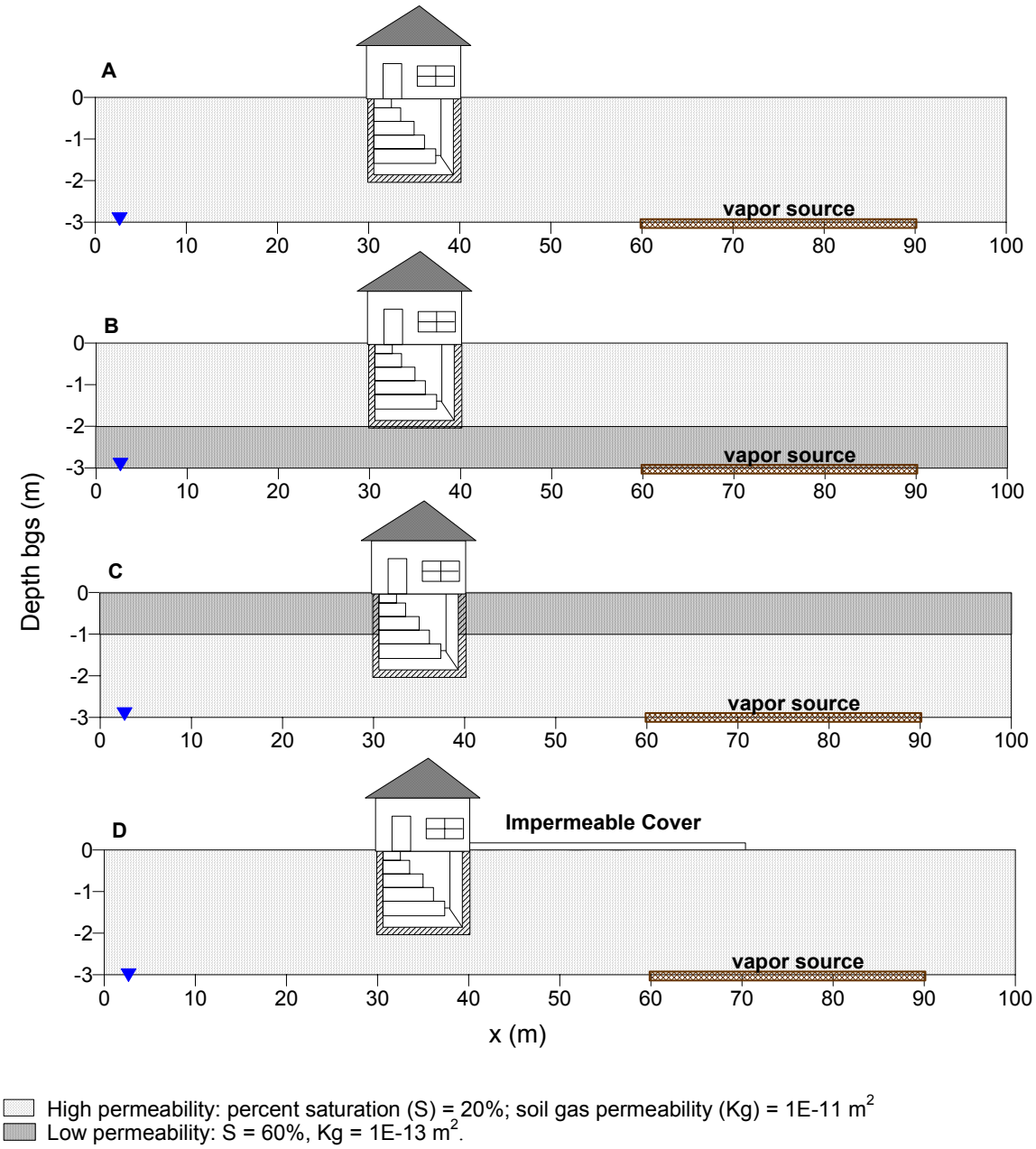

Figure 21a. Soil layers and ground cover scenarios used in the simulations presented in Figure 21b with a shallow laterally separated vapor source.

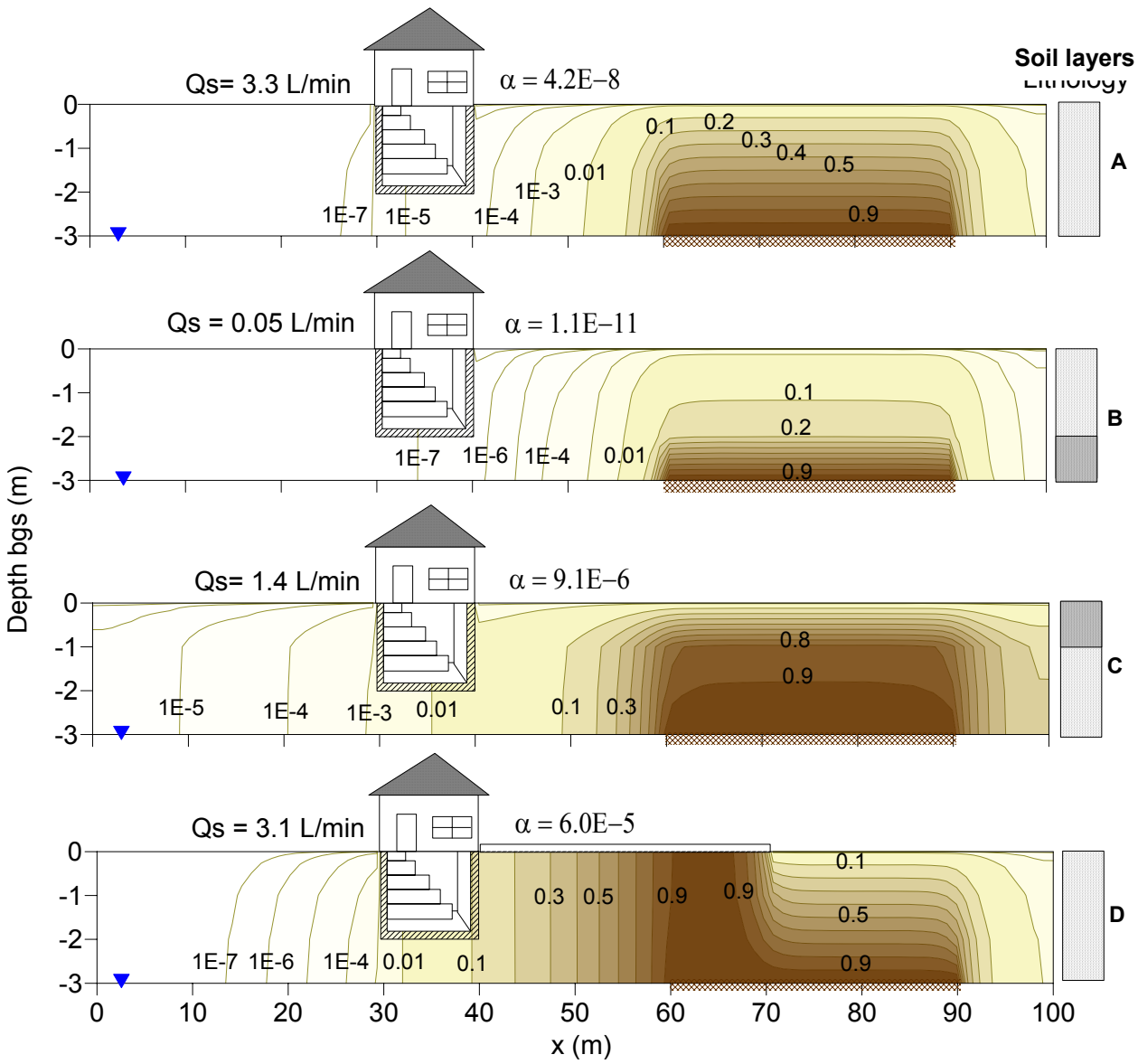

Figure 21b. Effect of soil layers and ground covers (Figure 21a) on soil vapor distribution and normalized indoor air concentration (α) for a shallow laterally separated vapor source.
The soil vapor concentration contour lines are normalized by the source vapor concentration. The source is at 3 m bgs. Qs is the soil gas flow rate predicted for building under-pressurized by 5 Pa.

Figure 22a presents a set of conceptual model scenarios that illustrate the effect of continuous layers for deep groundwater (8 m bgs) and a finite vapor source located at a lateral distance of 20 m from a building. Scenario A is the homogeneous baseline soil condition, used for comparison. In Scenario B, a layer of higher moisture content (3 m thick) is on top of the vapor source at groundwater level. In Scenario C, a 2 m thick layer of higher moisture content extends from depths of 3 to 5 m bgs between the foundation and the source. In Scenario D, a 1 m thick layer of higher moisture content is on the ground surface. **Figure 22b** presents the predicted normalized soil vapor concentration distribution, soil gas flow rate (Qs), and the indoor air concentration for the scenarios described in Figure 22a. In Scenario B, the high moisture content layer on top of

the source reduces the vapor concentrations in the subsurface close to the building and in the indoor air by about one order of magnitude compared with the homogeneous scenario (Scenario A). In Scenario C, the predicted soil vapor and indoor air concentrations are similar to those in Scenario A. Although there is a higher moisture content layer between the source and the foundation, there is substantial lateral migration through the lower moisture content layer right above the source. In Scenario D, the high moisture content layer on the ground surface increases the lateral migration of vapors and increases the vapor concentrations throughout the subsurface and in the indoor air by about one order of magnitude compared with Scenario A.

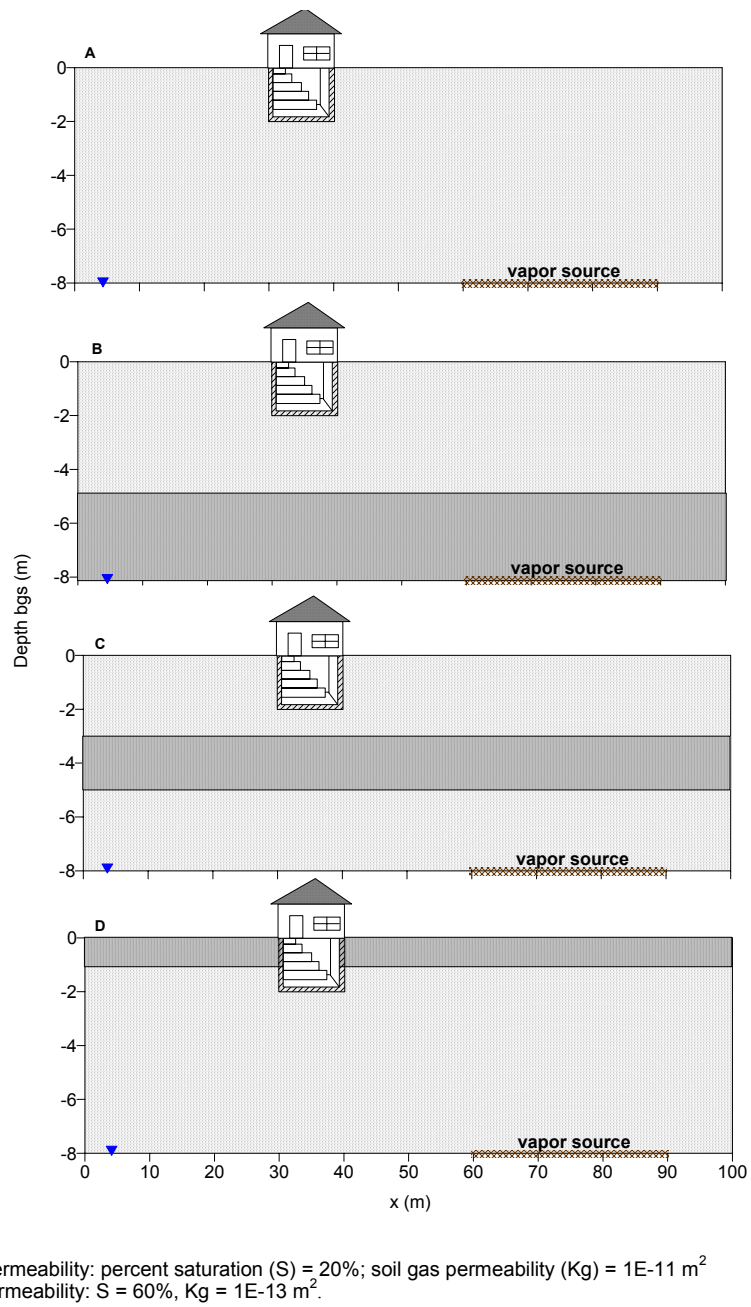

Figure 22a. Soil layer scenarios used in the simulations presented in Figure 22b with a deep laterally separated vapor source.

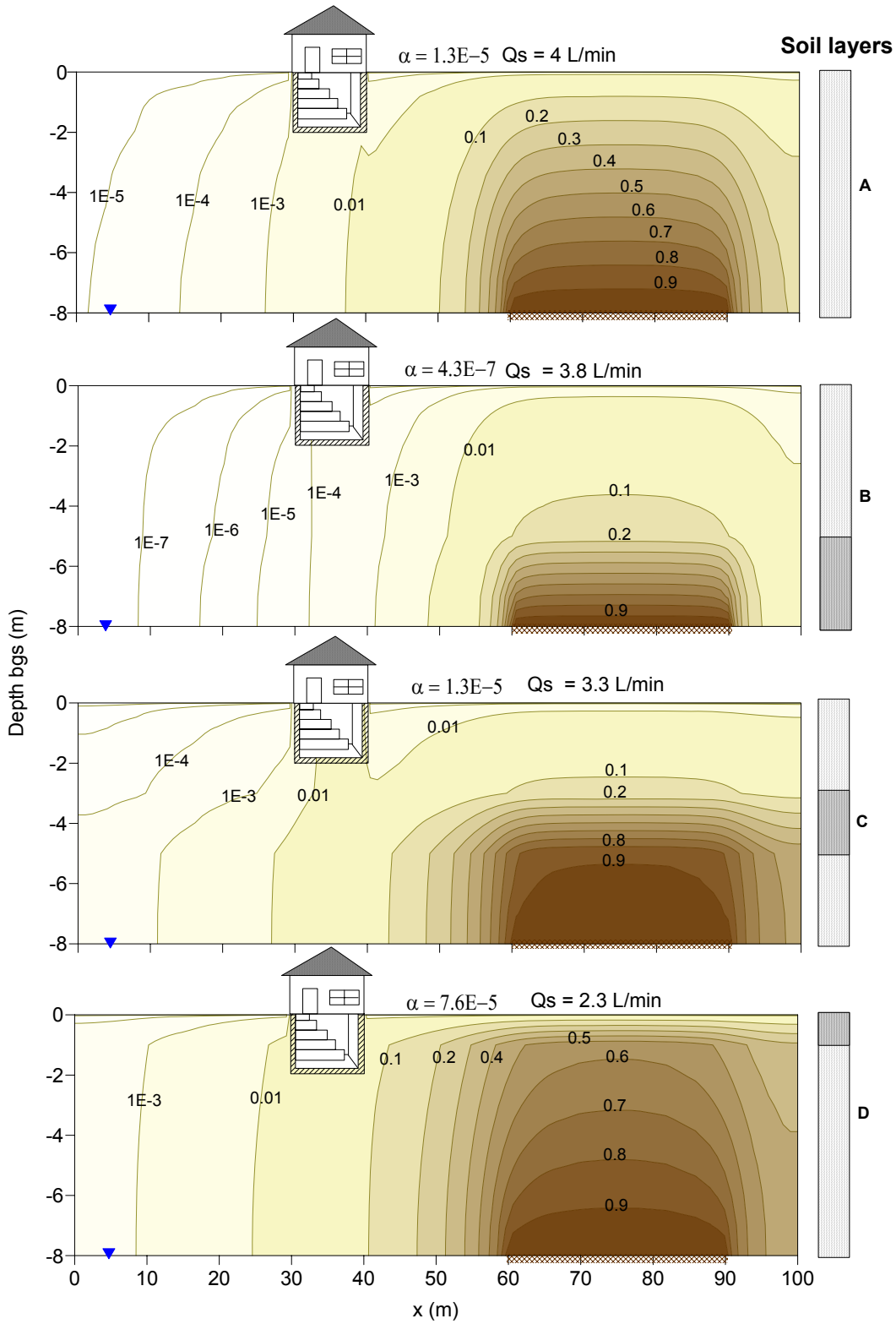

Figure 22b. Effect of soil layers (Figure 22a) on soil vapor distribution and normalized indoor air concentration (α) for a deep laterally separated vapor source.

The soil vapor concentration contour lines are normalized by the source vapor concentration. The source is at 8 m bgs. Qs is the soil gas flow rate predicted for building under-pressurized by 5 Pa.

Figure 23a presents a set of conceptual model scenarios that illustrate the effect of a heterogeneous subsurface and impermeable ground cover for deep groundwater (8 m bgs) and a finite vapor source located directly beneath two separated buildings with basements. Scenario A is the homogeneous baseline soil condition, used for comparison. In Scenario B, a discontinuous soil layer of higher moisture content (2 m thick) extends below the first foundation, but is discontinuous below the second foundation. In Scenario C, there is an impermeable cover at the ground surface between the two buildings that extends about 10 m away from the first building, which has the baseline homogeneous subsurface conditions. Scenario D has the same impermeable ground cover presented in Scenario C, with a discrete higher moisture content layer 2 m thick extending beneath the two buildings.

Figure 23b presents the predicted normalized soil vapor concentration distribution, soil gas flow rate (Qs), and the indoor air concentration for the scenarios described in Figure 23a. In Scenario B, the discontinuous layer beneath the buildings creates considerable spatial variability in the soil vapor concentrations, with the shallow concentrations on the sides of the buildings varying by about a factor of 10 and the indoor air concentration of the buildings varying by about a factor of four compared with the homogenous scenario (Scenario A). The indoor air concentration of the first building in Scenario B (with the layer beneath it) is a factor of four smaller than in Scenario A. The second building (without the layer beneath it) has a similar indoor air concentration to that in Scenario A. In Scenario C, the impermeable cover prevents the migration of vapors to the atmosphere, which increases the vapor concentrations in the subsurface beneath it by about a factor of eight compared with the concentration under the bare ground surface. Note that the concentration around the perimeter crack of Scenario C is about a factor of 1.6 higher than the concentration at the perimeter crack in Scenario A, and the soil gas flow rate (Qs) in Scenario C is about a factor of 1.4 smaller than the Qs in Scenario A; therefore, the contaminant emission rate to the enclosed space and the indoor air concentration are similar in both scenarios. In Scenario D, the continuous layer below the foundations reduces the vapor migration from the source to the buildings. The sub-slab concentrations and the indoor air concentrations of the two buildings are similar and about a factor of 10 smaller than in Scenarios A and C with homogeneous soil conditions.

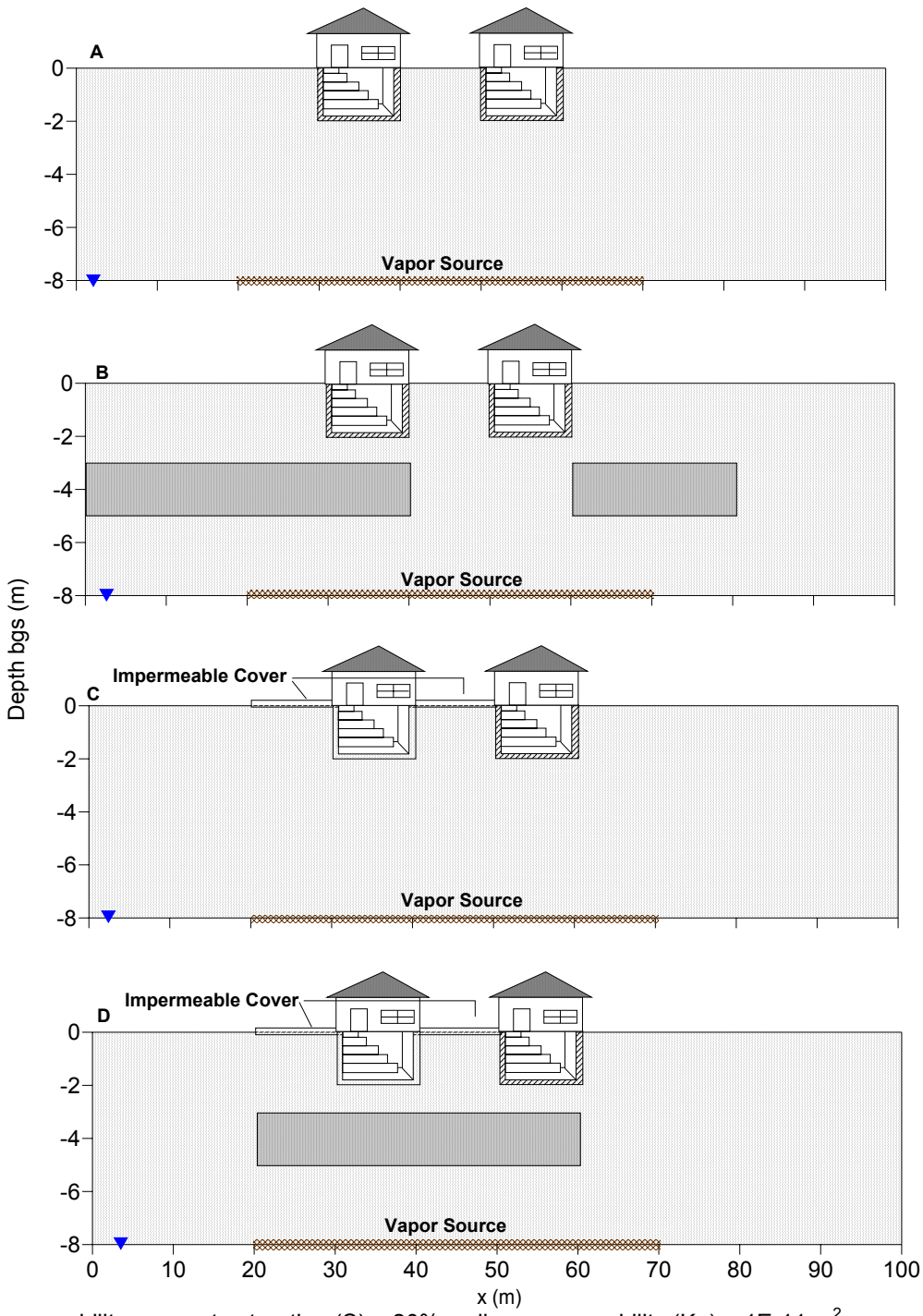

High permeability: percent saturation (S) = 20%; soil gas permeability (Kg) = 1E-11 m^2
Low permeability: S = 60%, Kg = 1E-13 m^2.

Figure 23a. Discontinuous soil layers and ground cover scenarios used in the simulations presented in Figure 23b for two buildings separated by 10 m overlying a plume.

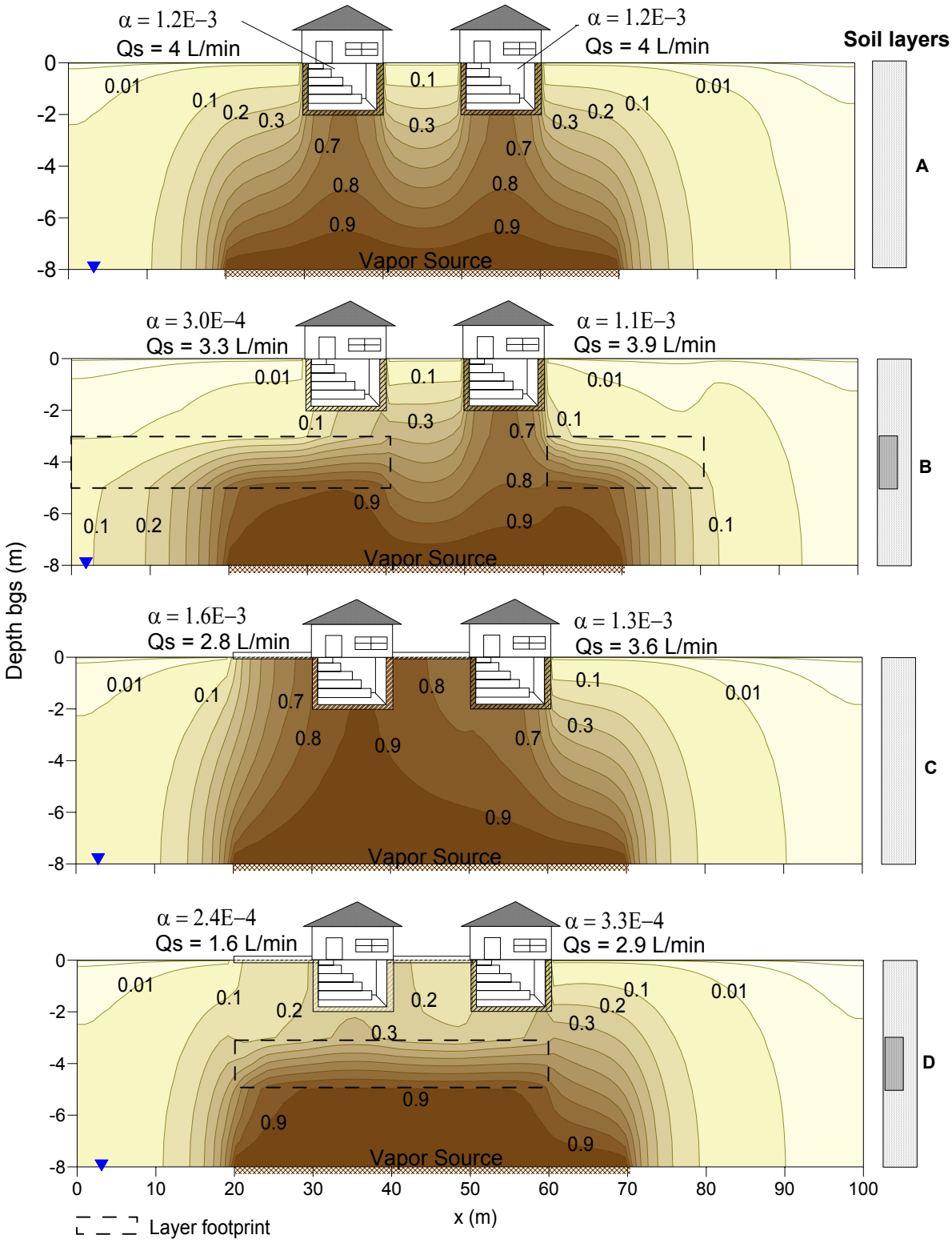

Figure 23b. Effect of discontinuous soil layers and ground cover (Figure 23a) on soil vapor distribution and normalized indoor air concentration (α) for two buildings separated by 10 m.

The soil vapor concentration contour lines are normalized by the source vapor concentration. The source is at 8 m bgs. Qs is the soil gas flow rate predicted for building under-pressurized by 5 Pa.

Figure 24a presents a set of conceptual model scenarios that illustrate the effect of a heterogeneous subsurface and impermeable ground cover for deep groundwater (8 m bgs) and a finite vapor source located at a lateral distance of 20 m from two adjacent buildings, one with a slab-on-grade foundation and another with a basement foundation. Scenario A is the homogeneous baseline soil condition, used for comparison. In Scenario B, there is an impermeable cover at the ground surface extending from the slab-on-grade building to about 10 m over the source, and the subsurface has the baseline homogeneous conditions. Scenario C has the same impermeable ground cover as Scenario B and a discrete higher moisture content layer (2 m thick) extending from beneath the slab-on-grade building to about 5 m beyond the source edge.

Figure 24b presents the predicted normalized soil vapor concentration distribution, soil gas flow rate (Qs), and the indoor air concentration for the scenarios described in Figure 24a. In Scenario B, the impermeable cover does not allow the migration of vapors to the atmosphere, increasing the vapor concentrations in the subsurface by about a factor of six compared with the concentration under the bare ground surface in Scenario A. The cover also promotes the migration of vapors to further lateral distances, increasing the vapor concentrations below the foundations and in the indoor air concentration by factors of 2.5 and 5, respectively, compared with Scenario A. In Scenario C, the discontinuous layer with higher moisture content does not have a substantial influence on the vapor concentration distribution because there is still considerable surface area with low moisture content in the subsurface for migration of the contaminant vapors and the vapors simply diffuse around and through the discrete high moisture content layer.

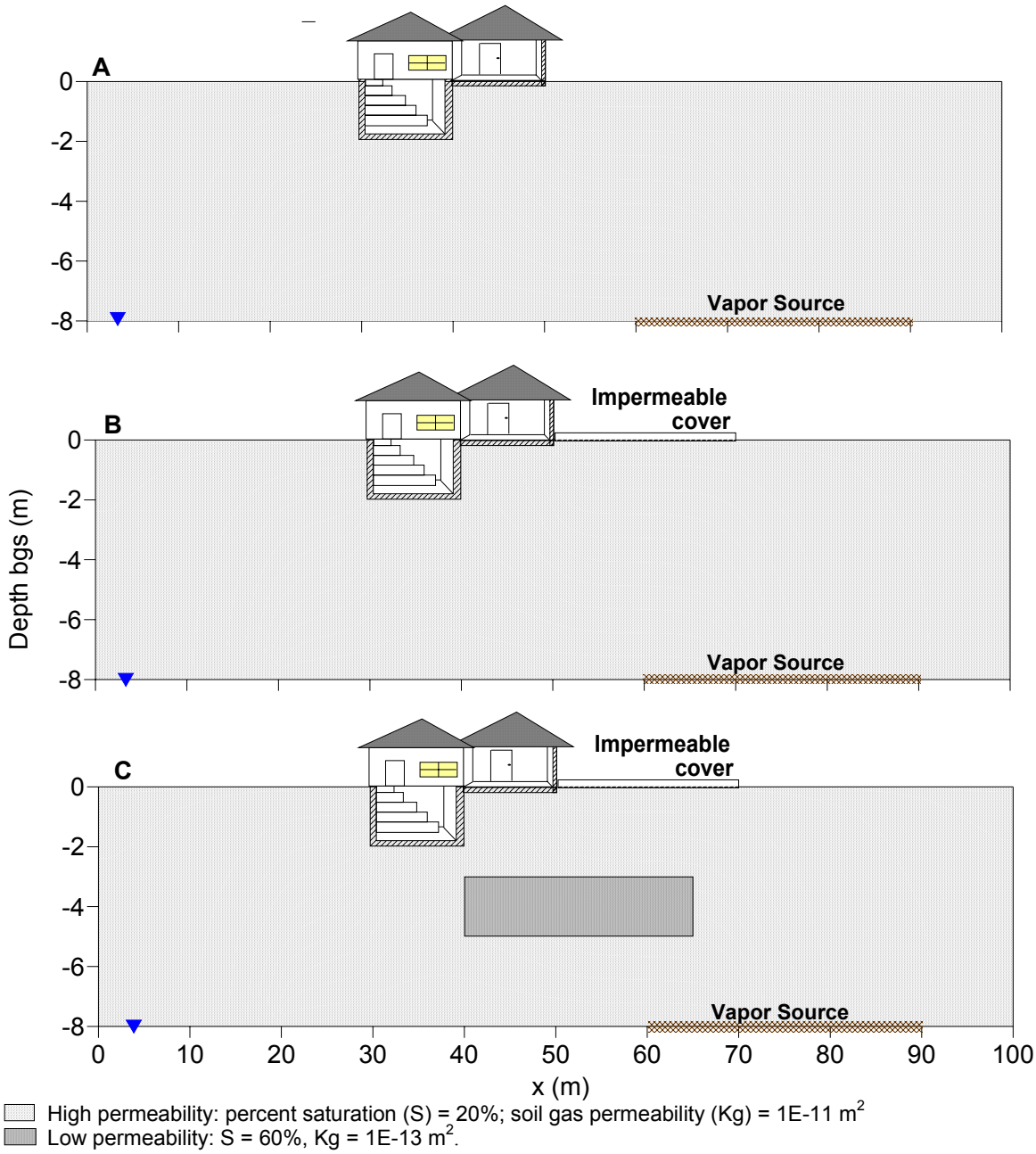

Figure 24a. Discontinuous soil layers and ground cover scenarios used in the simulations presented in Figure 24b for two adjacent buildings near a plume.

A finite vapor source is located laterally 20 m away from the closest building at groundwater level of 8 m bgs.

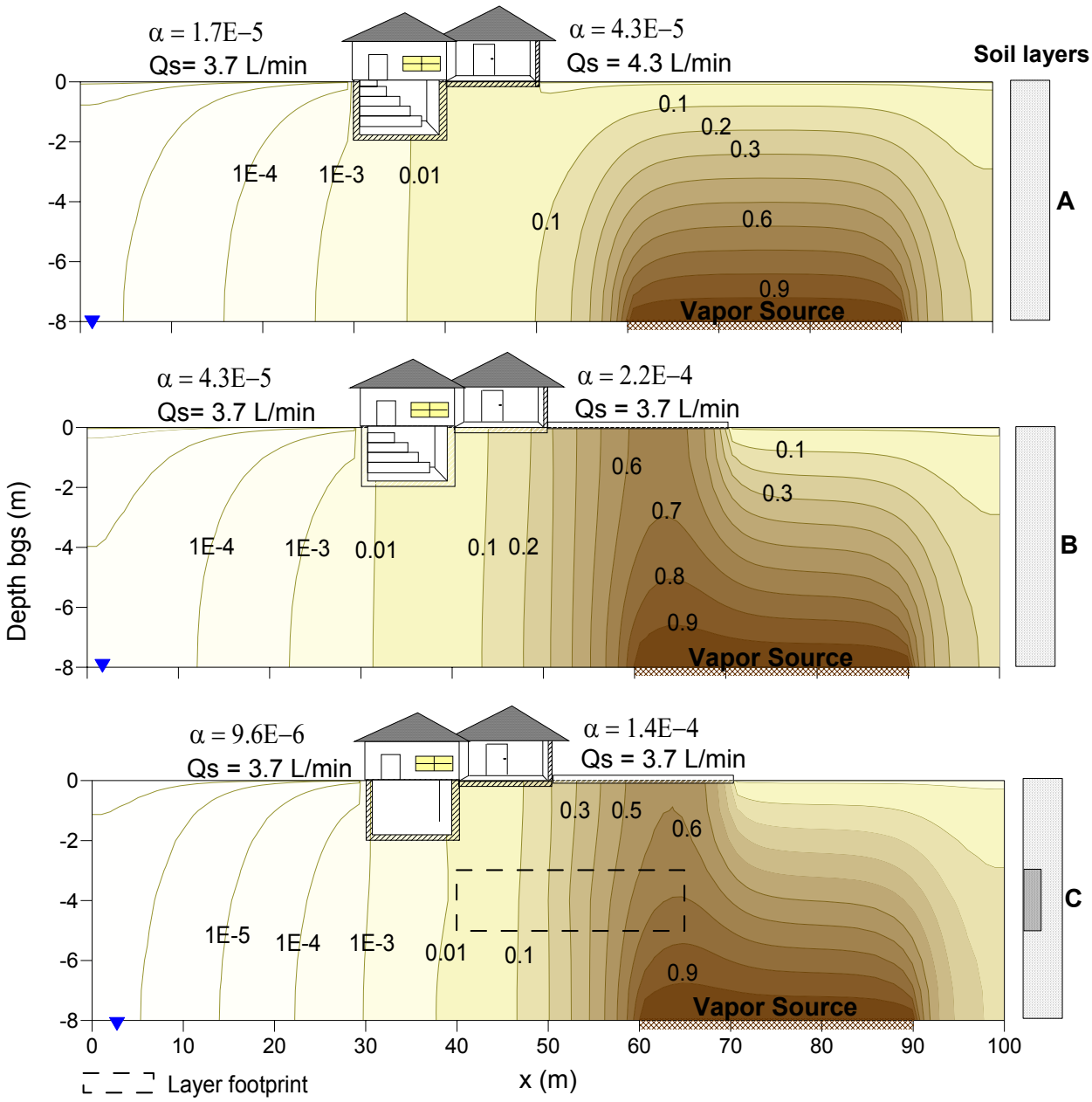

Figure 24b. Effect of discontinuous soil layers and ground cover (Figure 24a) on soil vapor concentration distribution and normalized indoor air concentration (α) for two adjacent buildings.
The soil vapor concentration contour lines are normalized by the source vapor concentration. The source is at 8 m bgs. Qs is the soil gas flow rate predicted for building under-pressurized by 5 Pa.

4.4.4 Geologic Barrier

The simulations in this section further illustrate how nonhomogeneous soil conditions can impact the soil gas flow into the building and VOC concentrations in soil gas in the vicinity of a building and in the indoor air. These simulations expand on the concepts in **Sections 4.4.1** through **4.4.3** by depicting the influence of low permeability soil layers that can act as "barriers" to gas migration (which are modeled here as soil layers with 95% pore water saturation) over a broad range of soil layering profiles, source depths and locations, and building scenarios. The simulations illustrate that such barrier layers can lead to a sharp concentration change with up to an order of magnitude decrease in concentrations between the area beneath the geologic barrier and the area above it (**Figure 25**). **Figures 26** and **27** highlight the fact that differences in the relative positions of the source, the barrier, and the structure can result in very different sub-slab contaminant profiles and indoor air concentrations.

In this document, "geologic barrier" is used to indicate a natural layer in the subsurface that hinders the movement of vapors to a greater extent than the soil layers modeled in the previous section. In the simulations presented in this section, a geologic barrier is represented as a thin soil layer with 95% pore water saturation (S). In natural settings, this condition could exist in areas where, for example, there is ponding of infiltrating water on top of a fine-grained soil layer (e.g., water from natural recharge or irrigation, leaky water or sewer pipes). The high moisture content layer properties used in these simulations may not be typical of real sites, but they are a convenient modeling mechanism for simulating low permeability barriers and their influence on the subsurface distribution of VOCs at a vapor intrusion site. The 95% saturated layer portrayed in this document has a soil gas permeability of 1×10^{-13} m^2, roughly equivalent to a soil layer of moist clay.

The effect of a geologic barrier depends on its position and size with respect to the source, the building foundation, and the ground surface. The scenarios simulated in this section illustrate different configurations of geologic barriers with respect to these conditions for single and multiple buildings. Similar trends were observed by Bozkurt et al. (2009).

Figure 25 presents the modeled scenarios and the predicted effect of geologic barriers on normalized soil vapor concentration distribution, soil gas flow rate (Qs), and indoor air concentration for conceptual model scenarios represented by a single building and a large vapor source directly beneath the building at groundwater level (5 m bgs). Scenario A is the homogeneous baseline soil condition, used for comparison. In Scenario B, the barrier is between the source and the building and extends laterally beneath the full extent of the foundation. In Scenario C, the barrier is between the source and the building but does not extend beneath the foundation. In Scenario D, the barrier is at the ground surface. Note that, in all scenarios, the barrier is discontinuous at locations away from the building.

The results presented in Figure 25 show that, for the conditions simulated, the predicted vapor concentration below the geologic barrier is about one order of magnitude higher than the vapor concentration above it. The geologic barriers reduced the soil gas flow rate (Qs) in Scenarios B, C, and D by about 40% compared with the homogeneous case (Scenario A). In Scenario B, where the geologic barrier extends below the foundation, the normalized indoor air concentration (α) is about one order of magnitude smaller than in the homogeneous case. For scenarios where the geologic barrier does not extend below the foundation (Scenarios C and D), the normalized indoor air concentrations are similar to the homogeneous case.

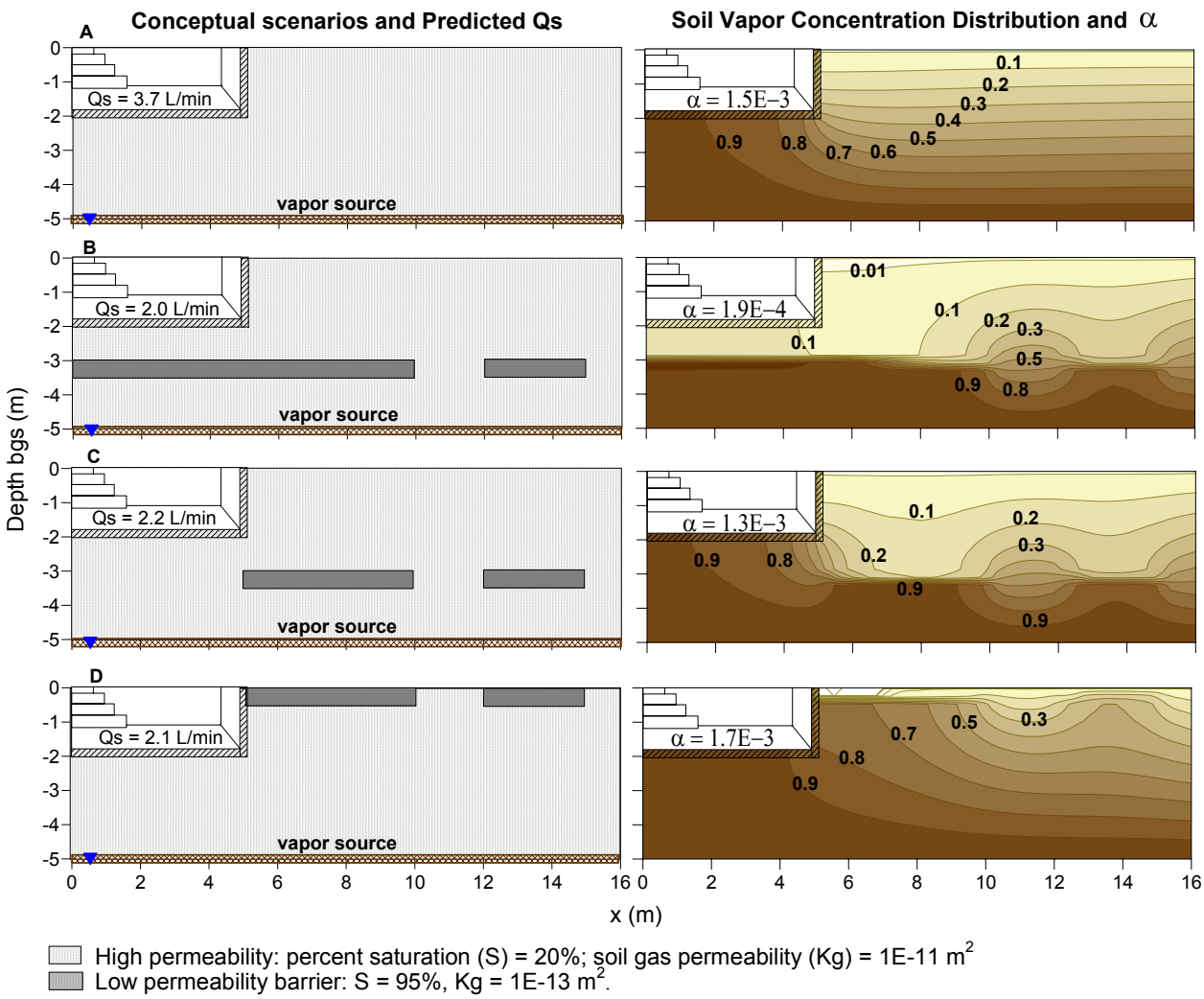

Figure 25. Effect of geologic vapor barriers on soil vapor distribution and normalized indoor air concentration (α).

The soil vapor concentration contour lines are normalized by the source vapor concentration. The source is at 5 m bgs. Qs is the soil gas flow rate predicted for building under-pressurized by 5 Pa.

The next two figures present scenarios with finite sources and multiple buildings. **Figure 26** shows two buildings with basements that are 10 m apart and a geologic barrier extending fully beneath only one of the two buildings. **Figure 27** shows two adjacent buildings with basements and a geologic barrier extending up to the edge of the second building. In Figure 26, the normalized indoor air concentration predicted for the building above the geologic barrier is more than a factor of 10 smaller than the concentration predicted for the building that is not above the barrier. In Figure 27, the indoor air concentration of the building right at the edge of the geologic barrier is a factor of four higher than the concentration of the building that is fully shielded by the geologic barrier. The examples in Figures 26 and 27 show that, although the primary reason for the reduced normalized indoor air concentration is the effect that the geologic barrier has on reducing vapor migration by diffusion, the barrier also reduces the soil gas flow rate into the building due to its low soil gas permeability. This effect is more pronounced in the scenario with two adjacent buildings (Figure 27).

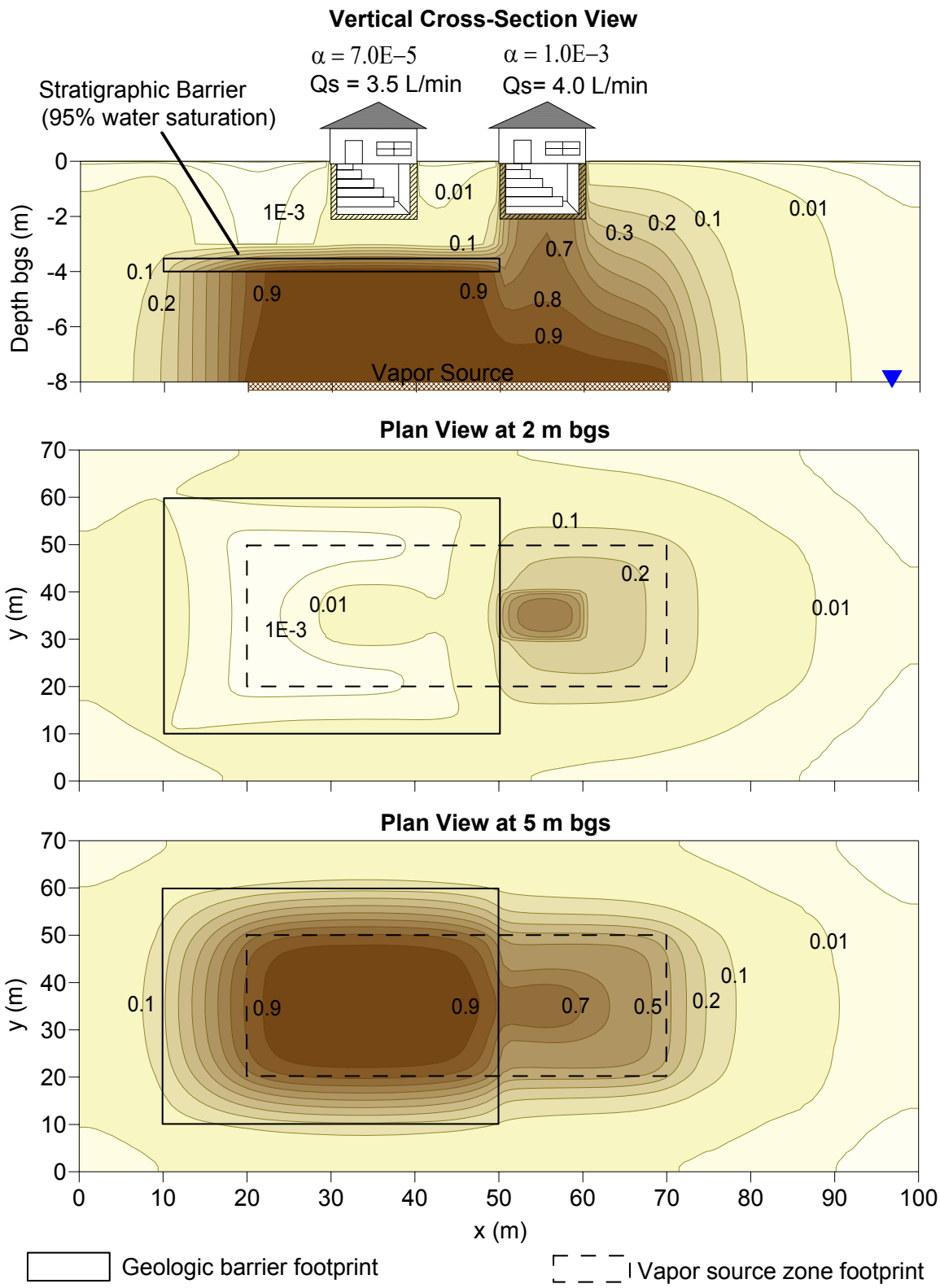

Figure 26. Effect of a geologic vapor barrier on soil vapor distribution and normalized indoor air concentration (α) for two buildings separated by 10 m.

The soil vapor concentration contour lines are normalized by the source vapor concentration. The source is at 8 m bgs. Qs is the soil gas flow rate predicted for building under-pressurized by 5 Pa.

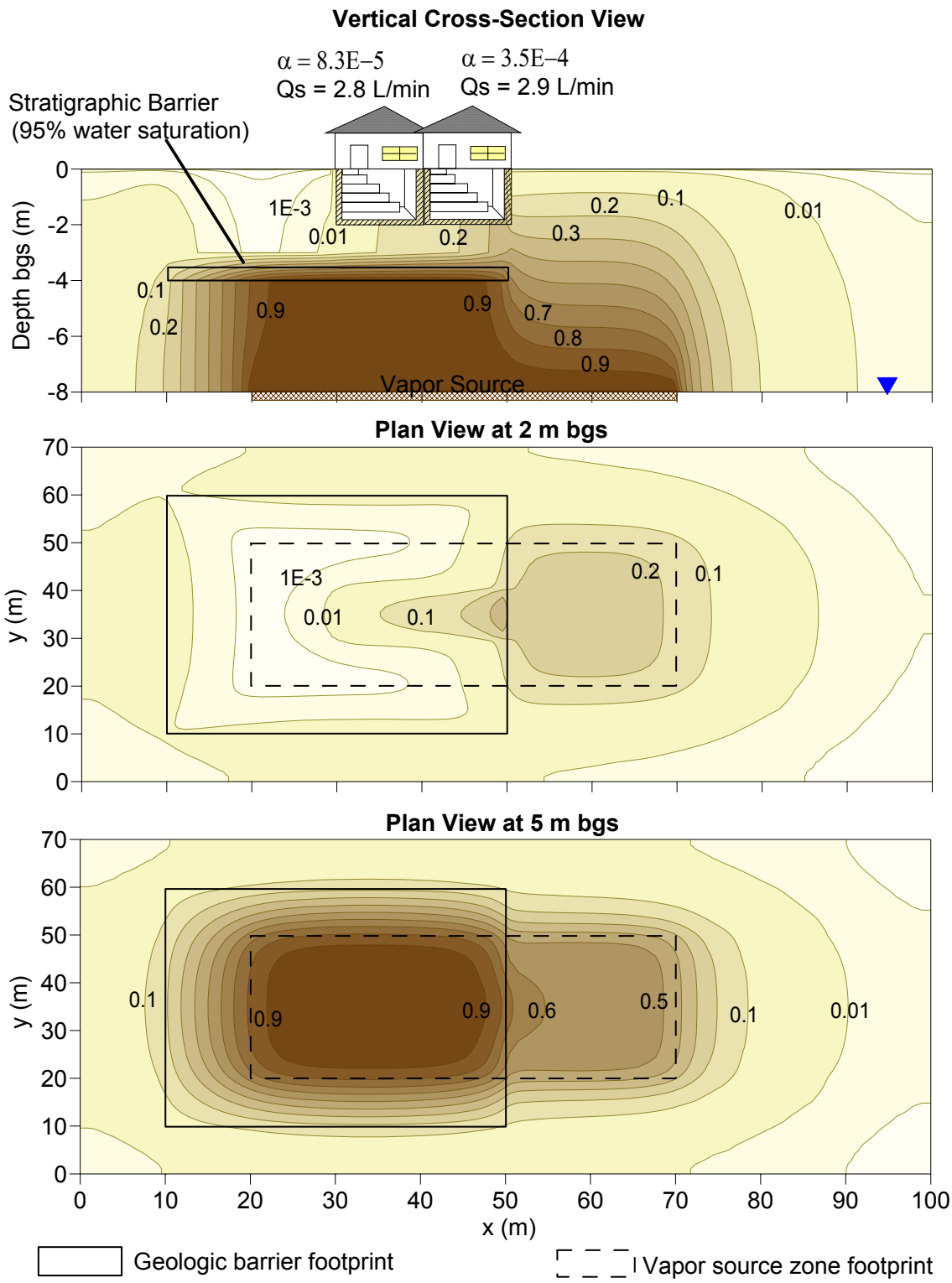

Figure 27. Effect of a geologic vapor barrier on soil vapor distribution and normalized indoor air concentration (α) for two adjacent buildings.

The soil vapor concentration contour lines are normalized by the source vapor concentration. The source is at 8 m bgs. Qs is the soil gas flow rate predicted for building under-pressurized by 5 Pa.

[This page intentionally left blank.]

5.0 Factors Affecting Vapor Migration and Indoor Air Concentrations of Biodegradable VOCs

In previous chapters, it was assumed that the VOCs depicted in the simulations were recalcitrant (i.e., were not subject to rapid breakdown in the subsurface). In this chapter, the VOCs depicted in the simulations are subject to aerobic biodegradation, or biodegradation that occurs in the presence of oxygen. Because oxygen is necessary to support the bacterial communities that foster aerobic biodegradation of the VOCs, the simulations include depictions of the distribution of oxygen concentrations in the subsurface as well as the distribution of the VOCs. The simulations cover many of the same topics covered in **Section 3** and **Section 4** where recalcitrant compounds were addressed. The simulations in this chapter are applicable to petroleum hydrocarbons.

Petroleum hydrocarbons and chlorinated hydrocarbons differ in their potential for vapor intrusion, mainly because petroleum compound vapors readily biodegrade in the subsurface (U.S. EPA, 2011). Biodegradation is the decomposition of organic contaminants by microorganisms, mainly bacteria. If the microorganisms use oxygen to break down the VOCs, the mechanism is called aerobic biodegradation. As summarized in U.S. EPA (2011), substantial reduction of the vapor concentration of many petroleum hydrocarbons via aerobic biodegradation has been observed by several researchers in natural settings (e.g., Roggemans et al., 2001; Hers et al., 2000) and in controlled experimental settings (e.g., Pasteris et al., 2002; Jin et al., 1994). Aerobic biodegradation does reduce vapor intrusion into buildings if the VOC is aerobically biodegradable and oxygen is present. Because aerobic biodegradation depends on the availability of oxygen, the simultaneous transport of atmospheric oxygen into the subsurface soil gas is an important factor in the aerobic biodegradation of hydrocarbons.

The fate and transport of aerobically biodegradable compounds includes the same processes of diffusion and advection discussed in **Section 3**, with the addition of aerobic biodegradation. This section presents the effect of several factors on the fate and vapor intrusion of biodegradable hydrocarbons, including subsurface oxygen availability: source vapor concentration, source depth and lateral distance from the building, building foundation type, layered soils moisture content distribution, and geologic barriers.

The 3-D model was used to simulate the simultaneous transport and biodegradation of hydrocarbons and oxygen. The atmosphere is a constant source of oxygen through the open ground surface area next to the building, and the VOC source is assumed to be infinite (i.e., it has constant concentration and does not deplete over time). Predicted concentration profiles for hydrocarbon and oxygen are presented and discussed for a variety of scenarios similar to those in **Section 4**. As before, the hydrocarbon concentration profiles are normalized by the source vapor concentration, and the oxygen concentration profiles are normalized by the atmospheric oxygen concentration.

In all simulations, the threshold oxygen concentration for biodegradation to occur was assumed to be 1% by volume (which corresponds to a normalized oxygen concentration of 0.05 in the contour plots). The simulations employ a first-order biodegradation model with a biodegradation rate (λ) of 0.18 h^{-1} for aromatic hydrocarbons, following Abreu and Johnson (2006). This biodegradation rate is smaller than the average of 0.79 h^{-1} reported for aromatic hydrocarbons in the analysis of DeVaull (2007), who compiled results from 84 data sets of laboratory and field

biodegradation rates for aromatic hydrocarbons measured by multiple investigators. A range of biodegradation rates (0–1.8 h^{-1}) was also assumed for comparative purposes in several scenarios.

All simulations presented in this technical document assume a single-component vapor source with physical-chemical properties for benzene, which are similar to those for the VOCs of interest in vapor intrusion. For recalcitrant chemicals, the model-predicted steady-state normalized soil vapor concentration distribution and normalized indoor air concentration (α) for each chemical are independent of presence and concentration of other chemicals; however, that is not true in aerobic biodegradation scenarios, because many chemicals utilize oxygen and contribute to its depletion in the subsurface. For example, petroleum hydrocarbon releases involve mixtures of aerobically biodegradable VOCs. A modeling study by Abreu et al. (2009a,b) compared predicted VOC concentrations and oxygen profiles for cases involving single- and multi-component sources with the same total source concentration. For cases where oxygen is limiting and biodegradation rates are variable but fast compared with diffusive time scales, the vapor profiles of individual components were similar. This behavior has been observed in the field (i.e., Roggemans et al., 2001). Therefore, the simulations presented below are for a single-component source but are likely also applicable to a range of multi-component scenarios involving aerobically biodegradable chemicals.

As discussed below, for certain source concentrations and depths, the oxygen concentrations in the subsurface may be depleted, creating anaerobic zones. Under those conditions, methane gas may be generated. Methane is readily biodegradable aerobically, so it would also contribute to oxygen utilization and affect the vapor profile. Methane production and transport are not addressed in this document, but it should be noted that methane may be the dominant vapor component (present at 1–20% by volume) at some petroleum sites.

5.1 Source Concentration

The simulations in this section illustrate the effect of source concentration on the distribution of biodegradable hydrocarbon vapors in the subsurface for buildings with basement (**Figures 28** and **30**) and slab-on-grade (**Figures 29** and **31**) foundations. Where the oxygen concentration is sufficient for biodegradation, hydrocarbons are broken down as oxygen is consumed. High hydrocarbon source concentrations can deplete oxygen, after which degradation diminishes and vapor transport is similar to that for recalcitrant compounds. Biodegradation typically reduces hydrocarbon vapor concentrations by several orders of magnitude over distances as short as a few meters or less. (*For comparisons with scenarios where the VOCs are recalcitrant, see **Figures 7** and **8**.*)

The source vapor concentration influences the soil vapor concentration distribution and the indoor air concentrations of aerobically biodegradable hydrocarbons. **Figures 28** and **29** present the simulated effect of source vapor concentration on normalized soil vapor concentration distributions for hydrocarbons and oxygen undergoing aerobic biodegradation for a building with a basement and a building with a slab-on-grade foundation, respectively. The source vapor concentrations simulated in each figure are 20,000, 100,000, and 200,000 mg/m^3. A hydrocarbon vapor source concentration of 20,000 mg/m^3 might be encountered at sites where the vapor source is gasoline or hydrocarbons dissolved in groundwater. A source vapor concentration of 200,000 mg/m^3 might be encountered at sites where the source is weathered gasoline NAPL just above the water table. In both Figures 28 and 29, the source is located at a depth of 8 m bgs.

The concentration profiles for the basement scenario (Figure 28) show that for source vapor concentrations of 100,000 and 200,000 mg/m^3 (representative of weathered gasoline NAPL sources), oxygen is consumed before it can penetrate beneath the foundation. Thus, no biodegradation is occurring beneath the foundation in the region below the 0.05 oxygen contour line, because of limited oxygen availability and supply. In this region, the vapor transport is not attenuated by biodegradation. As a result, the hydrocarbon concentration is higher below the foundation compared with similar depths away from the building with sufficient oxygen for biodegradation. For a source vapor concentration of 20,000 mg/m^3, oxygen penetrates beneath the entire foundation. The vapor transport is attenuated by biodegradation throughout much of the subsurface, and the vertical profile of the hydrocarbon concentration is similar beneath the building and away from the building.

The concentration profiles for the slab-on-grade scenario (Figure 29) show an increased oxygen supply beneath the foundation relative to the basement scenario, and the vapor transport is therefore attenuated by biodegradation beneath the entire building footprint, even for the highest source concentrations simulated. The differences in the aerobic zone (oxygen) distribution beneath the slab-on-grade foundation compared with the basement foundation are due to the combination of a smaller distance for oxygen transport from the atmosphere and an increased distance for hydrocarbon transport from the source to locations immediately beneath the slab. The concentration profiles in the subsurface away from the foundation are identical for both scenarios (basement and slab-on-grade).

For the conditions simulated in Figures 28 and 29, the normalized indoor air concentrations (α) decrease by about six orders of magnitude as the source vapor concentration decreases from 200,000 mg/m^3 to 20,000 mg/m^3 for both foundation types. The normalized indoor air concentrations for the slab-on-grade foundation are about three orders of magnitude smaller than those for the basement foundation. Biodegradation is influenced by the source vapor concentration and may significantly decrease the soil vapor concentration and indoor air concentration compared with the no biodegradation case (see Figure 7b).

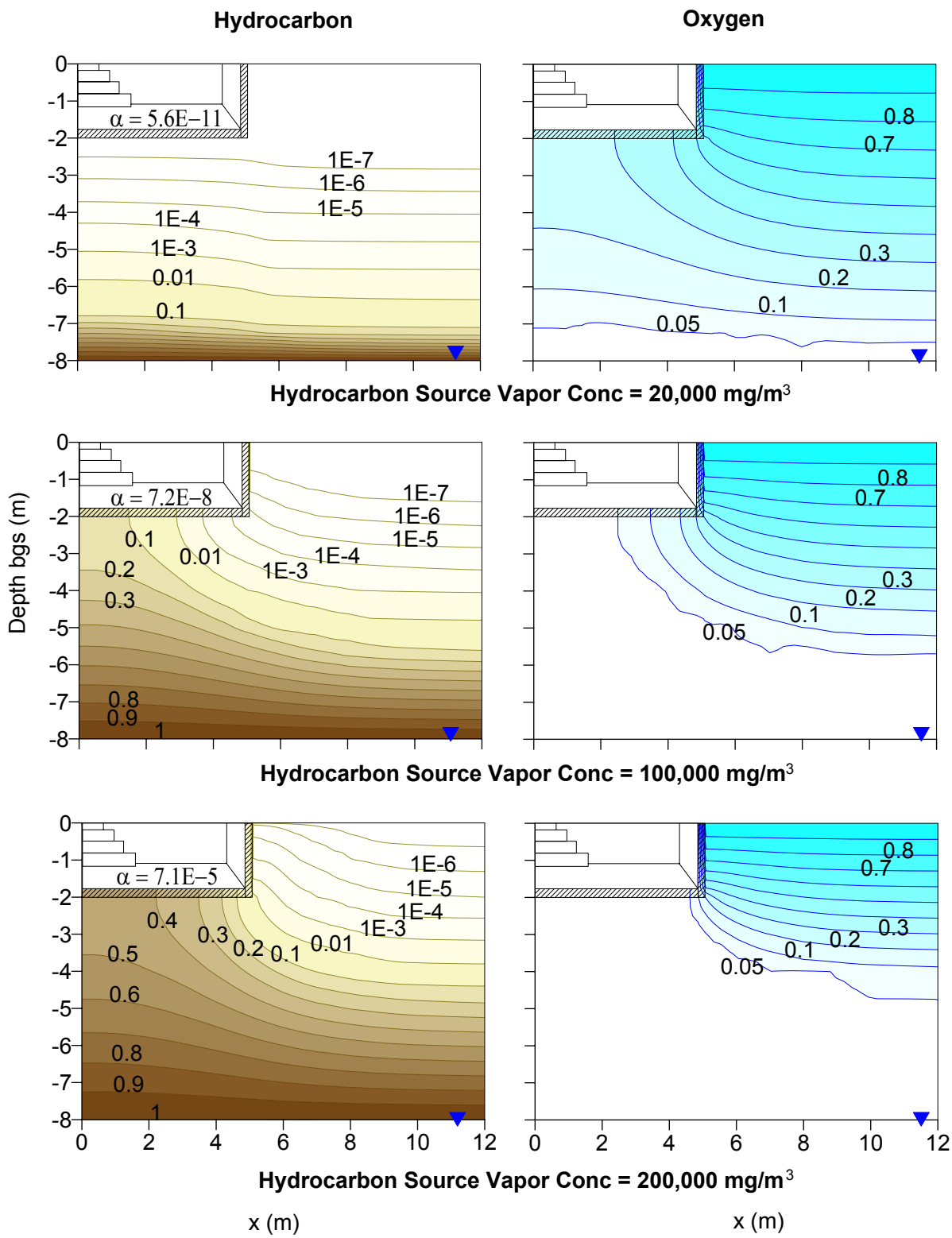

Figure 28. Effect of source vapor concentration on hydrocarbon and oxygen distribution in soil gas and normalized indoor air concentration (α) for a building with basement.

Hydrocarbon and oxygen concentration contour lines are normalized by source and atmospheric concentrations, respectively. The hydrocarbon vapor source is at 8 m bgs. Biodegradation rate (λ) = 0.18 h^{-1}.
(Abreu and Johnson, 2006)

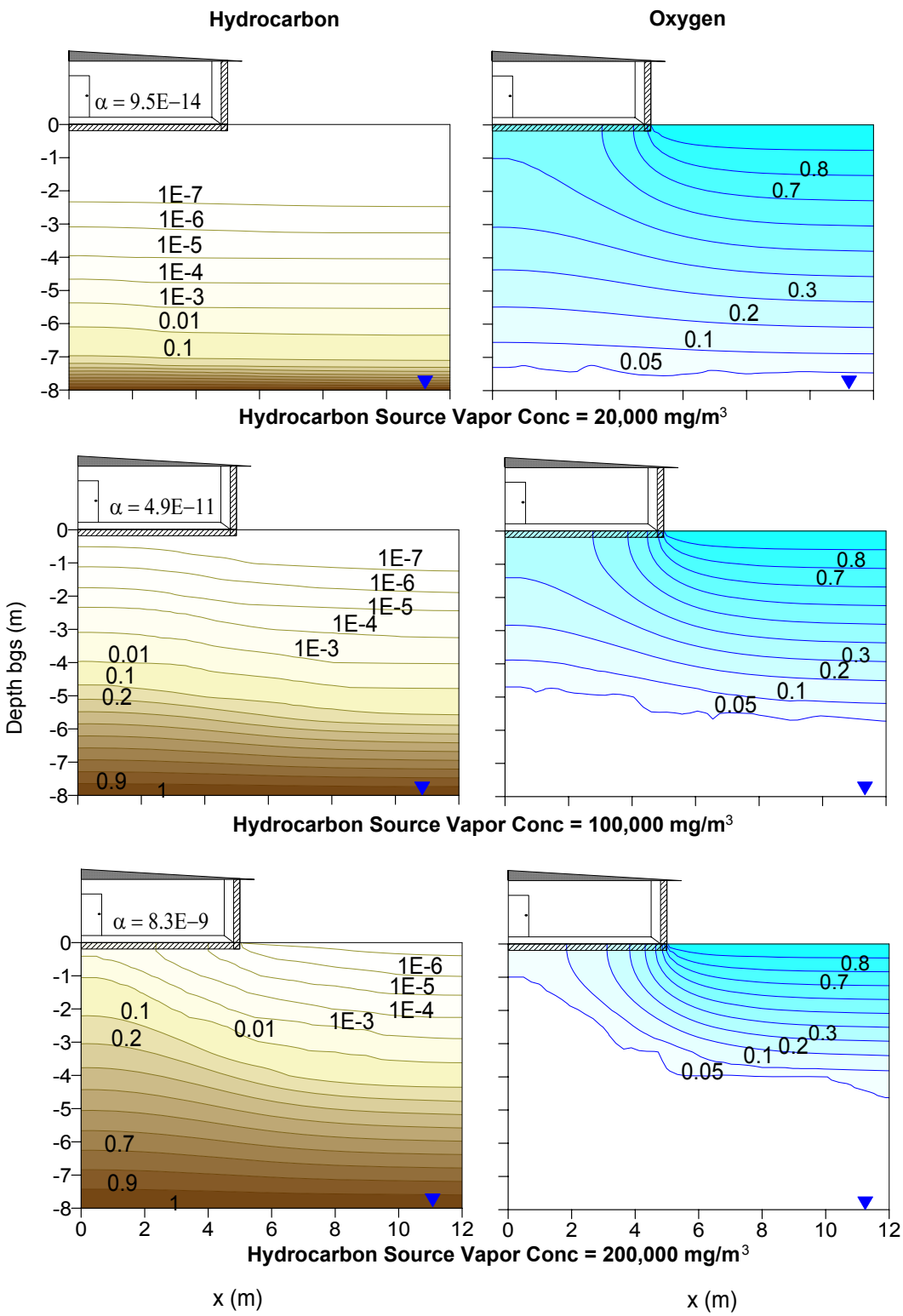

Figure 29. Effect of source vapor concentration on hydrocarbon and oxygen distribution in soil gas and normalized indoor air concentration (α) for a slab-on-grade building.

Hydrocarbon and oxygen concentration contour lines are normalized by source and atmospheric concentrations, respectively. The hydrocarbon vapor source is at 8 m bgs. Biodegradation rate (λ) = 0.18 h^{-1}.
(Abreu and Johnson, 2006)

Normalized indoor air concentrations for a broader range of source concentrations, depths, and biodegradation rates (λ) are presented in **Figure 30** for a basement scenario. Plots are presented for two source depths, 3 and 8 m bgs. The plot shows a family of curves with similar shapes and trends of decreasing normalized indoor air concentrations with a decreasing source vapor concentration, an increasing biodegradation rate, and an increasing source depth. For source vapor concentrations less than 10,000 mg/m^3, biodegradation occurs without oxygen limitations throughout the subsurface and normalized indoor air concentrations are relatively unaffected by changes in the source vapor concentration. For source vapor concentrations above 10,000 mg/m^3, normalized indoor air concentrations increase with increasing source vapor concentration, until they reach the value for the case of sub-slab oxygen depletion (when biodegradation beneath the foundation ceases), after which the results of the simulations are similar to those for chemicals that do not readily biodegrade aerobically (i.e., recalcitrant compounds). Increasing biodegradation rates generally correspond to decreasing normalized indoor air concentrations, except where oxygen depletion and anaerobic conditions occur beneath the foundation (i.e., at high vapor source concentrations), because aerobic biodegradation stops when oxygen is not present.

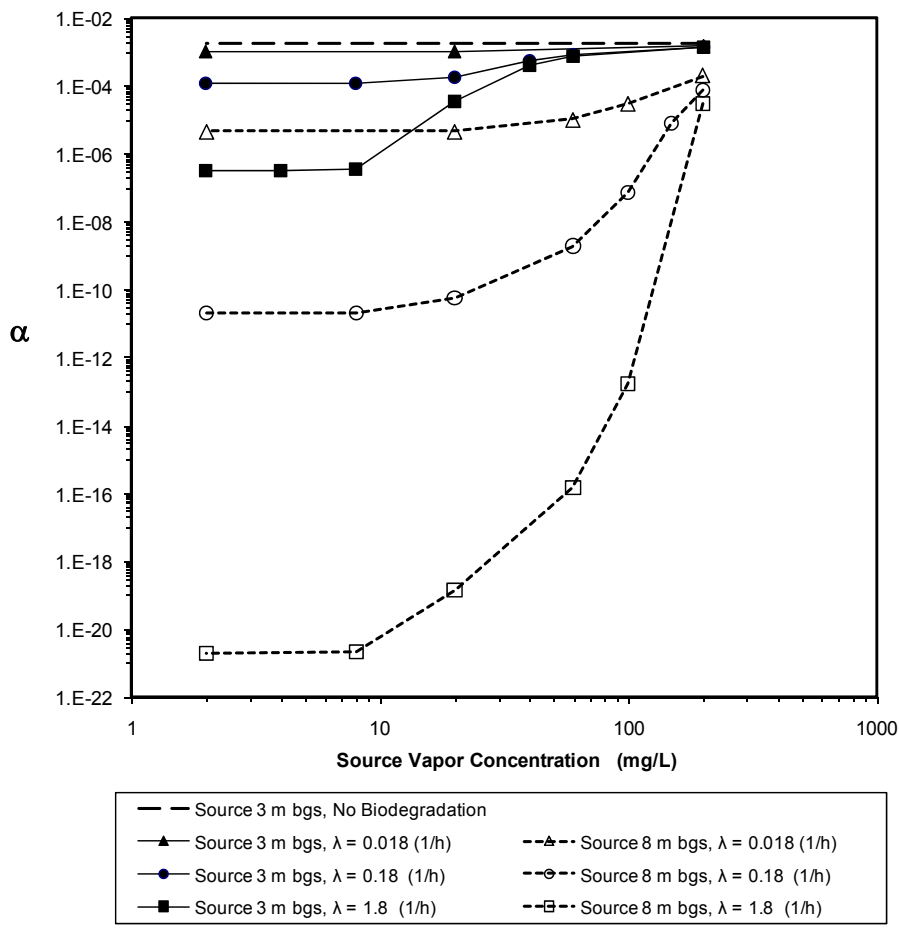

Figure 30. Relationship between source vapor concentration and normalized indoor air concentration (α) for three biodegradation rates (λ), two source depths and a building with basement.

(Abreu and Johnson, 2006)

For the same conditions of source concentration, biodegradation rate, and source depth, the normalized indoor air concentration for a slab-on-grade foundation (**Figure 31**) may be several orders of magnitude lower than the normalized indoor air concentrations for a basement foundation, because of the larger foundation-source separation for slab-on-grade buildings and the rapid rate of biodegradation relative to the rate of transport.

The plot for the no biodegradation case in Figures 30 and 31 shows that the normalized indoor air concentrations for recalcitrant compounds that do not readily biodegrade aerobically are independent of source concentration. The plots also show that biodegradation may reduce the normalized indoor air concentrations by many orders of magnitude compared with the no biodegradation case. This is a key difference between biodegradable and recalcitrant compounds.

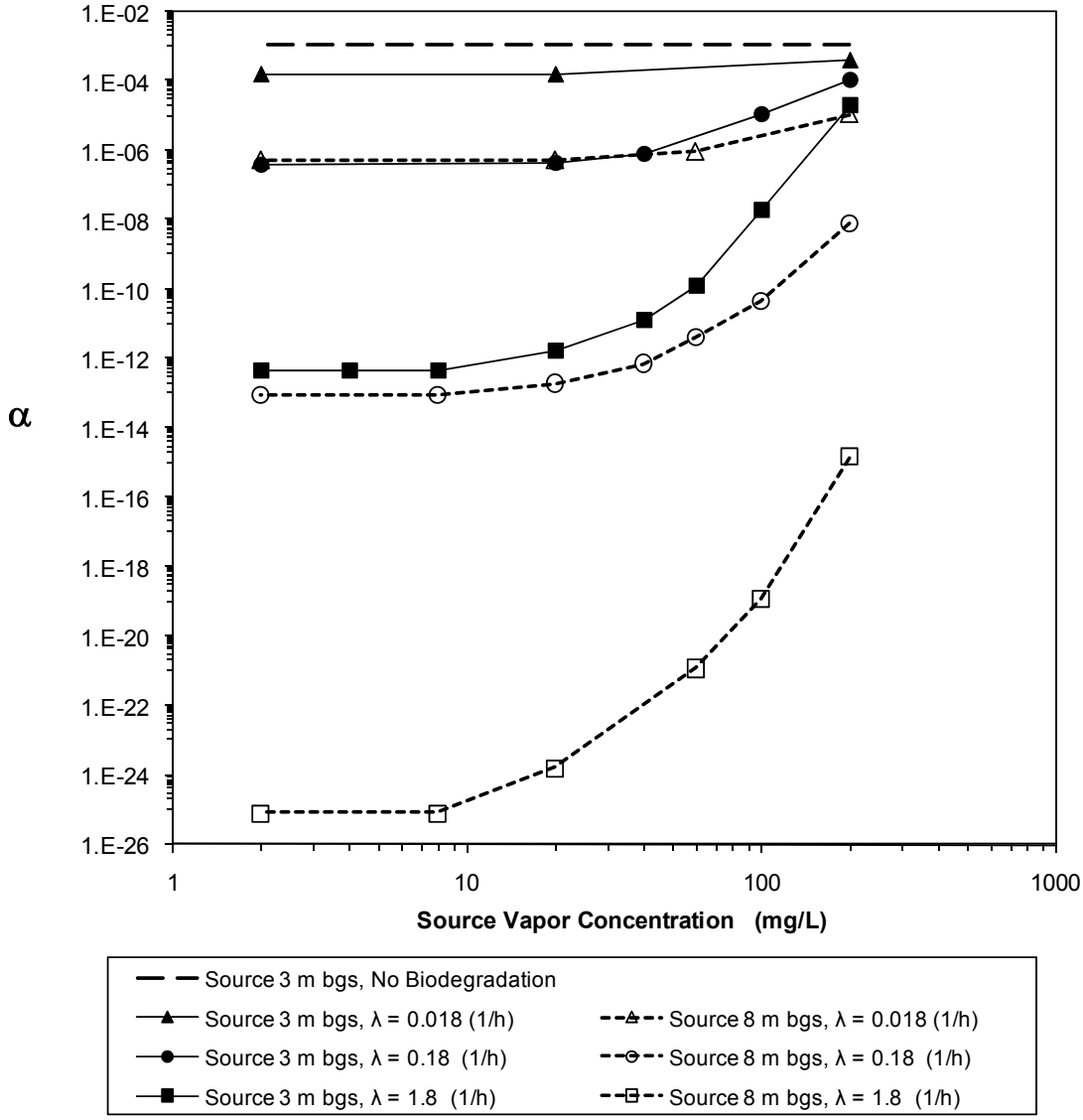

Figure 31. Relationship between source vapor concentration and normalized indoor air concentration (α) for three biodegradation rates (λ), two source depths and a slab-on-grade building.
(Abreu and Johnson, 2006)

5.2 Source Depth

The figures in this section illustrate the effect of vertical separation distance between the source and the building foundation on the distribution of biodegradable hydrocarbon vapors in the subsurface. Because the foundation slab inhibits downward diffusion of oxygen, for a given foundation area, degradation is likely to be more complete in settings where the separation between the source and the base of the foundation is greater and the source concentrations are smaller (**Figure 32**). Plots of normalized indoor air concentrations for a variety of conditions at a structure with a basement and one with a slab-on-grade are depicted in **Figures 33** and **34**, respectively. (*For comparisons with scenarios where the VOCs are recalcitrant, see **Figures 7b** and **8**.*)

The effect of source depth on the soil vapor concentration distribution profile for biodegradable hydrocarbons is illustrated in **Figure 32** for a slab-on-grade foundation, two source vapor concentrations (2,000 and 200,000 mg/m^3), and two source depths (3 and 8 m bgs). As illustrated in Figure 32, for a shallow source with a concentration representative of a weathered gasoline NAPL source, oxygen is depleted before reaching the subsurface beneath the building. Thus, because of oxygen limitations, little or no biodegradation is expected to occur beneath the slab. This scenario was observed in a field study conducted by Patterson and Davis (2009). As the source depth increases, oxygen fully penetrates below the foundation, and aerobic biodegradation reduces the soil vapor concentration by four orders of magnitude compared with the no biodegradation case (previously depicted in Figure 8). For a lower vapor concentration source, potentially representative of a dissolved groundwater source, oxygen concentrations in the entire subsurface are sufficient to allow biodegradation and reduce the soil vapor concentration by many orders of magnitude compared with the no biodegradation case.

For the conditions simulated in Figure 32, as the vapor source depth increases from 3 to 8 m (less than a factor of 3), the normalized indoor air concentration (α) decreases by about six orders of magnitude (a factor of 1,000,000) for the lower concentration scenario and by about four orders of magnitude (a factor of 10,000) for the higher concentration scenario. By comparison, the normalized indoor air concentration for the no biodegradation case presented in Figure 8 decreases by less than a factor of two as the source depth increases by 10 m.

Normalized indoor air concentrations for a broader set of source depths and biodegradation rates are presented in **Figures 33** and **34** for a basement and slab-on-grade scenarios, respectively. These figures show a family of curves with similar shapes and trends of decreasing normalized indoor air concentrations with increasing source depth. Increasing biodegradation rates generally correspond to decreasing normalized indoor air concentrations, except for shallow, high-concentration sources, where oxygen depletion and anaerobic conditions occur beneath the foundation, and biodegradation is stifled. These simulations indicate a decrease of multiple orders of magnitude in the normalized indoor air concentrations with an increase in source depth of approximately 2 m. The plots also show that biodegradation may reduce the normalized indoor air concentrations by six orders of magnitude compared with the no biodegradation case.

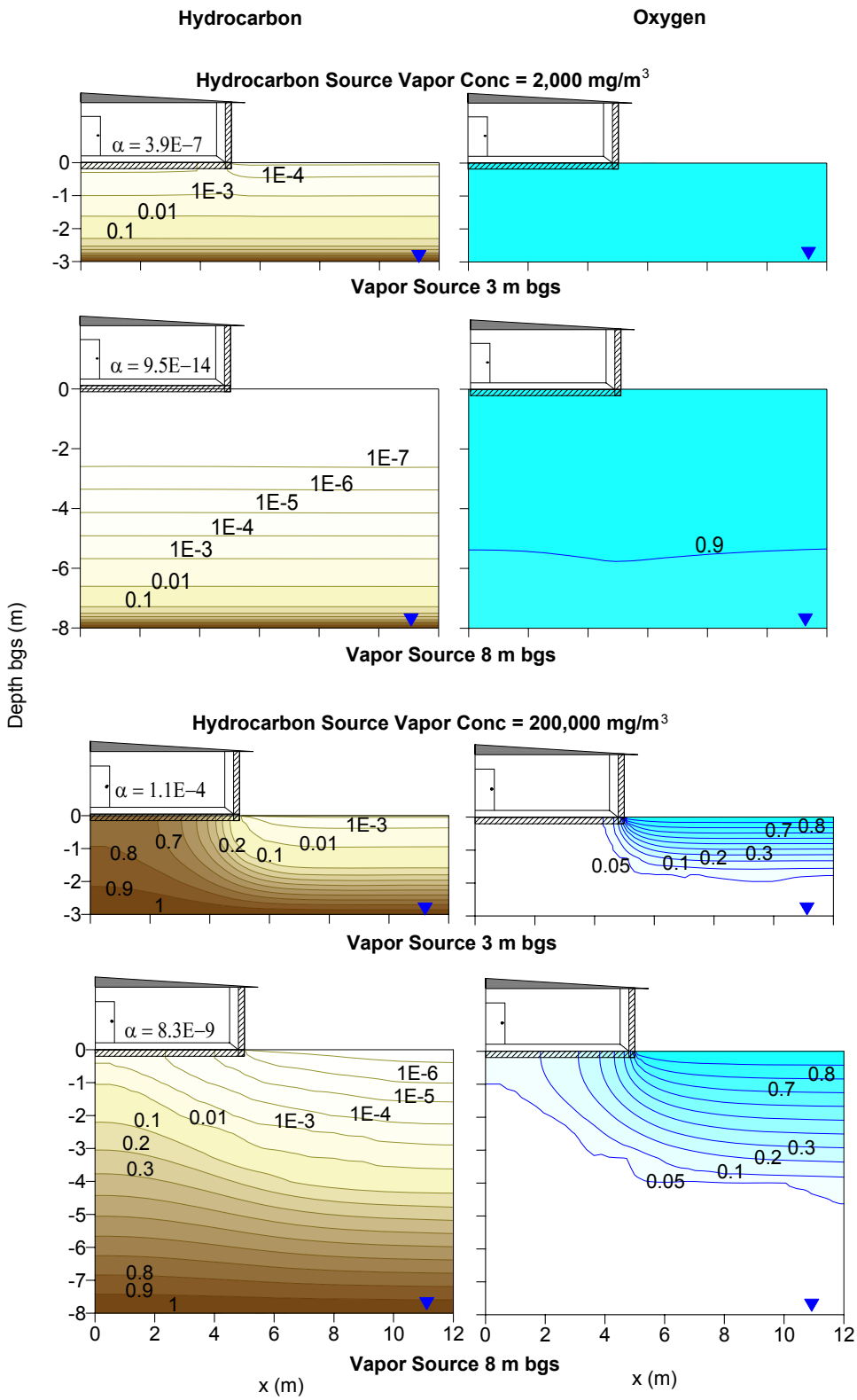

Figure 32. Effect of source depth and vapor concentration on hydrocarbon and oxygen distribution in soil gas and normalized indoor air concentration (α) for a slab-on-grade building.
Hydrocarbon and oxygen concentration contour lines are normalized by source and atmospheric concentrations, respectively. The hydrocarbon vapor source is at 8 m bgs. Biodegradation rate (λ) = 0.18 h^{-1}.

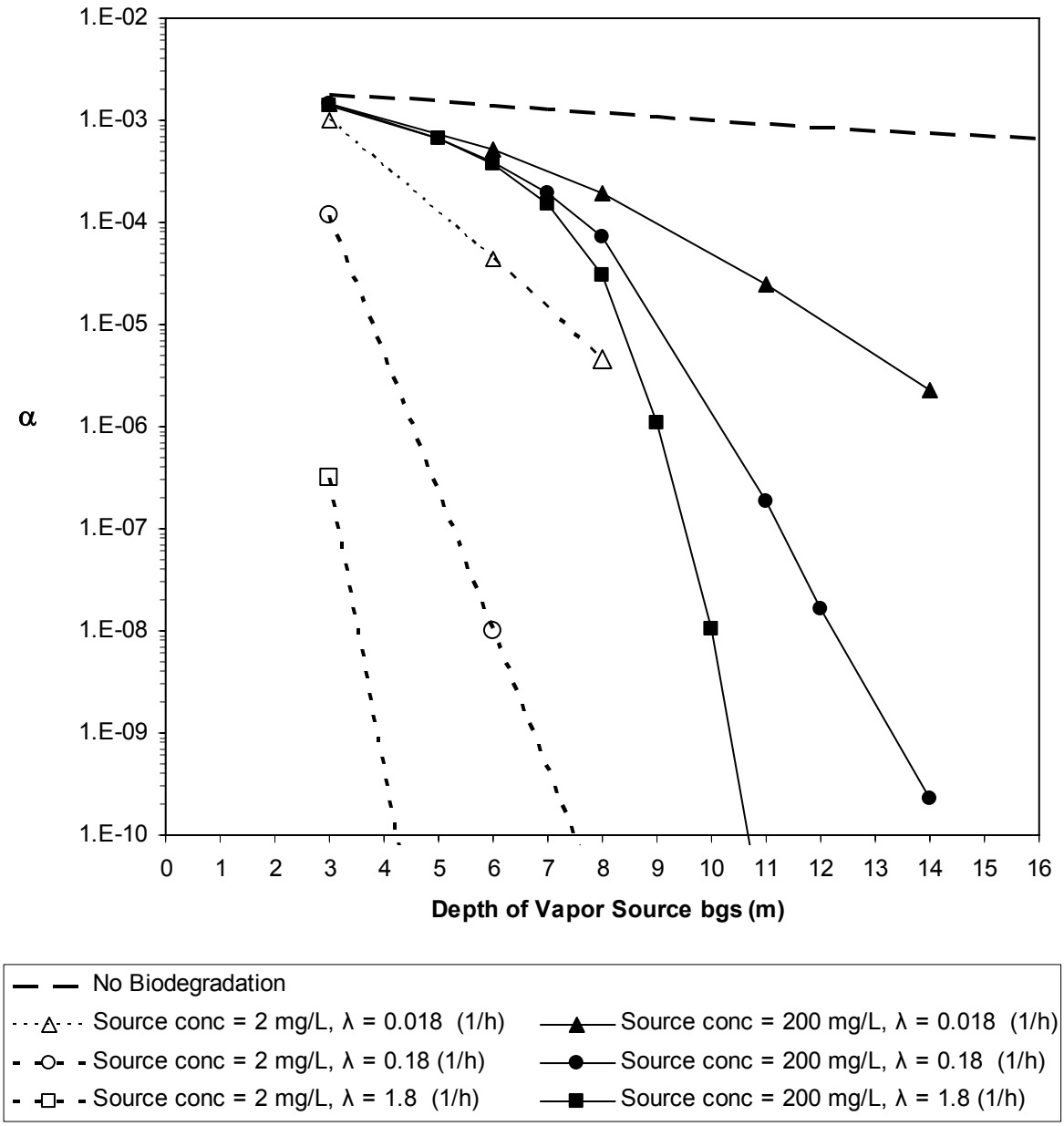

Figure 33. Relationship between source depth and normalized indoor air concentration (α) for a building with basement, two source vapor concentrations, and three biodegradation rates (λ) .
(Abreu and Johnson, 2006)

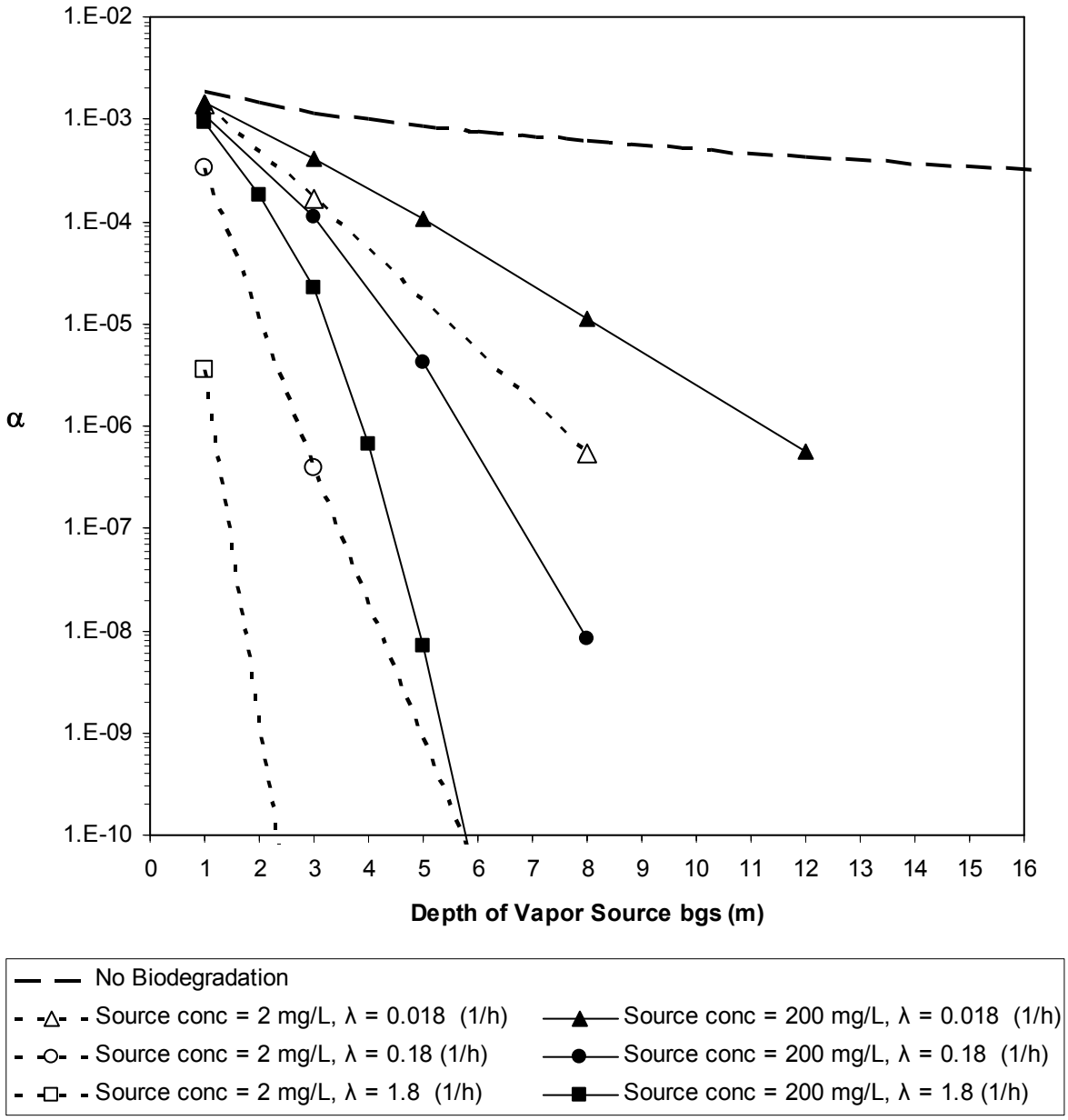

Figure 34. Relationship between source depth and normalized indoor air concentration (α) for a slab-on-grade building, two source vapor concentrations, and three biodegradation rates (λ).
(Abreu and Johnson, 2006)

5.3 Source Lateral Distance from Building

The figures in this section illustrate how the source depth and location influence soil vapor and indoor air contaminant concentrations for very concentrated (i.e., NAPL) biodegradable sources. Because the foundation slab inhibits downward diffusion of oxygen, biodegradation is likely to be more complete at settings where there is a lateral separation between the NAPL source and the base of the foundation than at settings where the NAPL source is below the foundation (**Figure 35**). Plots of normalized indoor air concentrations for a variety of conditions at a structure with a basement and a NAPL source are depicted in **Figure 36**. (*For comparisons with scenarios where the VOCs are recalcitrant, see **Figures 9** through **11**.*)

The effect of source-building lateral distance for aerobically biodegradable chemicals is illustrated in **Figure 35** for the basement scenario, a source vapor concentration representative of a weathered gasoline NAPL source (200 mg/L), two source depths (3 and 8 m bgs), and two lateral source-building separations (a source directly beneath the building basement on the left, and a source 5 m away from the edge of the building basement, on the right). The profiles show that a relatively small source-building lateral separation can result in a very large reduction in the normalized indoor air concentrations (α) for both shallow and deep sources, provided that the ground surface is open to allow oxygen to enter the subsurface.

Normalized indoor air concentrations for a broader set of source-building lateral distances and biodegradation rates are presented in **Figure 36** for the basement scenario, a source vapor concentration of 200 mg/L, and two source depths (3 and 8 m bgs). Figure 36 shows that the normalized indoor air concentrations decrease with increasing lateral distance and increasing biodegradation rates. If the source (or part of it) lies beneath the building (i.e., the source edge-building center lateral separation ranges from −15 to 5 m in Figure 36), normalized indoor air concentrations are relatively unaffected by the location of the source edge, but as the lateral distance increases and the source edge is no longer beneath the foundation (i.e., the source edge-building center lateral separation is >5 m), the effect of biodegradation may result in a large reduction in the normalized indoor air concentrations for both the shallow and deep sources at high concentrations representative of a weathered gasoline NAPL source, provided that the ground surface is open to supply oxygen to the subsurface. Figure 36 also shows that biodegradation may reduce the normalized indoor air concentrations by ten or more orders of magnitude compared with the no biodegradation case.

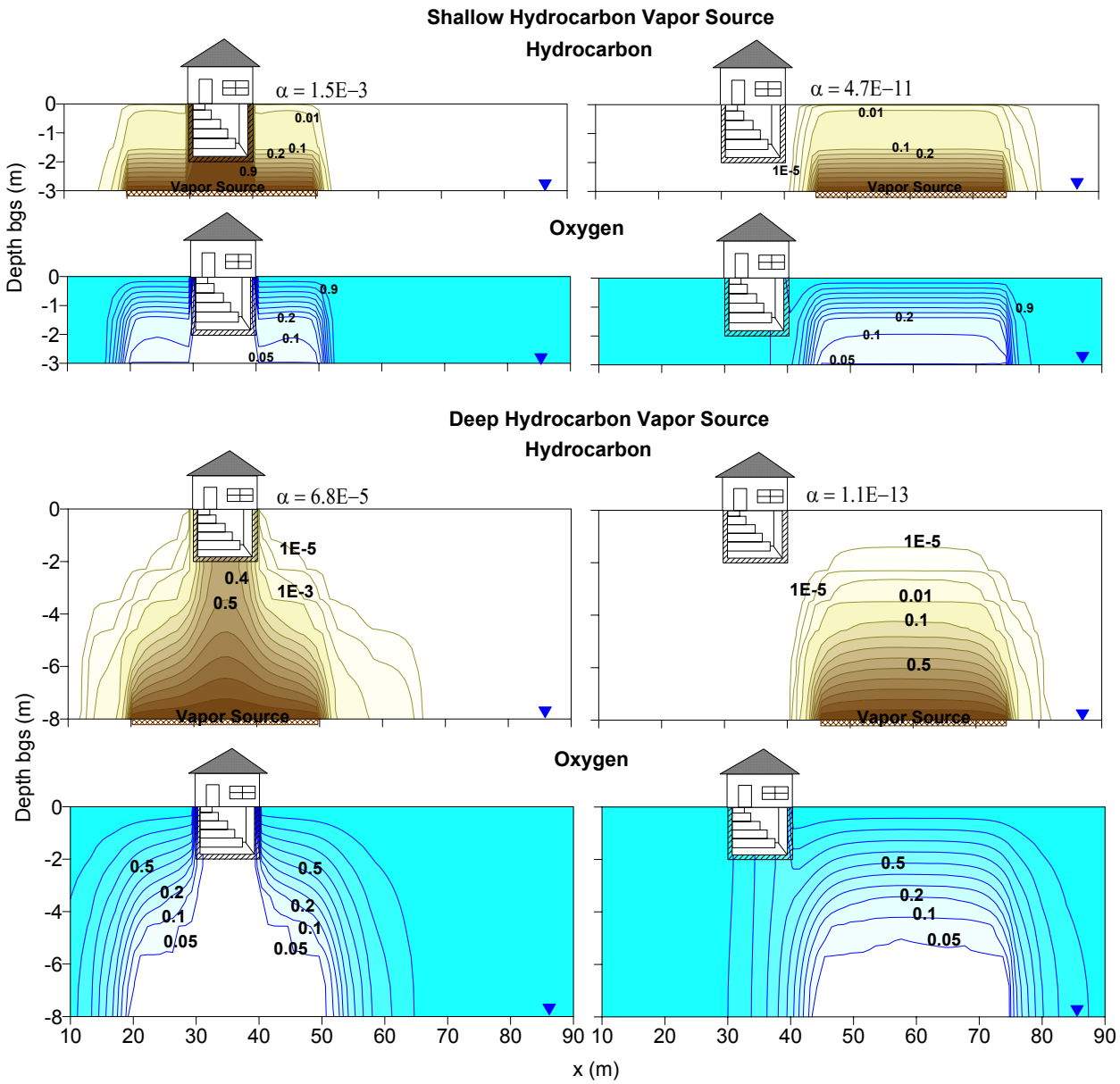

Figure 35. Effect of source depth and source-building lateral separation distance on the distribution of hydrocarbon and oxygen in soil gas for a NAPL source

Hydrocarbon and oxygen concentration contour lines are normalized by source and atmospheric concentrations, respectively. The source vapor concentration is 200 mg/L at two groundwater depth (3 m and 8 m). α is the normalized indoor air concentration (basement scenario). Biodegradation rate (λ) = 0.18 h^{-1}.

(Abreu, 2005)

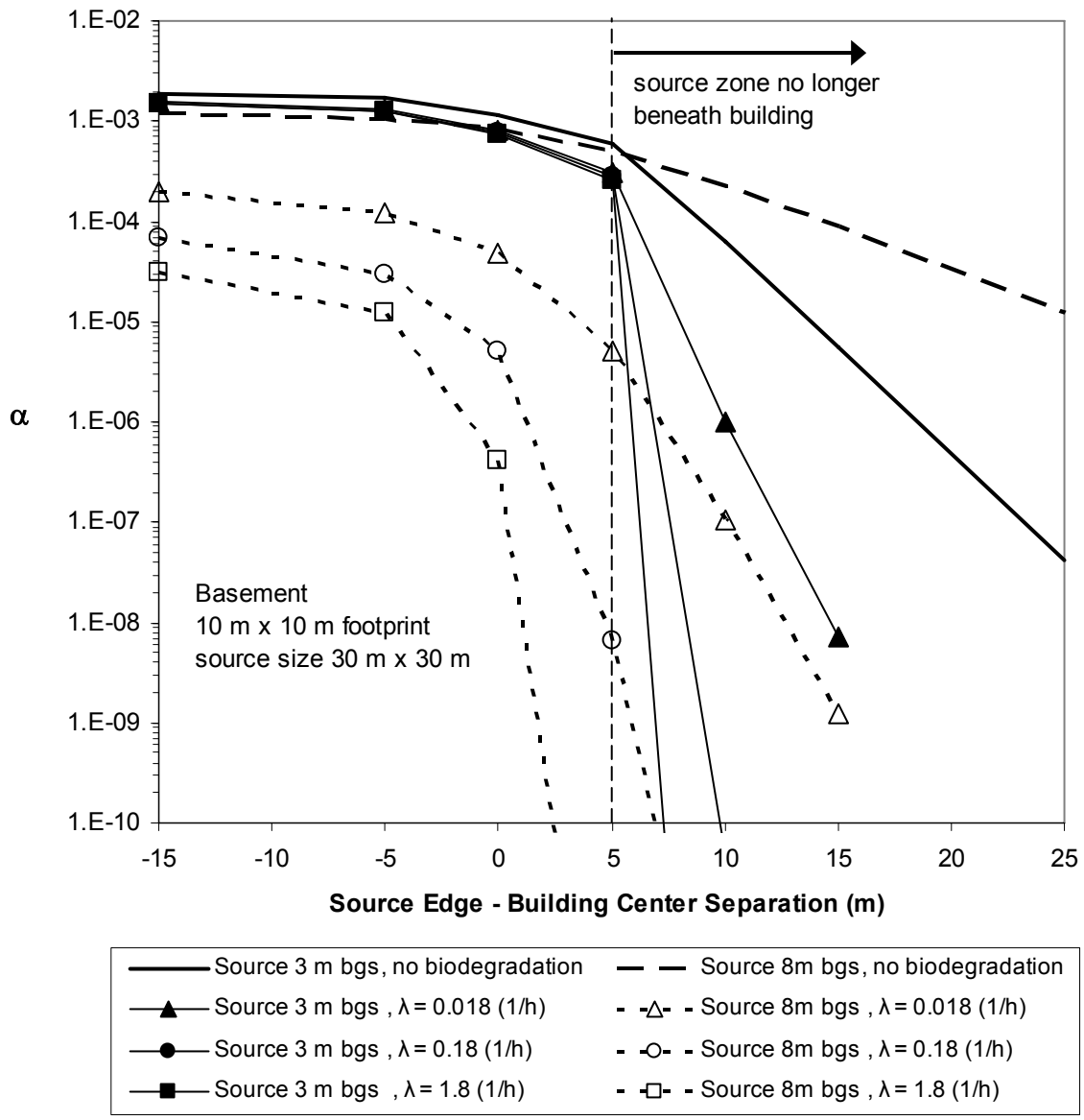

Figure 36. Relationship between source-building lateral separation distance and normalized indoor air concentration (α) for a NAPL source, two source depths, and three biodegradation rates (λ).

The source-building lateral separation is measured from the edge of the source zone to the center of the building with a basement; negative values and values <5 m indicate that the source is to some extent beneath the building. The source vapor concentration is 200 mg/L.

(Abreu, 2005)

5.4 Moisture Content in Layered Soil

The figures in this section use a single-building scenario to illustrate how nonhomogeneous soils (i.e., soils with layers of higher and lower moisture and associated soil gas permeability) can impact oxygen penetration and biodegradable hydrocarbon concentrations in soil gas in the vicinity of a building. The impact of the layers on the hydrocarbon and oxygen distributions depends on their location relative to the source and the building foundation, as well as the source strength. The degree of oxygen penetration also depends on whether the building is under-pressurized or over-pressurized. **Figure 37** depicts conditions with different soil configurations and a weathered NAPL source. **Figure 38** depicts conditions with low permeability materials at the ground surface for both a weathered NAPL source and a dissolved groundwater source. (*For comparisons with scenarios where the VOCs are recalcitrant, see **Figures 19** and **20**.*)

This section presents simulations illustrating the predicted effect of soil moisture content distribution on vapor transport and indoor air concentrations of aerobically biodegradable compounds for scenarios with a single building and a uniform vapor source at groundwater level (8 m bgs). The simulations were performed for buildings under- and over-pressurized to evaluate the predicted effect of steady air flow into and out of the building. The conceptual model scenarios simulated are the same as those presented in Figure 19a, and the predicted pressure field and soil gas flow rate (Qs) are the same as those presented in Figure 19b. As previously discussed, the moisture content in the soil affects vapor transport by diffusion (the diffusion coefficients decrease with increased moisture content) and may also affect advective transport because of lower permeability in higher moisture content soils. Moisture content of the soil will similarly affect the downward migration of oxygen from the atmosphere into the subsurface.

Figure 37 presents the soil vapor concentration profiles and indoor air concentrations predicted for a source strength representative of a weathered gasoline NAPL source (200,000 mg/m^3) vapor concentration (Johnson et al., 1990). For the homogeneous scenario (Scenario A), oxygen is depleted below the slab for both building pressurization conditions, and the hydrocarbon concentrations beneath the slab are not reduced by biodegradation. In Scenario B, with high-moisture content layers between the source and the foundation and a low-moisture content layer extending from the ground surface down to below the foundation, the contaminant migration toward the foundation is reduced and the oxygen supply beneath the slab is sufficient to promote biodegradation for both building pressurization conditions. In Scenario C, with high-moisture content layers between the source and the foundation and a high-moisture layer at the ground surface, oxygen is depleted below the foundation when the building is under-pressurized, but when the building is over-pressurized, the oxygen supply beneath the slab is sufficient to allow biodegradation. In Scenario D, with a high-moisture layer at the ground surface and a low-moisture content layer in the remaining subsurface, oxygen is depleted throughout the subsurface and no aerobic biodegradation is predicted to occur.

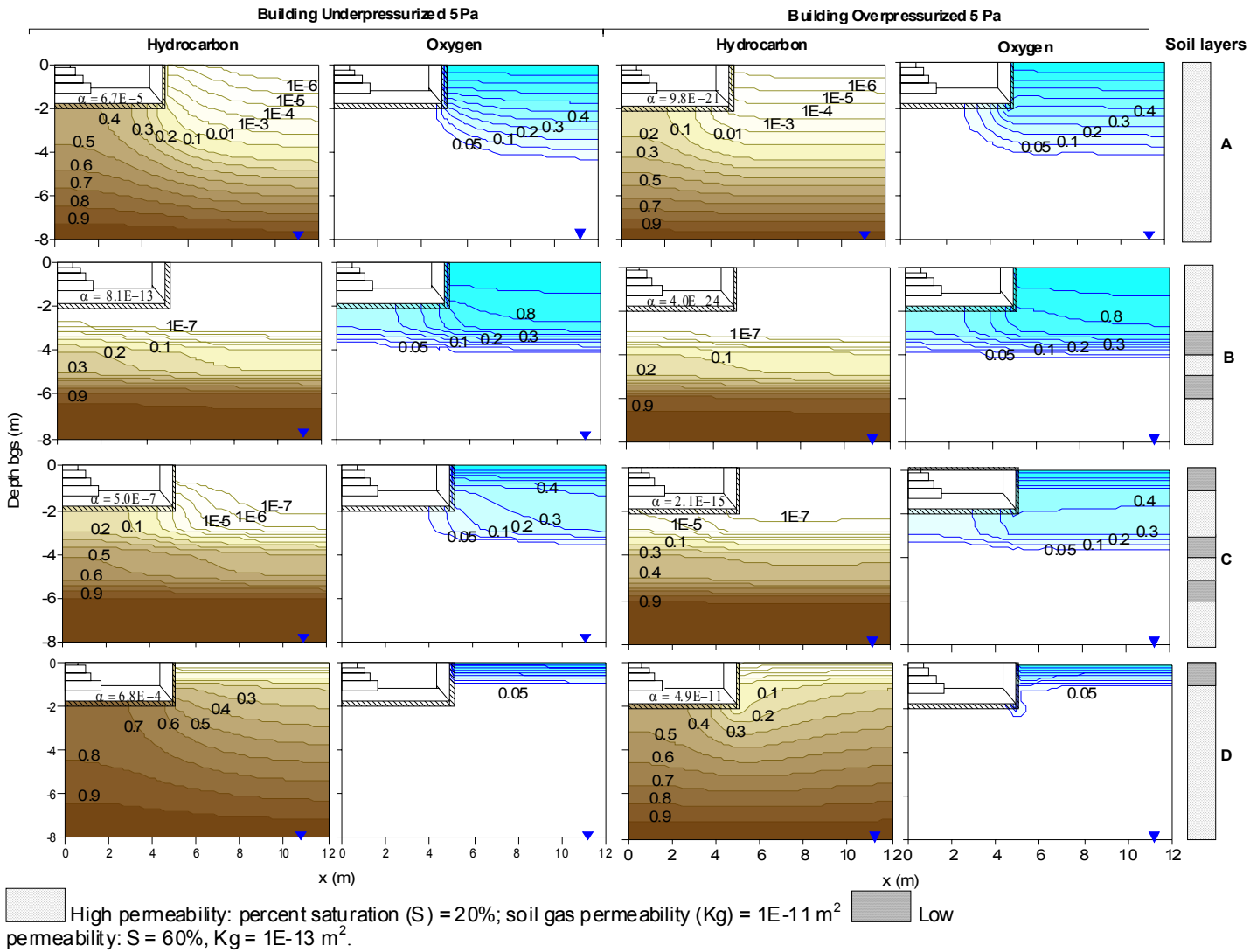

Figure 37. Effect of layered soils (rows A–D) on hydrocarbon and oxygen distribution in soil gas and normalized indoor air concentration (α) for two building pressures (basement scenario).

Hydrocarbon and oxygen concentration contour lines are normalized by source and atmospheric concentrations, respectively. The source vapor concentration is 200 mg/L located 8 m bgs. Biodegradation rate (λ) = 0.18 h^{-1}.

Note that the source concentration in Figure 37 is representative of weathered gasoline NAPL, which was used here to illustrate the regions of oxygen depletion. For dissolved groundwater sources (with lower source concentration), it is likely that the oxygen supply in the subsurface would be sufficient to allow biodegradation in most scenarios, provided that the soil above the source is clean (i.e., does not contain residual NAPL or any other second source of hydrocarbons that could deplete oxygen) and there are no physical or geologic barriers to oxygen entry to the subsurface. This conclusion generally agrees with the findings from field data analysis by Davis (2009). **Figure 38** illustrates the profiles predicted for a weathered gasoline NAPL source (200 mg/L vapor concentration) and for a dissolved groundwater source (2 mg/L vapor concentration), assuming Scenario D with a high moisture content layer on the ground surface and the building under-pressurized by 5 Pa. The predicted concentration profiles and normalized indoor air concentrations (α) show that, for the lower concentration source, there is sufficient oxygen in the subsurface, such that aerobic biodegradation reduces the contaminant concentration by nine orders of magnitude.

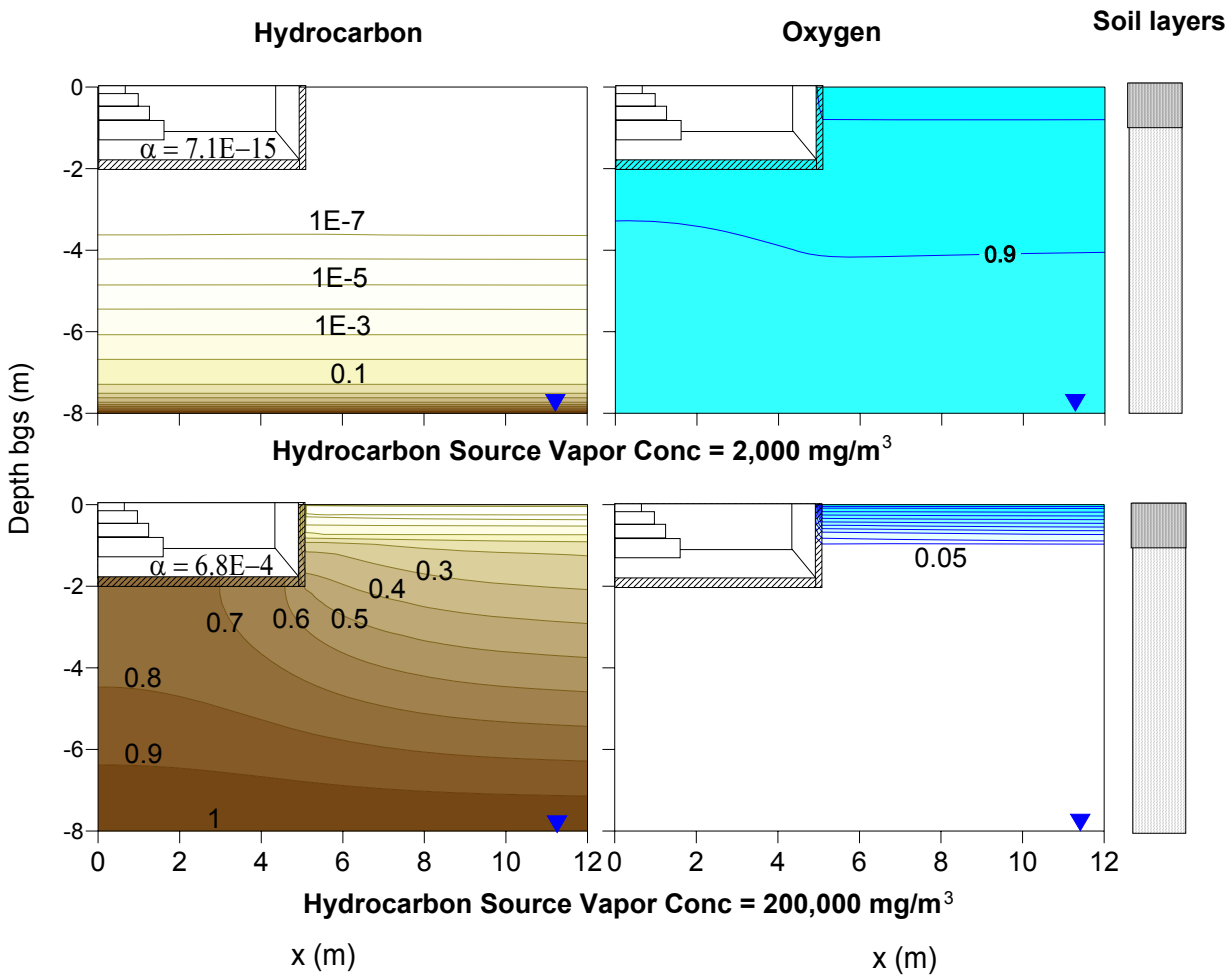

Figure 38. Effect of source vapor concentration on hydrocarbon and oxygen distribution in soil gas and normalized indoor air concentration (α) for scenarios with low permeability soils at the ground surface (e.g., soil layer scenario on row D of Figure 37).

Hydrocarbon and oxygen concentration contour lines are normalized by source and atmospheric concentrations, respectively. Source located at 8 m bgs (basement scenario). Biodegradation rate (λ) = 0.18 h^{-1}.

5.5 Geologic Barrier

The simulations in this section further illustrate how nonhomogeneous soil conditions can impact biodegradable hydrocarbon concentrations in soil gas. These simulations expand on the concepts in Section 5.4. by depicting the influence of low permeability soil layers that can act as "barriers" to gas migration (which are modeled here as soil layers with 95% pore water saturation) over a broad range of soil layering profiles for a vapor source at groundwater table at 5 m bgs and a building with a basement. The simulations illustrate that, depending on the location of the barrier relative to the source and the foundation, up to several orders of magnitude decrease in concentrations can occur between the area beneath a geologic soil barrier and the area above it for NAPL sources (**Figure 39**). They also illustrate that, despite the presence of a barrier, enough oxygen may penetrate the subsurface to effectively diminish the concentration of degradable VOCs in settings where the source strength concentrations are in the dissolved phase range (**Figure 40**). (*For comparisons with scenarios where the VOCs are recalcitrant, see **Figure 25**.*)

As illustrated in **Section 4.4.4** for recalcitrant chemicals, a low permeability geologic barrier may reduce the soil vapor concentration above it by at least one order of magnitude. This section examines the effect of geologic barriers for aerobically biodegradable compounds. The same conceptual models presented in Figure 25 are used in the simulations presented in this section (e.g., the barrier layer is assumed to be at 95% water saturation). As noted in Section 4.4.4, the particular properties assumed for the barriers in these simulations may or may not be typical of most sites but will serve to illustrate how a low permeability soil layer can influence the distribution of VOC concentrations in the subsurface and indoor air.

The source vapor concentration has a substantial effect on the predicted concentration profile of aerobically biodegradable chemicals. Therefore, simulations are presented here for two source types: a NAPL source with 200 mg/L vapor concentration and a dissolved groundwater source with a 2 mg/L vapor concentration. The predicted hydrocarbon and oxygen concentration profiles and normalized indoor air concentrations (α) are presented in **Figure 39** for the NAPL source and **Figure 40** for the dissolved groundwater source. The profiles suggest that, compared with homogeneous subsurface conditions, a geologic barrier may reduce the soil vapor concentration above it by many orders of magnitude for aerobically biodegradable hydrocarbons, provided that sufficient oxygen is present in the subsurface.

The results presented in Figure 39 for the weathered gasoline NAPL source show that in Scenario B, where the geologic barrier extends below the foundation, the normalized indoor air concentration is reduced by more than three orders of magnitude compared with the homogeneous case, because oxygen penetrates entirely below the foundation, allowing biodegradation and reducing the hydrocarbon concentration. For scenarios where the geologic barrier does not extend below the foundation (Scenarios C and D), oxygen is depleted below the foundation, no aerobic biodegradation is occurring there, and the predicted normalized indoor air concentrations are similar to the homogeneous case. The results presented in Figure 40 for the dissolved groundwater source show that predicted oxygen concentrations are elevated for all scenarios and that aerobic biodegradation reduces the vapor concentration in the subsurface and indoor air by many orders of magnitude, regardless of the location of the geologic barrier and how it extends beneath the foundation.

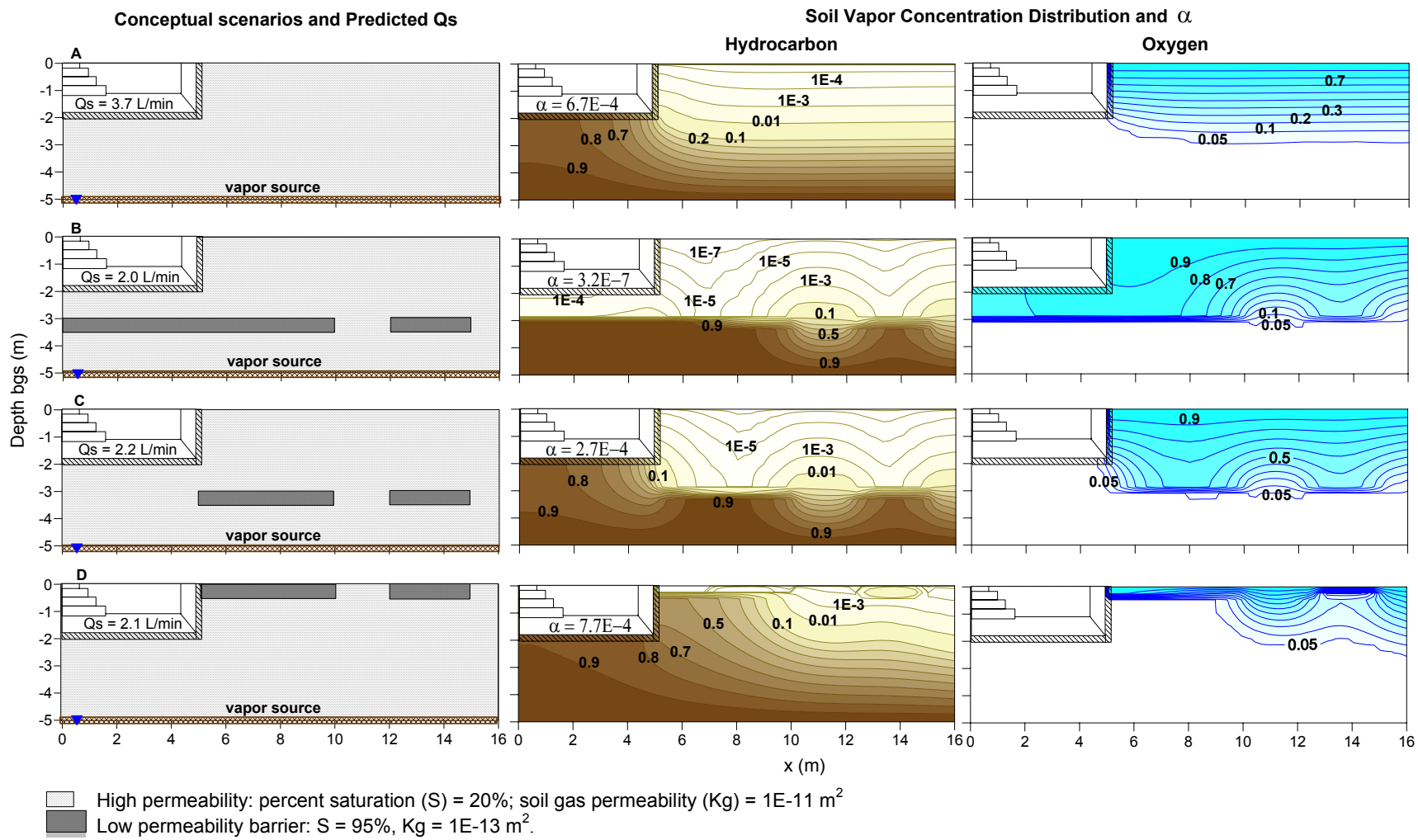

Figure 39. Effect of geologic barriers on hydrocarbon and oxygen distribution in soil gas and normalized indoor air concentration (α) for a NAPL source at 5m bgs.

Hydrocarbon and oxygen concentration contour lines are normalized by source and atmospheric concentrations, respectively. Source vapor concentration is 200 mg/L (basement scenario). Biodegradation rate (λ) = 0.18 h^{-1}. Qs is the soil gas flow rate predicted for building under-pressurized by 5 Pa. (Abreu et al., 2006)

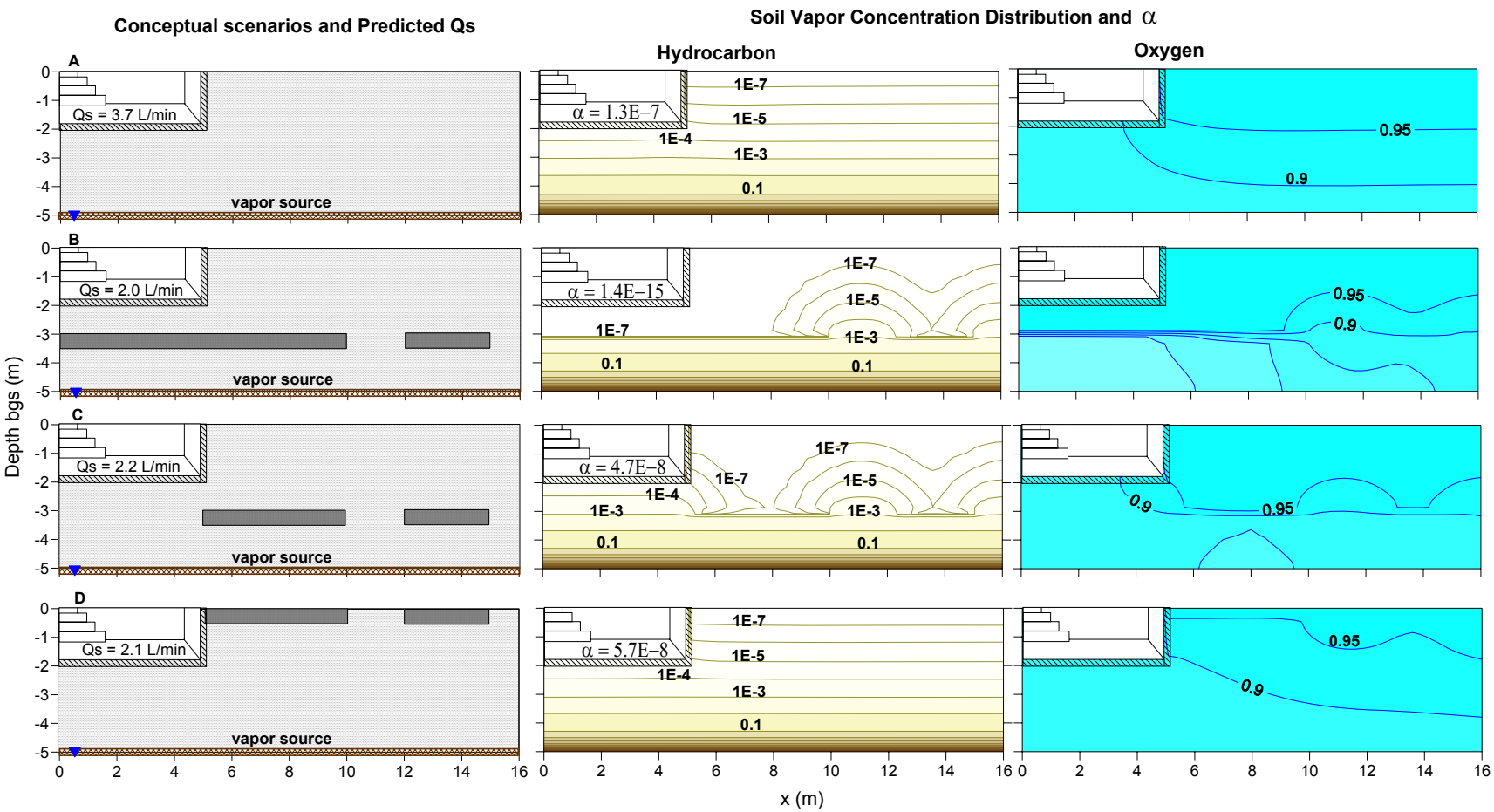

High permeability: percent saturation (S) = 20%; soil gas permeability (Kg) = 1E-11 m^2
Low permeability barrier: S = 95%, Kg = 1E-13 m^2.

Figure 40. Effect of geologic barriers on hydrocarbon and oxygen distribution in soil gas and normalized indoor air concentration for a dissolved groundwater source at 5m bgs.

Hydrocarbon and oxygen concentration contour lines are normalized by source and atmospheric concentrations, respectively. Source vapor concentration is 2 mg/L (basement scenario). Biodegradation rate (λ) = 0.18 h^{-1}. Qs is the soil gas flow rate predicted for building under-pressurized by 5 Pa.

6.0 Temporal and Spatial Variability in Subsurface and Indoor Air Concentrations

The figures in this section depict scenarios that illustrate possible temporal and spatial changes in the distribution of VOCs and the factors that can lead to those changes.

This section discusses the temporal and spatial variability that may occur in the subsurface, sub-slab, and indoor air concentrations caused by several factors: transient transport after a source is released, wind load on a building, fluctuations in atmospheric and indoor air pressures, and seasonal phenomena (e.g., rainfall events, fluctuation on water table elevation). Other conditions that result in spatial variability, such as sources located laterally away from buildings and discontinuous layers, have already been illustrated in previous sections.

6.1 Transient Transport Following Source Release

The simulations presented thus far assume that the vapor source has been in place long enough to fully develop the soil gas profiles (or reach near–steady-state conditions). Johnson et al. (1999) developed a simplified equation to estimate the time necessary to achieve near–steady-state subsurface vapor distributions and estimated that sites with shallow vapor sources (<1 m depth) take only a few hours to a few days to reach near–steady-state conditions. Sites with deeper vapor sources (>10 m depth) may take months or years to reach steady-state conditions. Aerobic biodegradation may reduce the time to reach steady-state soil gas distributions because once the VOCs are degraded, their migration path is shorter to the point that VOC concentrations are reduced substantially.

The time required for vapors to reach near-steady concentrations at any location in the subsurface increases with the square of the distance from the source. It is also affected by the chemical properties of the compound of interest. Johnson et al. (1999) developed a graph that provides the time for a non-retarded chemical to reach near-steady vapor concentrations (τ_{ss}/R_v) as a function of soil type and distance to the source (**Figure 41**). This graph can be used for any chemical, and the retardation time for any specific chemical can be calculated by multiplying τ_{ss}/R_v by the chemical retardation factor (R_v), which is calculated as follows:

$$R_v = \left(1 + \frac{\phi_w}{\phi_g H_n} + \frac{K_{oc,n} \cdot f_{oc} \cdot \rho_b}{\phi_g H_n}\right) \tag{1}$$

where

ϕ_w = water-filled porosity (m^3 water/m^3 soil)
ϕ_g = gas-filled porosity (m^3 gas/m^3 soil)
ρ_b = soil bulk density (kg soil/m^3 soil)
H_n = Henry's law constant for chemical *n* ([kg chemical/m^3 gas]/[kg chemical/m^3 water])
$K_{oc,n}$ = sorption coefficient of chemical n to organic carbon ([kg chemical/kg OC]/[kg chemical/m^3 water])
f_{oc} = mass fraction of organic carbon in the soil (kg OC/kg soil).

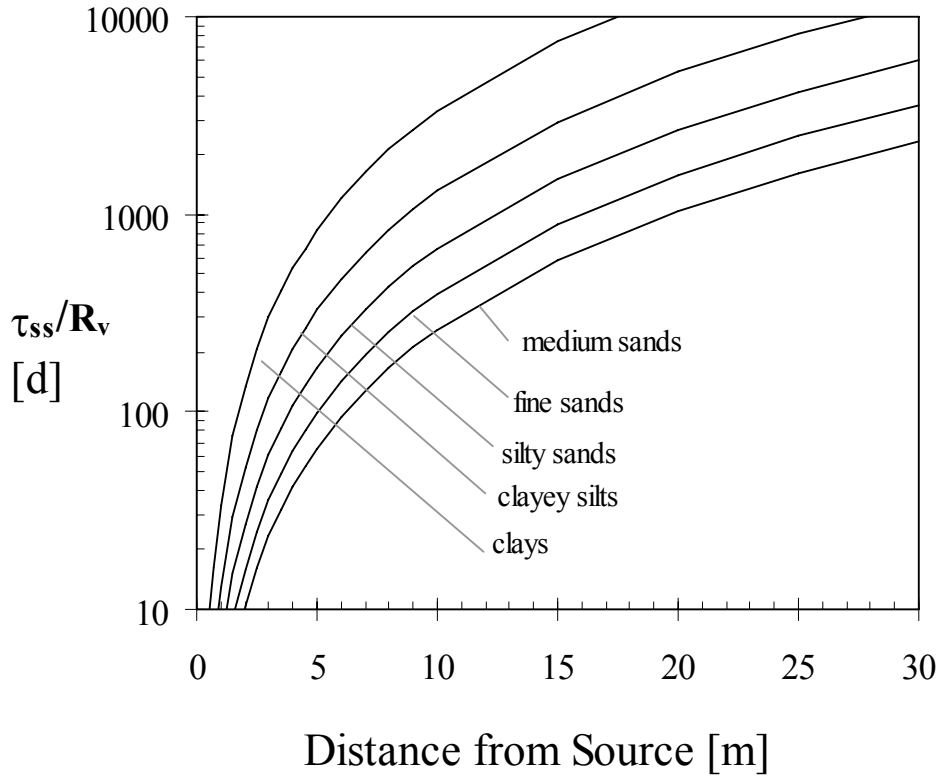

Figure 41. Estimated time (y-axis, d=days) for chemicals to reach near-steady vapor concentrations (τ_{ss}) as a function of the distance from a source. Time on the plot is normalized by the retardation factor (Rv).
(Johnson et al., 1999)

The sub-sections below provide examples illustrating the variation in concentration profiles with time following the release of the vapor source. The effect of moisture content and distribution on transient profiles is presented first, followed by an example illustrating how sorption of the VOCs to soil organic carbon (foc) attenuates the VOCs in the subsurface.

6.1.1 Effect of Moisture Content on Transient Transport

The figures in this section illustrate how the moisture content of the soils may impact VOC distributions through time after a source is released and vapors migrate beneath a structure. They include simulations where the groundwater vapor source is 8 m below the surface (**Figure 42**) and where it is 3 m below the surface (**Figure 43**). They also include simulations with a variety of layered soils and multiple building distances from the source (**Figure 44**). Areas closer to the source achieve near-steady conditions sooner than those farther away. Drier soils achieve near-steady conditions more quickly than soils with higher moisture content. Soil layers with higher moisture content can delay attainment of near-steady conditions in soils above them.

The effect of soil moisture content on the transient concentration profiles in the subsurface is described here for recalcitrant vapor sources located at groundwater level. In this case, the vapor migration may occur upwards toward the ground surface or laterally to regions of lower concentration. Simple scenarios involving a single building with a basement and a large source directly beneath the building illustrate the transient upward migration of vapors. Two homogeneous soils with pore water saturations (S) of 20% and 60% and two source depths (3 m and 8 m bgs) were used in the simulations. In all scenarios, the buildings were assumed to be at constant atmospheric pressure conditions and, as a result, the transport is due to diffusion only.

The results presented in **Figure 42** are for an 8 m deep vapor source and show the concentrations at three transport times after the source is released: 1 month, 1 year, and 3 years. In Scenario A, with a lower soil moisture content, the concentrations reach near–steady-state conditions about 1 year after the source release. In Scenario B, the higher soil moisture content leads to a concentration below the slab after 1 year that is more than an order of magnitude lower than in Scenario A. It takes about 9 years for Scenario B to reach steady state.

The results presented in **Figure 43** for a shallow vapor source show that the transport time is shorter if the source is shallow, and it may take just days or a few months to reach steady state. This is consistent with the time frames described by Johnson et al. (1999).

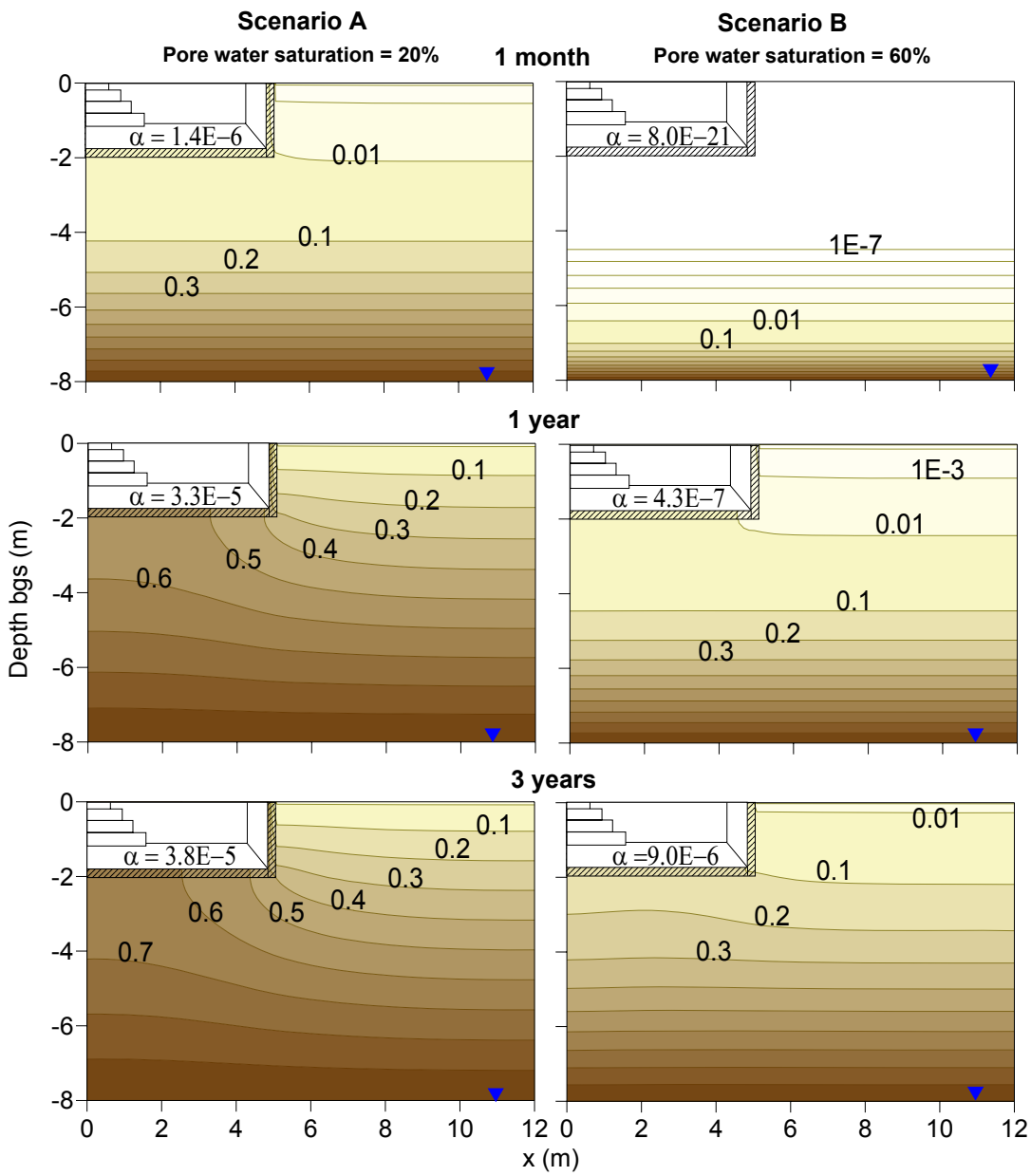

Figure 42. Effect of transport time on soil vapor distribution and normalized indoor air concentration (α) for different soil pore water saturation (deep source, 8 m bgs).
The soil vapor concentration contour lines are normalized by the source vapor concentration. The building is under atmospheric pressure.

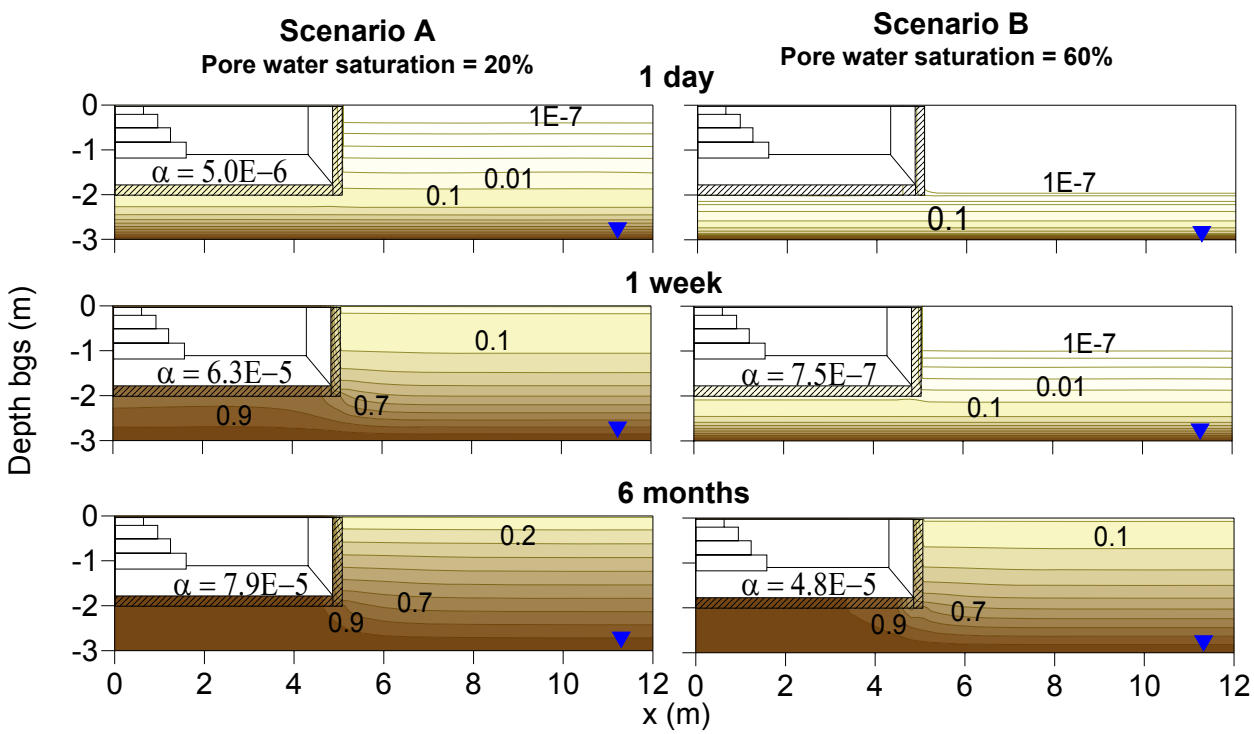

Figure 43. Effect of transport time on soil vapor distribution and normalized indoor air concentration (α) for different soil pore water saturation (shallow source, 3 m bgs).

The soil vapor concentration contour lines are normalized by the source vapor concentration. The building is at atmospheric pressure.

More complex scenarios with multiple buildings and a finite source are presented in **Figure 44** and illustrate the transient upward and lateral migration of vapors. Two scenarios are presented for comparison: Scenario 1 is a homogeneous subsurface with low moisture content and Scenario 2 is a layered subsurface with soil properties as shown in the figure. A vapor source is located at 8 m bgs and extends up to 25 m laterally. Each scenario has three slab-on-grade buildings. Building A has no cracks or openings in the foundation and is located above the vapor source; Buildings B and C have full-length perimeter cracks and are located 5 and 25 m laterally from the source edge, respectively. The buildings are assumed to be at steady atmospheric pressure, and the transport is due to diffusion only.

Figure 44 illustrates the profiles for three transport times after the source is released: 1 month, 1 year, and 3 years. In both scenarios, the concentration close to the source reaches near–steady-state conditions much faster than the concentration farther away from the source. The higher moisture content layer in Scenario 2 affects the soil vapor concentration distribution and increases the transport time. The farther the building is from the vapor source, the longer it takes for the vapor to reach it, and the time increases as the moisture content of the subsurface increases.

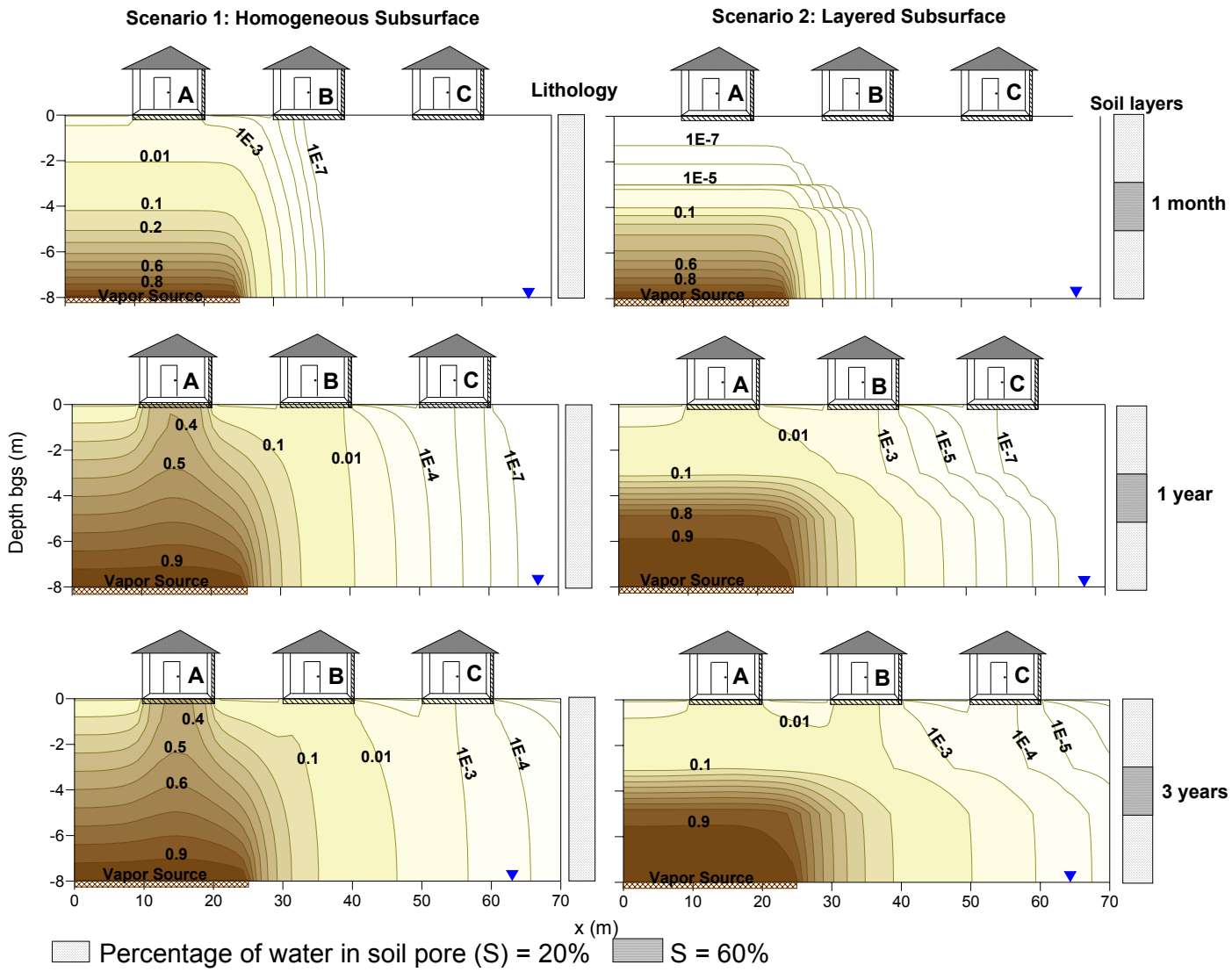

Figure 44. Effect of transport times on soil vapor distribution for scenarios with homogeneous lithology and layered soils, and multiple buildings over spatially finite vapor source.

The soil vapor concentration contour lines are normalized by the source vapor concentration.

6.1.2 Effect of Sorption on Transient Transport

The figures in this section illustrate the effect of soil sorption on the estimated time that vapor concentrations take to reach a near-steady condition after a source is released and vapors migrate beneath a structure (i.e., transient transport) for two different sorption scenarios (**Figure 45**). Soils with higher organic carbon content (foc) and contaminants with higher organic carbon-water partitioning coefficients (Koc) tend to sorb more and, therefore, delay attainment of near-steady conditions.

For transient transport conditions, the mass fraction of organic carbon in soil (foc) and a chemical's sorption coefficient to organic carbon (Koc) determine the amount of the chemical that is adsorbed to the soil particles, which retards chemical transport.

The effects of foc and Koc on the soil vapor concentration distribution under transient transport conditions are illustrated in **Figure 45**. Two scenarios, A and B, are presented for comparison: both include a homogeneous subsurface, but Scenario B has higher foc and Koc values than Scenario A, as shown in the figure. The vapor source of recalcitrant VOC is located beneath the foundation at a depth of 8 m bgs. The scenarios illustrate two buildings with a basement, both of which have full-length perimeter cracks and are at atmospheric pressure conditions, so the transport in the subsurface is due to diffusion.

Figure 45 illustrates the concentration profiles for three transport times after the source is released: 1 month, 1 year, and 3 years. The substantial difference in soil vapor concentration distribution between Scenarios A and B illustrates the strong influence that foc and Koc have on the transient concentration distribution. Higher foc and Koc values increase the transport time; therefore, the concentrations in Scenario B are lower compared with the concentrations in Scenario A at each transport time. The concentrations in Scenario A (lower foc and Koc) reached near–steady-state conditions about 1 year after the source release. In Scenario B, it takes more than 3 years to reach steady-state conditions. The transport time decreases if the source is shallow, and it may take just days or a few months to reach steady state. Once near–steady-state conditions are reached, sorption sites are saturated and the foc and Koc values no longer affect vapor distribution.

At sites with conditions that lead to a greater amount of contaminant sorption (i.e., sites with high soil foc, high-Koc chemicals, or deep sources), changes over time in soil gas profiles might not occur in parallel with changes over time in source conditions, because the available sorption sites will tend to buffer changes in soil gas concentrations over time.

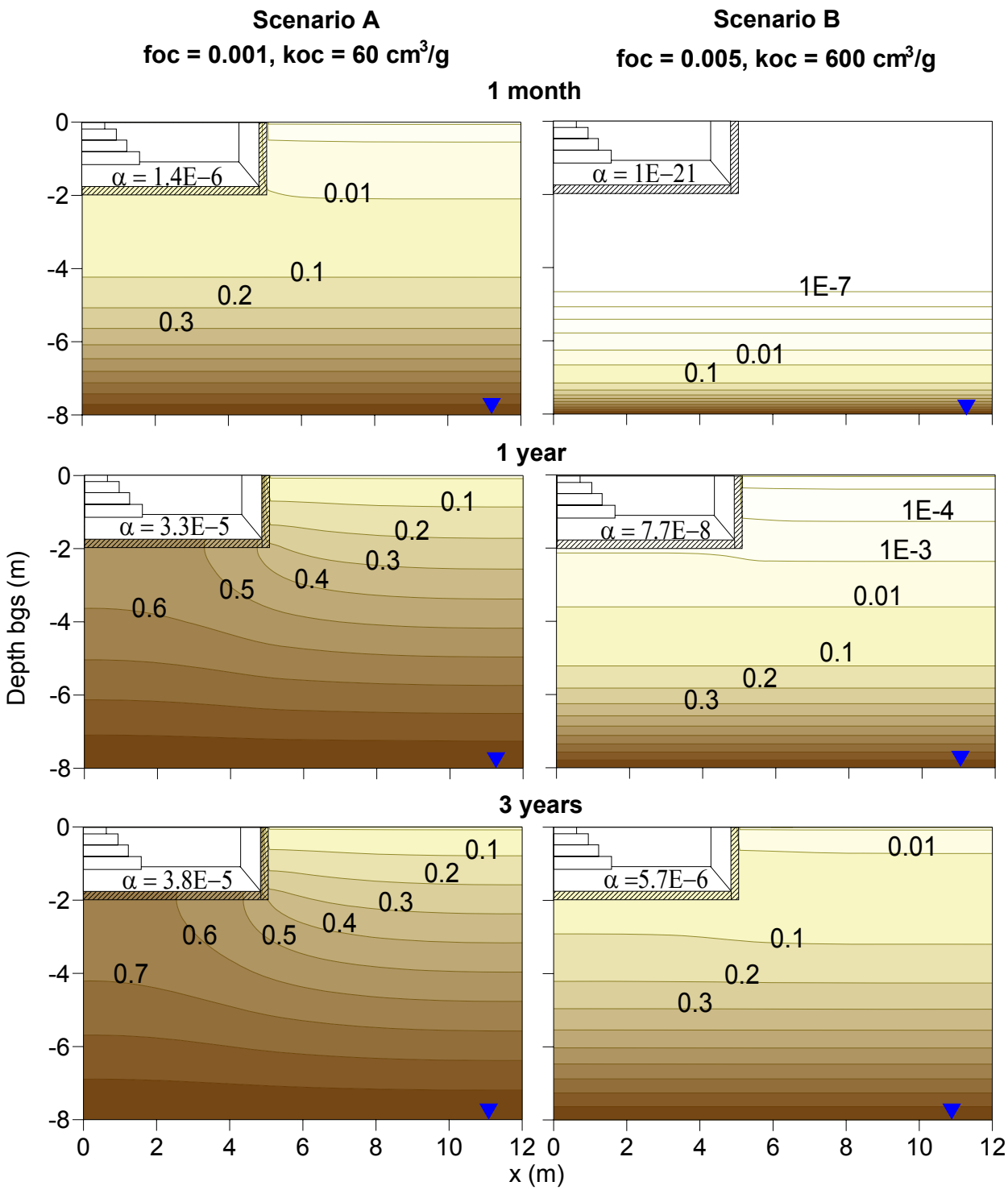

Figure 45. Effect of transport time on soil vapor distribution and normalized indoor air concentrations (α) for scenarios with varying koc and foc.

The soil vapor concentration contour lines are normalized by the source vapor concentration. The building is at atmospheric pressure.

6.2 Wind Load on Buildings

The figures in this section illustrate that the wind load on a building wall can affect the pressure distribution on the ground surface around the building and in its sub-slab (**Figure 46a**), which can affect the sub-slab distribution of recalcitrant and aerobically biodegradable VOCs (**Figure 46b**). Note that these simulations assume steady-state conditions. In reality, the wind load and its concomitant impact on sub-slab VOC concentrations will likely vary over time.

Wind blowing on the walls of a building will create a non-uniform atmospheric pressure distribution on the ground surface. The wind speed falls to zero as it strikes the side of a building, and the change in momentum from the free-stream speed can be related to the increase in pressure at the wall. On the downwind side of the building, the increase in wind speed creates a decrease in pressure. A wind-induced non-uniform pressure distribution on the ground surface on either side of a building may cause spatial and temporal variability in the sub-slab soil vapor concentration distribution. Luo et al. (2006) show this temporal and spatial variability at a site with soils with high soil gas permeability and strong winds. The actual building, soil, and wind data from that site were used as inputs to simulate the effect of wind on the sub-slab soil gas distribution. As described below, the model predictions are consistent with the field data.

To simulate a steady wind load effect, a wind-induced non-uniform pressure distribution at ground surface was applied as a boundary condition to the 3-D model. This pressure distribution was calculated according to the method described by Riley et al. (1999) and Nazaroff and Nero (1988). The simulations were performed for two contamination scenarios, a recalcitrant VOC and a biodegradable hydrocarbon, both with a source vapor concentration of 160 mg/L. The vapor source extends from 2 to 6 m bgs, there is a slab-on-grade foundation, and the water table is 6 m bgs. The soil is homogeneous and has a relatively high gas permeability (1E-10 m^2). The pressure inside the building is assumed to be the same as the free-stream conditions (i.e., gauge pressure is zero). Simulations were performed for two steady wind directions, north and northeast, both at a velocity of 5 m/s (11 mph). The reader is cautioned that, in most areas of the country, wind loads are unlikely to remain at steady directions or velocities for long, and that normal shifts in wind load (i.e., gusts) or direction can change the magnitude and direction of the pressure differentials across a slab.

The wind-induced ground-surface gauge pressure distribution applied as a boundary condition and the predicted sub-slab gauge pressure distribution for each wind direction are presented in **Figure 46a** and suggest about 10 Pa of pressure difference in the sub-surface across building walls in the wind direction. This pressure difference depends on wind speed. The predicted soil gas sub-slab concentration distribution for each wind direction is presented in **Figure 46b** and suggests about two orders of magnitude variability in sub-slab concentrations across the foundation for recalcitrant chemicals and about three orders of magnitude variability for biodegradable hydrocarbons with a high source concentration. The model simulations represent predictions for relatively high soil gas permeability and wind speed. The effect of wind will be less as soil gas permeability and wind decrease (Riley et al., 1996). However, these simulations are performed at steady state, and in reality, wind is variable over time, which would contribute to temporal variability in shallow subsurface vapor concentrations as shown by Luo et al. (2006).

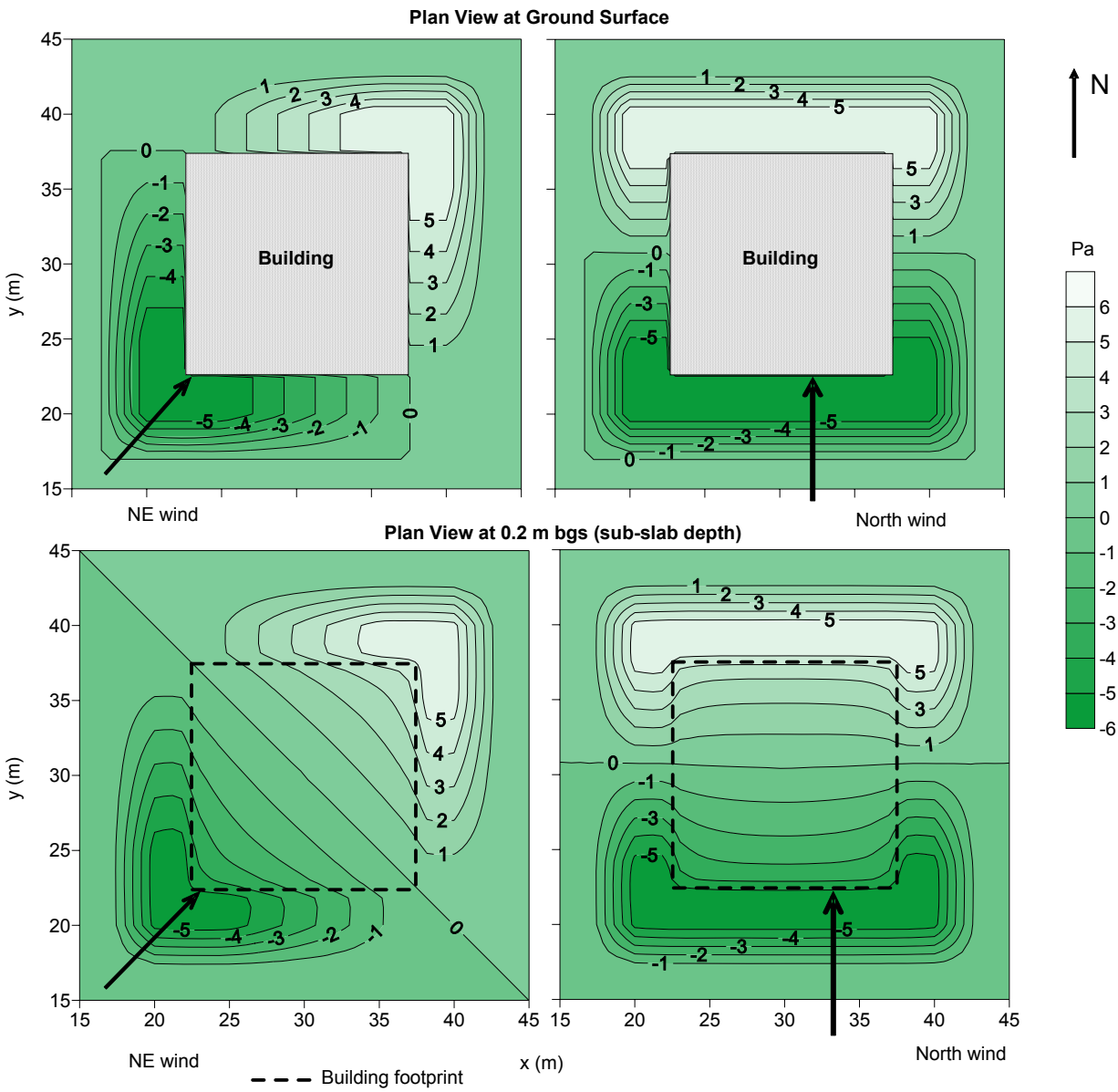

Figure 46a. Effect of building wind load on ground surface and sub-slab gauge pressure distribution.

The gauge pressure contour lines are in Pa; negative values reflect over-pressurization and positive values reflect under-pressurization.

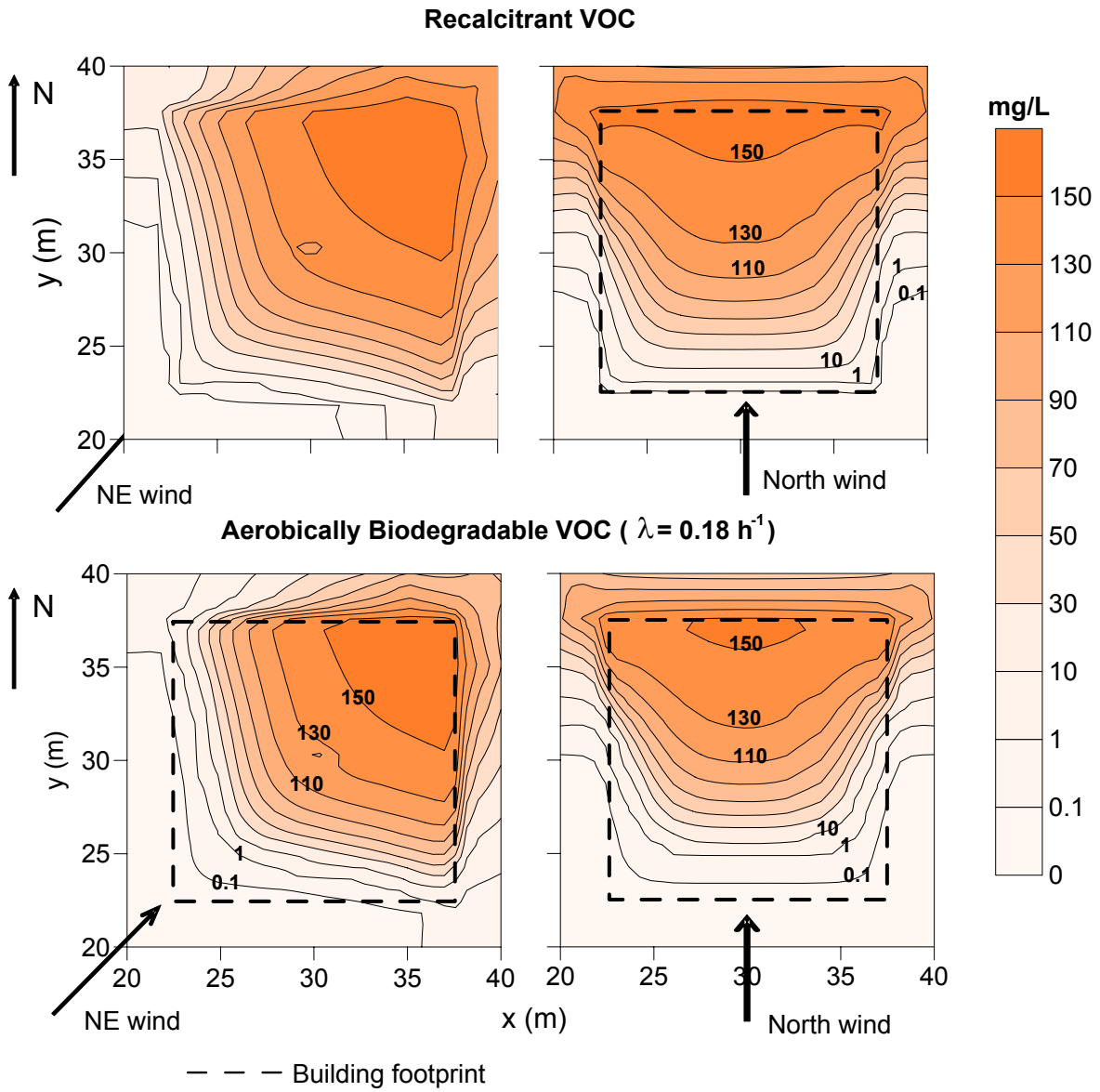

Figure 46b. Effect of building wind load on sub-slab soil vapor distribution for recalcitrant and aerobically biodegradable VOCs.

The vapor concentration contour lines are in mg/L. The source vapor concentration is 160 mg/L. (Abreu et al., 2006)

6.3 Atmospheric and Indoor Air Pressure Fluctuations

The figures in this section illustrate the effect of barometric pressure fluctuations on the transport of soil gas into a building. **Figure 47** depicts the barometric pressure fluctuations that were used in the simulations. **Figure 48** depicts the fluctuations in soil gas–indoor air pressure difference resulting from the barometric pressure cycling, and **Figure 49** depicts the resulting changes in the magnitude and direction of air flow between the sub-slab and the building. As the atmospheric pressure decreases, sub-slab air tends to flow into the building and the indoor concentrations of VOCs increase. As the atmospheric pressure increases, basement air tends to flow into the sub-slab and the indoor air concentrations of VOCs decrease (**Figure 50**). Subslab concentrations also change in response to the magnitude and direction of air flow (**Figure 51**). The air permeability of the sub-slab affects the magnitude of the change in the pressure difference and the flow into or out of the building. The pressure difference between the building and the sub-slab are greater for less permeable soils, but the flow rates are smaller.

Several published studies have demonstrated that barometric pressure fluctuations affect the transport of soil gas into buildings (Robinson and Sextro, 1997; Robinson, Sextro, and Fisk, 1997; Robinson, Sextro, and Riley, 1997; Narasimhan et al., 1990). These atmospheric pressure changes typically occur over several hours and affect the difference between soil gas pressure and indoor air pressure, which is a driving force for vapor intrusion. The magnitude of the induced pressure difference is related to the soil permeability and the magnitude of the barometric pressure changes; the pressure difference generally decreases as the soil permeability increases, and increases as the magnitude and rate of the barometric pressure change increases. The pressure difference between a building and the subsurface may also have higher frequency fluctuations due to changing wind load and lower frequency changes due to changing temperature. Use of doors and windows, ventilation fans, exhaust fans (stovetops, bathrooms), central vacuum cleaners, window-mount air conditioners, and the like can also cause episodic changes in pressure differentials. In combination, these variations in environmental and building conditions lead to complex soil gas–indoor air pressure differential histories and temporal changes in vapor intrusion rates; in some cases, these variations can also lead to flow from the building to the soil (Luo et al, 2006, 2007; Johnson, 2008).

In this section, 3-D model simulations[3] are presented to illustrate that transient fluctuations in the soil gas–indoor air pressure differential can affect air flow rates, indoor air concentrations, and sub-slab vapor concentrations below a slab crack. For the purposes of illustration, a simple idealized scenario was selected in which a sinusoidal barometric cycle fluctuates by 100 Pa over 4 hours (amplitude of 50 Pa and period of 4 hours), as illustrated in **Figure 47**. This idealized barometric cycle does not represent the wide range of barometric pressure behaviors that occur in real-world conditions, and it is used as an example for illustration purposes only.

[3] The simulations used a revised indoor air mixing equation to properly account for the accumulation term resulting from the transient pressure fluctuations. Details are provided in **Appendix A**.

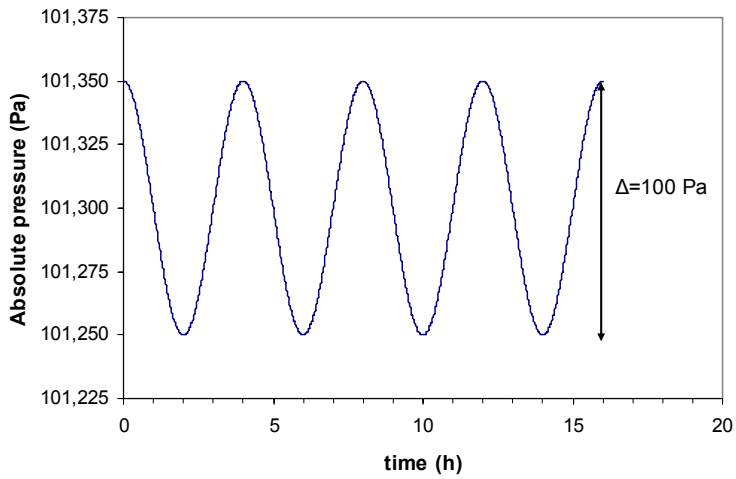

Figure 47. Barometric pressure fluctuations used in the simulations presented in Figures 48 through 51.

Two soil gas permeability conditions were simulated: 1E-12 m^2 and 1E-11 m^2. In each case, the subsurface is homogeneous and a very extensive recalcitrant vapor source with a vapor concentration of 10,000 $\mu g/m^3$ is located 8 m bgs at the water table. The intention is to evaluate the effects of one parameter at a time, so all other parameters that could also influence the results presented here are held constant (e.g., air exchange rates).

In these simulations, building indoor air pressure is set at atmospheric pressure conditions so that the indoor-outdoor pressure differential is always zero. It should be noted that many buildings are naturally under-pressurized relative to ambient conditions, so the assumption of equal indoor and outdoor pressures has implications for the results presented below, in particular the issue of flow reversal (i.e., flow from the building into the soil), which may not occur to the same degree as shown in these simulations.

Figure 48 presents the fluctuations in soil gas–indoor air pressure differential resulting from the barometric pressure cycling. It shows that the soil gas–indoor air pressure differential oscillates between positive and negative values. **Figure 49** shows that in response to the transient fluctuations of the soil gas–indoor air pressure differential, the air flow rate also oscillates with approximately the same period, with the air flow reversing direction at times when the indoor air pressure exceeds the soil gas air pressure. This aspect of the model behavior is related to prescribing equal indoor and outdoor pressures and would not occur in a situation where the baseline building under-pressurization is greater than the soil gas–indoor air pressure differentials seen in these simulations.

Figures 50 and **51** show that, when there is a reversal of flow direction from the building into the soil, then the indoor air and the vapor concentration right below the slab crack may also oscillate. For the simulations involving the higher air permeability, the indoor air concentration varies within a factor of three (from 2 to 6 $\mu g/m^3$), and the sub-slab soil gas concentration variation is within 40% (from 3,000 to 4,200 $\mu g/m^3$). These results are specific for the conditions simulated. As the soil gas permeability decreases, the range of temporal variation in air flow rates and concentrations decreases as well.

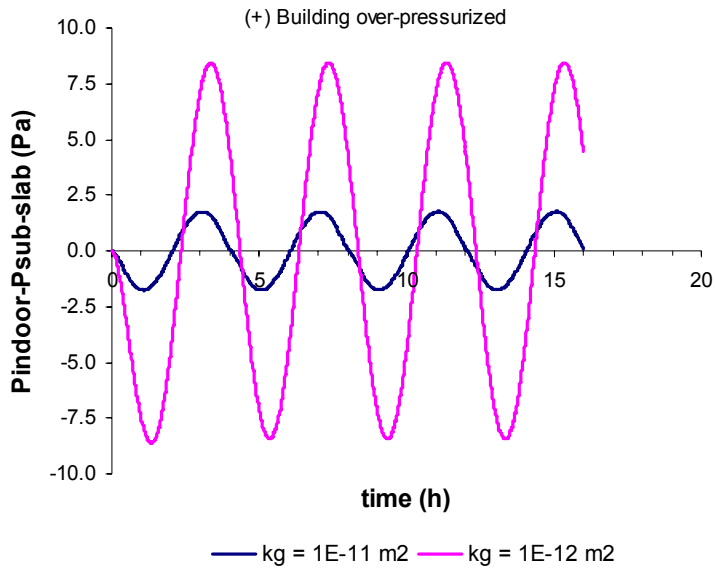

Figure 48. Temporal variation in the pressure difference between indoor air and sub-slab air resulting from fluctuations in barometric pressure (Figure 47) for two soil types.
Soil gas permeabilities (kg) of 1E-12 m^2 and 1E-11 m^2.

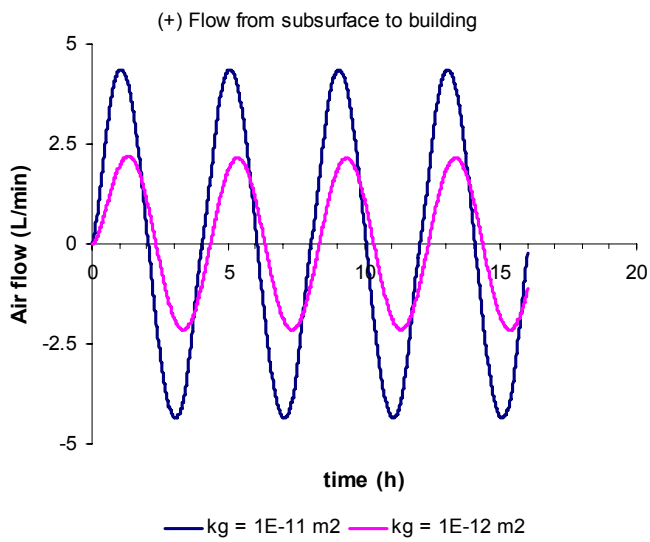

Figure 49. Temporal reversal of the air flow direction resulting from fluctuations in indoor-sub-slab pressure difference (Figure 48).
Soil gas permeabilities (kg) are 1E-12 m^2 and 1E-11 m^2.

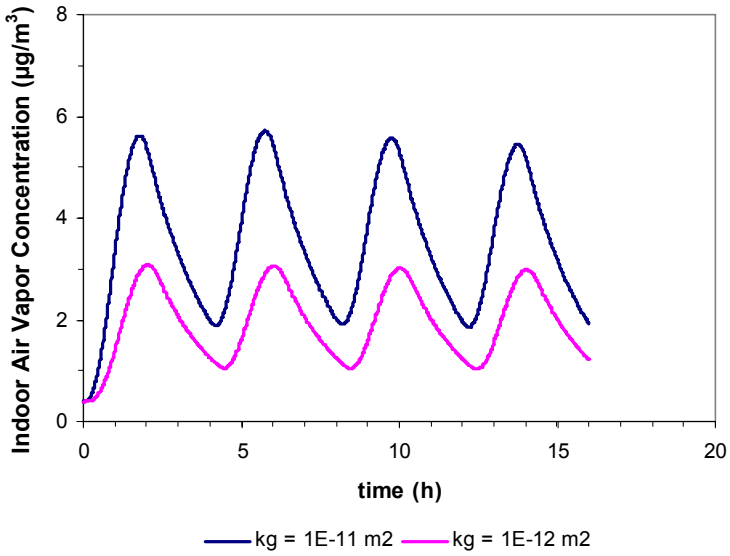

Figure 50. Temporal variation of the indoor air VOC concentration (y-axis) resulting from fluctuations in indoor sub-slab pressure difference and reversals of air flow direction (Figures 48 and 49).

Source vapor concentration is 10,000 µg/m^3 at 8 m bgs. Soil gas permeabilities (kg) are 1E-12 m^2 and 1E-11 m$^{2.}$

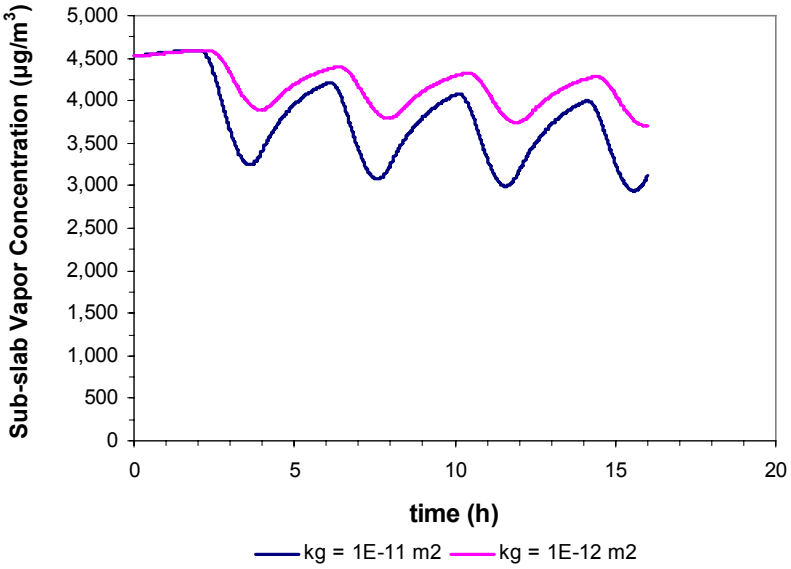

Figure 51. Temporal variation of the sub-slab VOC concentration (y-axis) resulting from fluctuations in indoor-sub-slab pressure difference and reversals of air flow direction (Figures 48 and 49). Concentration measured at location below slab crack.

Source vapor concentration is 10,000 µg/m^3 at 8 m bgs. Soil gas permeabilities (kg) are 1E-12 m^2 and 1E-11 m$^{2.}$

6.4 Seasonal Phenomena

The following subsections describe possible temporal and spatial changes in the distribution of VOCs that might take place from season to season. Although no model simulations of these seasonal changes were performed, the conceptual scenarios are illustrated to familiarize the reader with their potential impacts.

Seasonal variability is the change in vapor intrusion that occurs according to a season or a period of the year associated with a particular seasonal phenomenon. For example, seasonal changes in outdoor air temperature (and the resulting difference between indoor and outdoor air temperatures) can affect building pressure via the stack effect, and seasonal changes in air exchange rates can contribute to seasonal variations in the magnitude of vapor intrusion to indoor air. Simulations showing the effects associated with such building conditions that can vary seasonally are discussed in **Section 4.3.3**. This section briefly introduces two processes that can cause seasonal variability in vapor intrusion that were not simulated for this document: fluctuations in water table elevations and rainfall events.

6.4.1 Fluctuations in Water Table Elevation

The figures in this section illustrate the effect that fluctuations in the water table elevation might have on the vapor source concentration. **Figure 52** depicts conditions where a falling water table exposes a soil zone containing a hydrocarbon NAPL (i.e., a "smear zone"), thus increasing the available vapor source. **Figure 53** depicts a case where a rising water table encounters soil zone NAPL. The NAPL dissolves into the formerly clean groundwater, and aqueous phase constituents are transported away from the source, expanding the area of contamination.

Fluctuations in the water table elevation may affect the distribution of contaminants in the subsurface, the source-foundation separation, and, consequently, the magnitude of any vapor intrusion. The extent of this effect depends on the location of the original vapor source. If the contaminant vapor source is originally at the water table (e.g., dissolved groundwater or NAPL plume) and the subsurface soil in the vadose zone above the water table is initially clean, as shown in **Figure 52**, as the groundwater table rises and falls again, it leaves a contaminated soil zone above the water table as a second source of contamination (or NAPL smear zone). The water table will also act like a piston, forcing soil gas upward or drawing soil gas downward as the water table rises and falls.

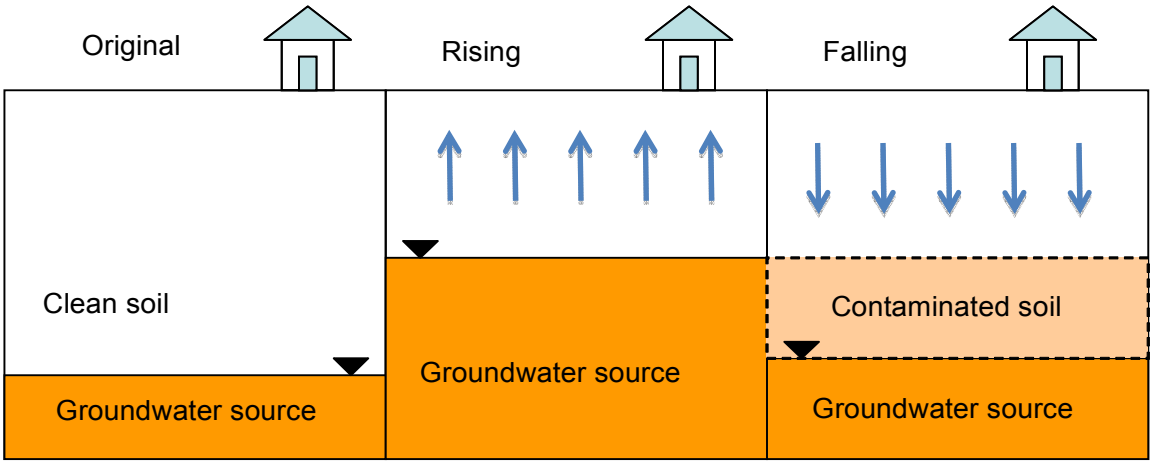

Figure 52. Schematic illustration of water table fluctuations and the increase of VOC-impacted area from a groundwater source.

A second scenario, shown in **Figure 53**, can occur when the original vapor source is residual NAPL in soil, and the groundwater below it is initially clean. As the groundwater table rises and reaches the NAPL-contaminated soil, contaminants dissolve into the groundwater and may migrate with the groundwater flow to an area of larger extent than the original soil source and may ultimately migrate to beneath a nearby building, increasing the subsurface VOC concentration beneath it. As the now-contaminated groundwater table falls after a rising cycle, it generates a contaminated soil zone that was initially clean. Thus, two new source zones were created: a contaminated groundwater zone and a larger soil contamination zone extending beneath the building.

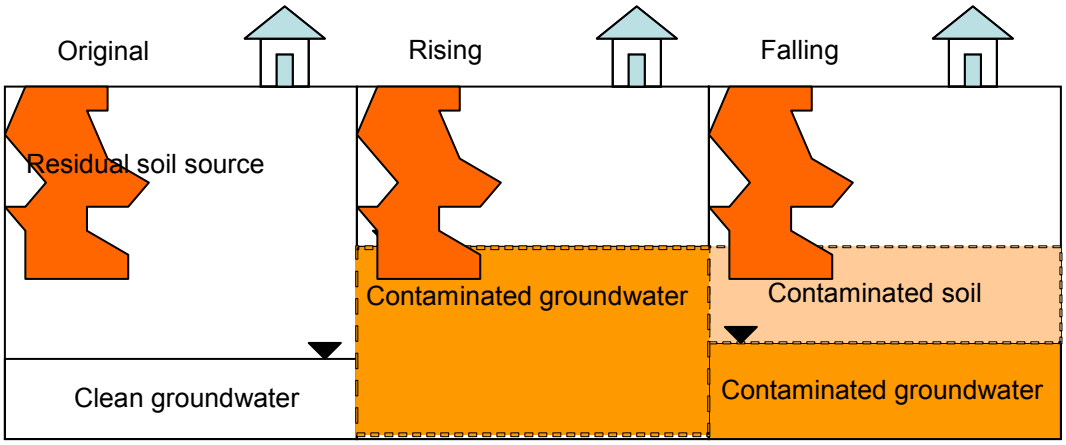

Figure 53. Schematic illustration of water table fluctuations and the increase of VOC-impacted area from a vadose zone (unsaturated soil) source.

In cases where lighter-than-water NAPL is present near the water table, the rate of mass transfer to overlying soil gas increases when the water table falls because the drainage of water exposes more of the NAPL to the gas phase. A falling water table can allow the LNAPL to migrate to deeper depths (the NAPL smear zone), and when the water table rises again, some of that mass will remain trapped by capillary forces below the water table, which would reduce the generation of vapors.

6.4.2 Rainfall Events and Water Infiltration

There are no figures in this section, but the role of a structure as a moisture barrier and the role of a lens of fresh water at the water table overlying a zone of dissolved phase contamination are briefly discussed.

A building structure may represent a barrier for infiltration of rain water into the subsurface immediately below the building footprint, which may result in a non-uniform distribution of soil moisture content (Tillman and Weaver, 2007). During or after a rainfall event, the subsurface beneath the building may have a lower moisture content than the adjacent areas. Localized wet soil layers on the ground surface adjacent to the building may act as barriers to vertical vapor transport toward the atmosphere, and the vapor migration may be diverted toward the building and may increase the sub-slab concentration. The significance of this process depends on the duration of the rainfall event, the soil type, the subsurface water infiltration and drainage capacity, run-off, and evaporation and transpiration.

In locations where there is significant infiltration through the unsaturated zone, a layer of clean groundwater may build up on top of the contaminated groundwater plume and act as a barrier to VOC volatilization from the groundwater to soil gas and may decrease the soil vapor concentration distribution in the subsurface. This process has been referred to as clean water lens (Fitzpatrick and Fitzgerald, 1996) and diving plumes (Griesemer, 2001). Also, if the soil is coarse grained and there is high downwards drainage of the infiltrating water through the soil, the water may flush the contaminant from the soil gas as it infiltrates down the subsurface, which may also decrease the soil vapor concentration (Mendoza and McAlary, 1990).

[This page intentionally left blank.]

7.0 Examples Comparing Soil Gas Concentration at Different Locations

This section uses examples from simulations presented in this report to illustrate the impacts of sample location selection and to highlight the fact that vapor concentrations at exterior sample locations may be either similar to or different from sub-slab concentrations depending on site-specific conditions and sampling depth. In the simulations, the red circles depict concentrations that would be obtained from samples at sub-slab locations. The red triangles depict concentrations that would be obtained from soil gas samples at their respective locations. **Figure 54** depicts a scenario with a laterally extensive groundwater vapor source. **Figure 55** depicts scenarios where a finite groundwater vapor source is at varying lateral distances from a building. **Figure 56** depicts a scenario with multiple buildings and multiple sources. These simulations highlight the importance of developing and using an accurate site conceptual model when choosing sampling locations and interpreting sampling results.

This document is intended to provide a theoretical understanding of vapor intrusion processes and to illustrate how different site conditions might influence the distribution of VOCs in the subsurface and the indoor air of buildings in the vicinity of a soil or groundwater contaminant source. The previous sections indicate that VOC concentration distributions in the subsurface may not be uniform (including the sub-slab concentration distribution). This section uses the previous results and makes comparisons between concentrations in different locations, highlighting, for example, how the simulations indicate that vapor concentration at exterior sample locations may be similar to or different from sub-slab concentration, depending on site-specific conditions (including depth).

As described earlier and illustrated in the figures below, when interpreting the nature and extent of soil gas contamination, it is important to discern the source of VOCs in soil gas (soil or groundwater), as well as the subsurface conditions (e.g., homogeneous, heterogeneous), the types of ground cover and buildings, and the persistence of the chemicals of interest.

The simulations presented in this section are examples illustrating soil and groundwater sources at different locations. **Figure 54** illustrates a vapor concentration distribution for a laterally extensive groundwater source directly below a residential building overlying homogeneous subsurface soils and recalcitrant VOCs. This figure shows that the concentration at exterior locations right above the source (if groundwater is shallow) or somewhat deeper than the foundation depth (e.g., more than 3 m below the foundation depth) could approximate the concentrations expected in sub-slab locations. Some limited field data with an adequate number of observations from groundwater-source scenarios have observations that are in general agreement with the results presented in Figure 54 (e.g., Wertz, 2006; DiGiulio, 2006; Patterson and Davis, 2009).

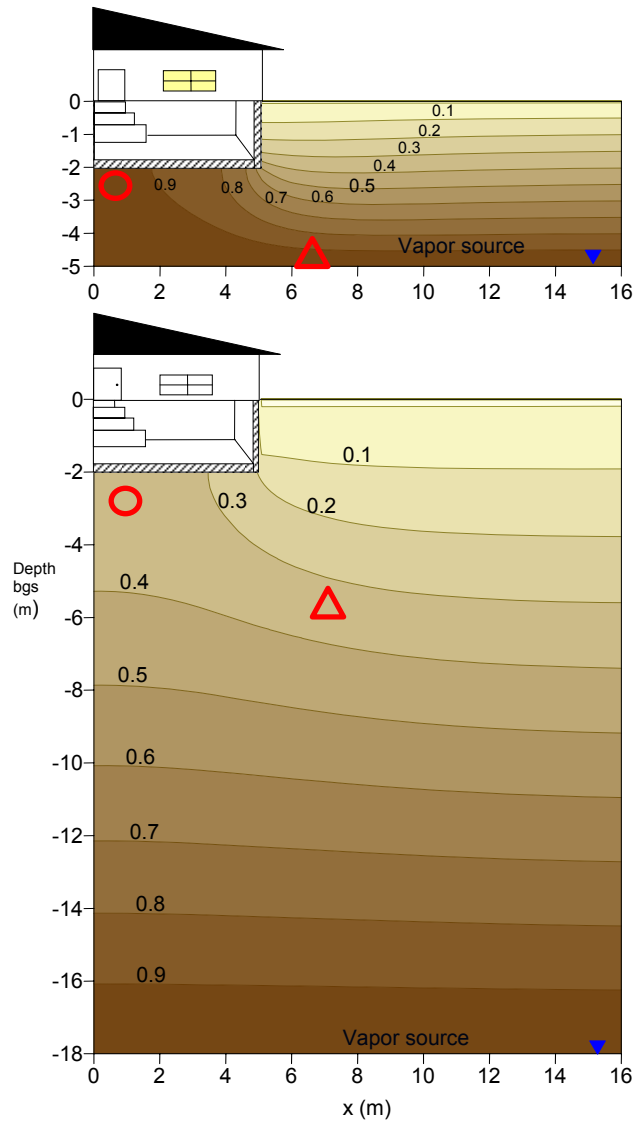

Figure 54. Scenarios with extensive groundwater source directly below a building. The symbols highlight areas for comparing soil vapor concentrations.
Circles are sub-slab locations; triangles are exterior locations.

Figure 55 illustrates a set of related scenarios where the VOC source, which is located at the groundwater table, is positioned at a different lateral distance from a building with a basement. **Figure 56** illustrates a scenario with two distinct VOC sources: one located at the groundwater table near a building with a basement and the other in the unsaturated soil zone near a building with a slab-on-grade foundation. From Figures 55 and 56, it should be noted that in some exterior locations (i.e., red triangles), soil gas concentrations are constant with depth, while in other exterior locations, the soil gas concentrations increase with depth (i.e., above the groundwater source), and in other locations, the soil gas concentrations increase and decrease with depth (i.e., where there is a soil source). These figures also illustrate that the sub-slab soil gas concentrations (i.e., red circles) can be higher, lower, or similar to the exterior locations, depending on the VOC source location(s) and the specific exterior location and depth.

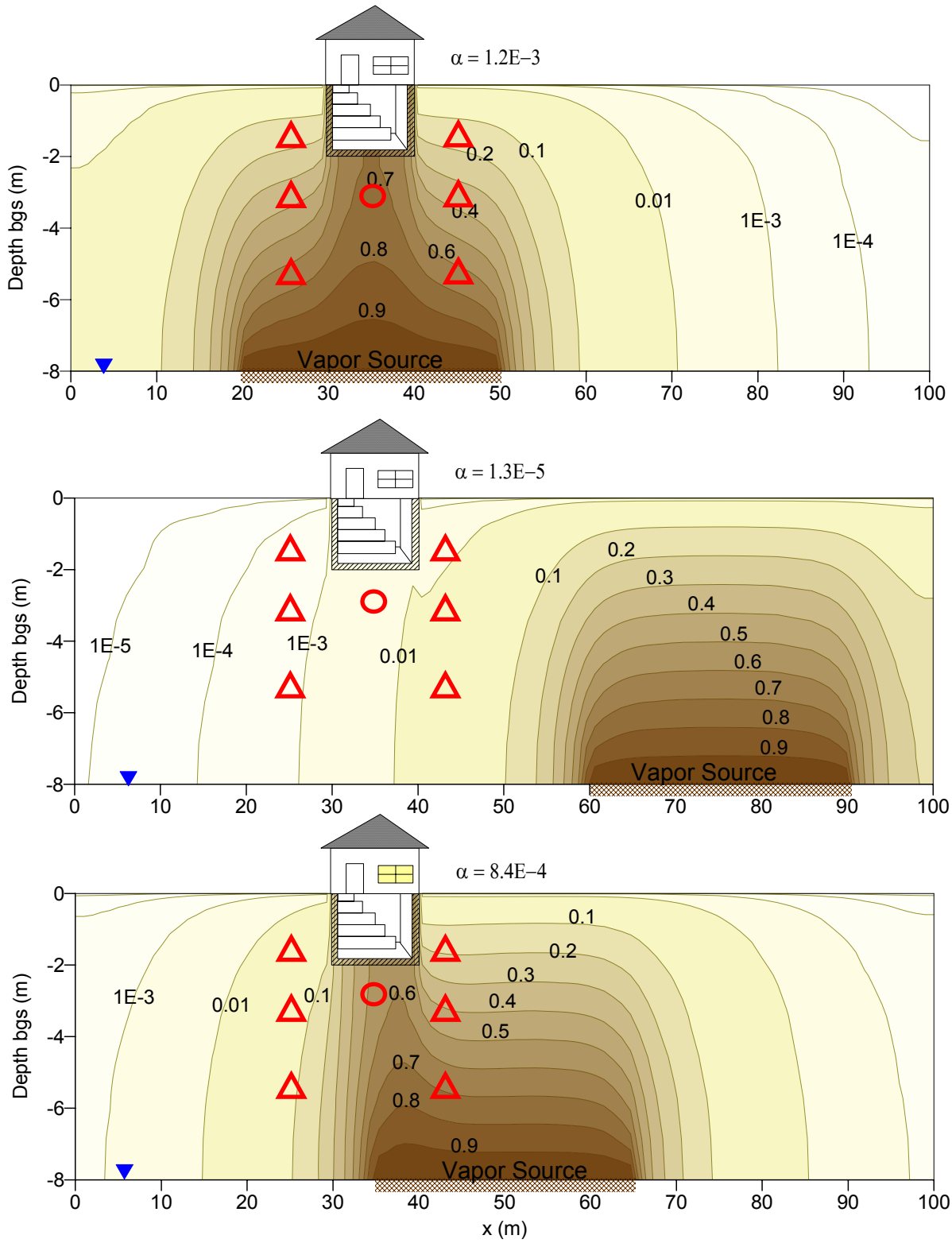

Figure 55. Scenarios with a groundwater source at different lateral distances from a building. The symbols highlight areas for comparing soil vapor concentrations.

Circles are sub-slab locations; triangles are exterior locations.

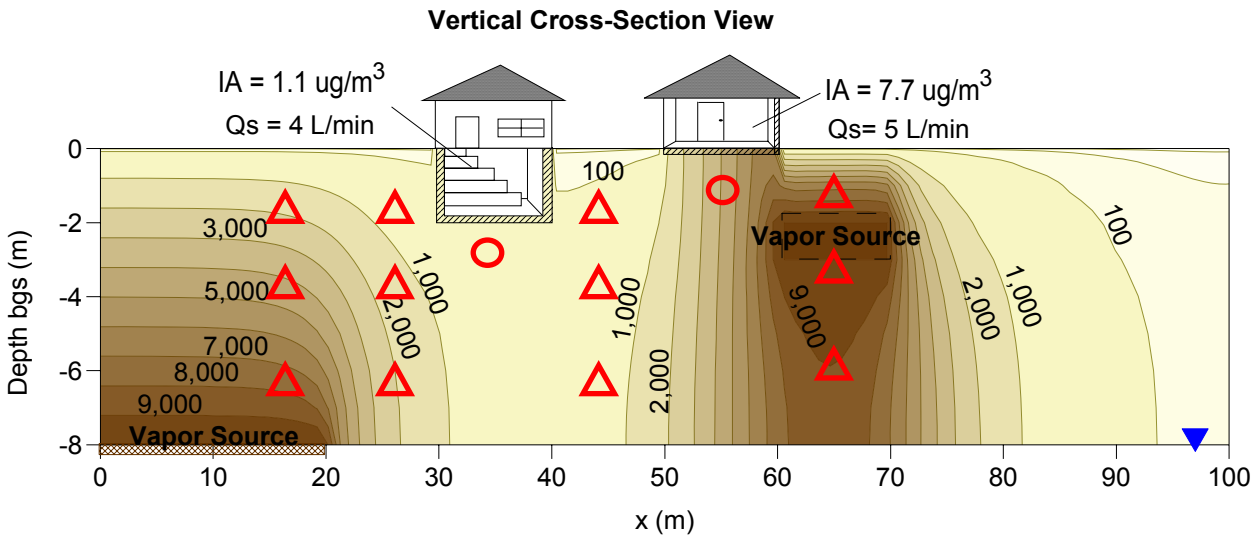

Figure 56. Scenario with multiple buildings and multiple sources. The symbols highlight areas for comparing soil vapor concentrations.

Circles are sub-slab locations; triangles are exterior locations.

The analysis provided in this section is based on just a few examples. The reader should keep in mind that many other scenarios are presented in this technical document (e.g., scenarios with heterogeneous subsurface, scenarios with biodegradation, scenarios under transient conditions). The exact depth, number, and locations of soil gas samples can depend on site-specific conditions and should be decided based on the nature, extent, and fate and transport of vapors; and the conceptual model of the source, pathway, and receptor relationships.

8.0 Summary of Results

This document was prepared to help environmental practitioners gain insight into the processes and variables involved in the vapor intrusion pathway and to provide a theoretical framework with which to better understand the complex vapor fate and transport conditions typically encountered at actual contaminated sites. Site-specific conditions may lead to more complex VOC distributions than shown for the simplified conceptual model scenarios used in this technical document. Nevertheless, the following general observations can be made from these theoretical analyses and may be useful when considering the vapor intrusion pathway at a particular site. Report sections are provided so the reader can review examples and understand the basis and limitations for each observation:

- The horizontal and vertical distance over which vapors may migrate in the subsurface (primarily by diffusion) depends on the concentration of the source (**Sections 4.1** and **5.1**), the source depth (**Sections 4.2** and **5.2**), the soil matrix properties (e.g., porosity and moisture content, **Sections 4.4** and **5.4**), the thickness of the vadose zone, and the time since the release occurred (**Section 6.1**).
- Subsurface heterogeneities in site geology (e.g., layering, moisture content; see **Sections 4.4**, **5.4**, and **5.5**) influence the extent of vapor transport from a contaminant source to overlying or adjacent buildings.
- Advective flow occurs predominantly near cracks and openings in the building foundation slab and may affect the distribution of VOCs directly beneath the structure (**Section 3.2**). Heterogeneities in the permeability of geologic materials and backfill (**Section 4.3.2**), along with wind effects and building and atmospheric pressure temporal variation, may contribute to spatial and temporal variability of VOC concentrations in sub-slab soil gas and indoor air (**Section 6**).
- The distribution of VOCs in soil gas beneath a building is not the only factor that determines the indoor air concentration. The indoor air VOC concentration is also influenced by building conditions, including the existence of cracks in the foundation, building pressurization, and air exchange rate, which in turn can be related to other factors such as temperature, wind, barometric pressure, occupant behavior, and building operations (**Section 4.3**).
- In cases where the subsurface is homogeneous, building conditions are the same (e.g., air exchange rate, pressurization), and the source vapor concentration extends evenly beneath each building, the presence of multiple single-family residences at typical spacing would be expected to have little or no effect on the predicted indoor air VOC concentrations for a single building under these specific conditions (**Section 4.3**).
- Simulations assuming an impermeable ground cover suggest that shallow soil gas VOC concentrations can be higher under low permeability ground covers than under open soil (**Section 4.4.3**). Note that this document illustrates simulation output for idealized (i.e., impermeable) engineered surfaces, which is a simplification.

- The soil gas distribution of aerobically biodegradable chemicals (e.g., many petroleum compounds) can be significantly different from that of recalcitrant chemicals that do not readily degrade aerobically (e.g., chlorinated solvents) in similar settings (**Section 5**).
- The simulations presented in this technical document illustrate that the VOC concentrations in the subsurface may not be uniform (either in sub-slab soil gas or in soil gas at similar depths exterior to the building of concern). Therefore, VOC concentrations at exterior locations may be similar to or different from the sub-slab concentration, depending on site-specific conditions and the location and depth of the sample. **Section 7** shows examples for some different scenarios.

The conceptual scenarios simulated in this technical document illustrate that several factors influence the distribution of VOC concentrations in soil gas and in indoor air and suggest that assessment of the distribution of VOC concentrations in soil gas at sites and in indoor air can be supported by characterization of the source extent, site geology, building conditions, biodegradation, and other site-specific factors that can influence the distribution of VOCs in the subsurface and their migration into the indoor air of overlying buildings.

9.0 References

Abreu, L.D.V. 2005. *A Transient Three-dimensional Numerical Model to Simulate Vapor Intrusion into Buildings*. UMI 3166060, Ph.D. Dissertation, Arizona State University, Tempe, AZ.

Abreu, L.D.V., and P.C. Johnson. 2005. Effect of vapor source-building separation and building construction on soil vapor intrusion as studied with a three-dimensional numerical model. *Environmental Science and Technology* 39(12):4550–4561.

Abreu, L.D.V., and P.C. Johnson. 2006. Simulating the effect of aerobic biodegradation on soil vapor intrusion into buildings: influence of degradation rate, source concentration, and depth. *Environmental Science and Technology* 40(7):2304–2315.

Abreu, L.D.V., P.C. Johnson, and T.A. McAlary. 2006. *3-D Model Simulations and Implications to Near-Building Sampling*. Presented at the Summary Workshop in the Context of EPA's VI Guidance Revisions, Association for Environmental Health and Sciences (AEHS) 16th Annual West Coast Conference on Soils, Sediment, and Water; San Diego, CA, March 16. Available at http://iavi.rti.org/WorkshopsAndConferences.cfm.

Abreu, L.D.V.; R. A. Ettinger, and T. McAlary. 2009a. Simulated vapor intrusion attenuation factors including biodegradation for petroleum hydrocarbons. *Ground Water Monitoring and Remediation* 29(1):105–117.

Abreu, L.D.V., R.A. Ettinger, and T.A. McAlary. 2009b. *Simulating the Effect of Aerobic Biodegradation on Soil Vapor Intrusion into Buildings: Evaluation of Low Strength Sources associated with Dissolved Gasoline Plumes.* API Publication 4775. API: Washington, DC. April.

Bozkurt, O., K. Pennell, and E.M. Suubery. 2009. Simulation of the vapor intrusion process for nonhomogeneous soils using a three-dimensional numerical model. *Ground Water Monitoring and Remediation* 29(1):92–104.

Davis, R. 2009. Bioattenuation of petroleum hydrocarbon vapors in the subsurface: Update on recent studies and proposed screening criteria for the vapor intrusion pathway. *L.U.S.T. Line Bulletin* 61(May):11–14.

Denman, A.R., R.G.M. Crockett, C.J. Groves-Kirkby, P.S. Phillips, G.K. Gillmore, and A.C. Woolridge. 2007. The value of seasonal correction factors in assessing the health risk from domestic radon—A case study in Northamptonshire, UK. *Environment International* 33:34–44.

DeVaull, G.E. 2007. Indoor vapor intrusion with oxygen-limited biodegradation for a subsurface gasoline source. *Environmental Science and Technology* 41(9):3241–3248.

DiGiulio, D. 2006. *Evaluation of the "Constrained Version" of the J&E Model and Comparison of Soil-Gas and Sub-Slab Air Concentrations at the Raymark Superfund Site*. Presented at the Summary Workshop in the Context of EPA's VI Guidance Revisions, AEHS 16th

Annual West Coast Conference on Soils, Sediment, and Water; San Diego, CA, March 16. Available at http://iavi.rti.org/WorkshopsAnd Conferences.cfm.

Falta, R.W., I. Javandel, K. Pruess, and P.A. Witherspoon. 1989. Density-driven flow of gas in the unsaturated zone due to the evaporation of volatile organic compounds. *Water Resources Research* 25(10):2159–2169.

Fitzpatrick, N.A., and J.J. Fitzgerald. 1996. *An Evaluation of Vapor Intrusion into Buildings Through a Study of Field Data*. Presented at the 11th Annual Conference on Contaminated Soils, University of Massachusetts at Amherst, October.

Folkes D., W. Wertz, J. Kurtz, and T. Kuehster. 2009. Observed spatial and temporal distributions of CVOCs at Colorado and New York vapor intrusion sites. *Groundwater Monitoring and Remediation* 29(1):70–80.

Freeze, A. and J. Cherry, 1979. *Groundwater*. Prentice Hall, Inc., Englewood Cliffs, New Jersey.

Griesemer, J. 2001. Diving plumes: The development and investigation of dissolved contaminant plumes that migrate vertically downward to depths below the water table. *NJDEP Site Remediation News* 13(1), May.

Groves-Kirkby, C.J., A.R. Denman, R.G.M. Crockett, P.S. Phillips, A.C. Woolridge, and G.K. Gillmore. 2006. Time-integrating radon gas measurements in domestic premises: Comparison of short-, medium- and long-term exposures. *Journal of Environmental Radioactivity* 86(1):92–109.

Hers, I., J. Atwater, L. Li, and R. Zapf-Gilje. 2000. Evaluation of vadose zone biodegradation of BTX vapours. *Journal of Contaminant Hydrology* 46:233–264.

Hers, I., R. Zapf-Gilje, P.C. Johnson, and L. Li, 2003. Evaluation of the Johnson and Ettinger model for prediction of indoor air quality. *Ground Water Monitoring and Remediation* 23(1):62–76.

Hughes, B., Frind, E. and C. Mendoza, 1996. Vapor transport of trichloroethylene in the unsaturated zone: Field and numerical modeling investigations. *Water Resources Research* 32(1): 9–22.

ITRC (Interstate Technology and Regulatory Council). 2007. *Vapor Intrusion Pathway: A Practical Guideline.* VI-1. Interstate Technology & Regulatory Council, Vapor Intrusion Team, Washington, DC. Available at www.itrcweb.org.

Jin, Y., T. Streck, and W.A. Jury. 1994. Transport and biodegradation of toluene in unsaturated soil. *Journal of Contaminant Hydrology* 17:111–127.

Johnson, P.C. 2002. *Identification of Critical Parameters for the Johnson and Ettinger (1991) Vapor Intrusion Model*. API Soil and Groundwater Research Bulletin Number 17. May. Available at http://www.api.org/ehs/groundwater/criticalparameters.cfm.

Johnson, P.C. 2005. Identification of application-specific critical inputs for the 1991 Johnson and Ettinger vapor intrusion algorithm. *Ground Water Monitoring & Remediation* 25(1):63–78.

Johnson, P.C. 2008. *The Path to More Confident and Cost-Effective Vapor Intrusion Pathway Assessment*. Presented at the Association for Environmental Health and Sciences (AEHS), March 12, San Diego, CA. Available at http://iavi.rti.org/attachments /WorkshopsAndConferences/01_Johnson_Presentation.pdf.

Johnson, P.C., and R.A. Ettinger. 1991. Heuristic model for predicting the intrusion rate of contaminant vapors into buildings. *Environmental Science and Technology* 25:1445–1452.

Johnson, P. C., C.C. Stanley, M.W. Kemblowski, D.L. Byers, and J.D. Colthart. 1990. A practical approach to the design, operation, and monitoring of in situ soil-venting systems. *Ground Water Monitoring and Remediation* 10(2):159–178.

Johnson, R.L., K.A. McCarthy, M. Perrott, and C.A. Mendoza. 1992. Density-driven vapor transport: Physical and numerical modeling. In Weyer (ed.), *Subsurface Contamination by Immiscible Fluids.* Balkema: Rotterdam.

Johnson, P.C., M.W. Kemblowski, and R.L. Johnson. 1999. Assessing the significance of subsurface contaminant vapor migration to enclosed spaces: Site-specific alternatives to generic estimates*. Journal of Soil Contamination* 8(3):389–421.

Johnson, P.C., R.A. Ettinger, J. Kurtz, R. Bryan, and J.E. Kester, 2002. *Migration of Soil Gas Vapors to Indoor Air: Determining Vapor Attenuation Factors Using a Screening-Level Model and Field Data from the CDOT-MTL Denver, Colorado*. API Soil and Groundwater Task Force Bulletin No. 16; American Petroleum Institute: Washington, DC.

Lowell, P.S., and B. Eklund. 2004. VOC emission fluxes as a function of lateral distance from the source. *Environmental Progress* 23(1):52–58.

Luo, H., P. Dahlen, P. Johnson, T. Creamer, T. Peargin, P. Lundegard, B. Hartman, L. Abreu, and T. McAlary. 2006. *Spatial and Temporal Variability in Hydrocarbon and Oxygen Concentrations Beneath a Building Above a Shallow NAPL Source.* Presented at the Battelle Conference on Remediation of Chlorinated and Recalcitrant Compounds, Monterey, CA. May.

Luo, H., P. Dahlen, P.C. Johnson, T. Creamer, T, Peargin, and T. McAlary. 2007. *Spatial and Temporal Variability of Sub-Slab Soil Gas Concentrations at a Petroleum-Impacted Site*. Presented at the American Waste Management Association (AWMA) Conference: Vapor Intrusion: Learning from the Challenges. September 26–28. Providence, RI.

Marley, F. 2001. Investigation of the influences of atmospheric conditions on the variability of radon and radon progeny in buildings. *Atmospheric Environment* 35:5347–5360.

McAlary, T.A., Nicholson, P., Yik, L.K., Bertrand, D. and G. Thrupp. 2010. High purge volume sampling—A new paradigm for sub-slab soil gas monitoring. *Groundwater Monitoring and Remediation* 30(2):73–85.

Mendoza, C.A., and E.O. Frind. 1990. Advective-dispersive transport of dense organic vapors in the unsaturated zone, 2. Sensitivity analysis. *Water Resources Research* 26(3):388–398.

Mendoza, C.A. and T.A. McAlary. 1990. Modeling of groundwater contamination caused by organic solvent vapours. *Ground Water* 28(2):199–206.

Mosley, R.B. 2007. *Use of Radon Measurements to Analyze Vapor Intrusion Problems.* Workshop on Soil-Gas Sample Collection and Analysis. Presented at the 17th Annual Association for Environmental Health and Sciences (AEHS) Meeting and West Coast Conference on Soils, Sediments, and Water. San Diego, CA. March. Available at http://iavi.rti.org/WorkshopsAndConferences.cfm?PageID=documentDetails&AttachID=363.

Narasimhan, T.N., Y.W. Tsang, and H.Y. Holman. 1990. On the importance of transient air flow in advective entry into buildings. *Geophysical Research Letters* 17(6):821–824.

Nazaroff, W.W., and A.V. Nero. 1988. *Radon and Its Decay Products in Indoor Air*. New York, NY: J. Wiley & Sons.

Nazaroff, W.W., S.R. Lewis, S.M. Doyle, B.S. Moed, and A.V. Nero. 1987. Experiments on pollutant transport from soil into residential basements by pressure-driven airflow. *Environmental Science and Technology* 21(5):459–466.

Nielson, K.K., V.C. Rogers, R.B. Holt, T.D. Pugh, W.A. Grondzik, and R.J. Meijer. 1997. Radon penetration of concrete slab cracks, joints, pipe penetrations, and sealants. *Health Physics* 73(4):669–678.

Pasteris, G., D. Werner, K. Kaufmann, and P. Hohener. 2002. Vapor phase transport and biodegradation of volatile fuel compounds in the unsaturated zone: A large scale lysimeter experiment. *Environmental Science and Technology* 36(1):30–39.

Patterson, B.M., and G.B. Davis. 2009. Quantification of vapor intrusion pathways into a slab-on-ground building under varying environmental conditions. *Environmental Science and Technology* 43(3):650–656.

Pennell, K.G., O. Bozkurt, and E.M. Suuberg. 2009. Development and application of a three-dimensional finite element vapor intrusion model. *Journal of the Air and Waste Management Association* 59:447–460. DOI:10.3155/1047-3289.59.4.447.

Renken, K.J., and T. Rosenberg. 1995. Laboratory measurements of the transport of radon gas through concrete samples. *Health Physics* 68(6):800–808.

Riley, W.J., A.J. Gadgil, Y.C. Bonnefoud, W.W. Nazaroff. 1996. The effect of steady winds on radon-222 entry from soil into houses. *Atmospheric Environment* 30(7):1167–1176.

Riley, W.J., A.L. Robinson, A.J. Gadgil, W.W. Nazaroff. 1999. Effects of variable wind speed and direction on radon transport from soil into buildings: model development and exploratory results. *Atmospheric Environment* 33:2157–2168.

Rivett, M.O. 1995. Soil-gas signatures from volatile chlorinated solvents: Borden Field experiments. *Ground Water* 33(1):84–98.

Robinson, A.L., and R.G. Sextro. 1997. Radon entry into buildings driven by atmospheric pressure fluctuations. *Environmental Science and Technology* 31:1742–1748

Robinson, A.L., R.G. Sextro, and W.J. Fisk. 1997. Soil-gas entry into an experimental basement driven by atmospheric pressure fluctuations—Measurements, spectral analysis and model comparison. *Atmospheric Environment* 31(10):1477–1485.

Robinson, A.L., R.G. Sextro, and W.J. Riley. 1997. Soil-gas entry into houses driven by atmospheric pressure fluctuations—The influence of soil properties. *Atmospheric Environment* 31(10):1487–1495.

Rogers, V.C, K.K. Nielson, R.B. Holt, and R. Snoddy. 1994. Radon diffusion coefficients for residential concretes. *Health Physics* 67(3):261–265.

Roggemans, S., C.L. Bruce, and P.C. Johnson. 2001. *Vadose Zone Natural Attenuation of Hydrocarbon Vapors: An Empirical Assessment of Soil Gas Vertical Profile Data*. API Technical Bulletin No. 15. American Petroleum Institute: Washington, DC.

Rowe J.E., M. Kelly, and L.E. Price. 2002. Weather system scale variation in radon-222 concentration of indoor air. *Science of the Total Environment* 284(1–3):157–166.

Steck, D.J. 1992. Spatial and temporal indoor radon variations. *Health Physics* 62(4):351–355.

Tillman, F.D. and J.W. Weaver. 2007. Temporal moisture content variability beneath and external to a building and the potential effects on vapor intrusion risk assessment. *Science of the Total Environment* 379:1–15.

U.S. Census Bureau. 2006. *American Housing Survey for the United States: 2005.* Current Housing Reports, Series H150/05. U.S. Government Printing Office, Washington, DC. Available at http://www.census.gov/prod/2006pubs/h150-05.pdf.

U.S. EPA (Environmental Protection Agency). 2002. *OSWER Draft Guidance for Evaluating the Vapor Intrusion to Indoor Air Pathway from Groundwater and Soils (Subsurface Vapor Intrusion Guidance).* EPA530-D-02-004. U.S. EPA, Office of Solid Waste and Emergency Response, Washington, DC. November.

U.S. EPA (Environmental Protection Agency). 2004. *User's Guide for Evaluating Subsurface Vapor Intrusion into Buildings.* Prepared by Environmental Quality Management, Inc. for U.S. EPA Office of Emergency and Remedial Response, Washington DC, February 22. Available at http://www.epa.gov/oswer/riskassessment/airmodel/pdf/ 2004_0222_3phase_users_guide.pdf.

U.S. EPA (Environmental Protection Agency). 2011a. *Background Indoor Air Concentrations of Volatile Organic Compounds in North American Residences: A Compilation and Implications for Vapor Intrusion*. EPA 530-R-10-001. U.S. EPA, Office of Solid Waste and Emergency Response, Washington, DC. June. Available at http://www.epa.gov/oswer/vaporintrusion/documents/oswer-vapor-intrusion-background-Report-062411.pdf.

U.S. EPA (Environmental Protection Agency). 2011b. *Petroleum Hydrocarbons And Chlorinated Hydrocarbons Differ In Their Potential For Vapor Intrusion*. U.S. EPA, Office of Underground Storage Tanks, Washington, DC. September. Available at http://www.epa.gov/swerust1/cat/pvi/pvicvi.pdf.

Wertz, W. 2006. *Near-Building and Sub-slab Sampling at the Endicott (NY) Site, Implications for Site Screening Approaches*. Presented at the Summary Workshop in the Context of EPA's VI Guidance Revisions, AEHS 16th Annual West Coast Conference on Soils, Sediment, and Water; San Diego, CA, March 16. Available at http://iavi.rti.org/ WorkshopsAndConferences.cfm.

Appendix A

Model Equations

[This page intentionally left blank.]

A.1 Summary of Model Equations

Table A-1 shows the equations solved by the numerical code, and **Table A-2** shows the boundary conditions used. The symbols used are defined following each table.

Table A-1. Equations Solved by the Numerical Code

Parameter	Equation
Soil gas disturbance pressure field	$$\frac{\partial p}{\partial t} - \left(\frac{\overline{P}}{\phi_g \mu_g}\right) \cdot \vec{\nabla} \bullet (K_g \cdot \vec{\nabla} p) = 0$$
Soil gas flow field	$$\vec{q}_g = \frac{K_g}{\mu_g} (\vec{\nabla} p)$$
Chemical transport: advection, diffusion, and aerobic biodegradation	$$a \cdot \frac{\partial C_{ig}}{\partial t} = -\vec{\nabla} \bullet (C_{ig} \cdot \vec{q}_g) - \vec{\nabla} \bullet \left(\frac{C_{ig}}{H_i} \cdot \vec{q}_w\right) + \vec{\nabla} \bullet (D \cdot \vec{\nabla} C_{ig}) - R_i$$ where $$a = \left(\phi_g + \frac{\phi_w}{H_i} + \frac{K_{oc,i} \cdot f_{oc} \cdot \rho_b}{H_i}\right)$$ $$D = \left[D_{ig} + \frac{D_{iw}}{H_i}\right] \;,\; D_{ig} = d_i^a \frac{\phi_g^{10/3}}{\phi_T^2} \;,\; D_{iw} = d_i^w \frac{\phi_w^{10/3}}{\phi_T^2}$$ R_i is zero if the chemical is recalcitrant. If the chemical is biodegradable then the R_i used in this work is a first-order model limited by oxygen concentration: $$\begin{cases} R_i = \phi_w \cdot \lambda_i \cdot C_{iw} & if \quad C_{oxygen} > C_{og}^{\min} \\ R_i = 0 & if \quad C_{oxygen} \le C_{og}^{\min} \end{cases}$$ The reaction rate for oxygen (R_o) is determined stoichiometrically: $$R_o = \sum_{i=1}^{m} rk_o \cdot R_i$$
Indoor air concentration	$$C_{ig}^{indoor} = \frac{E_s + V_b \cdot A_{ex} \cdot C_{i,amb}}{V_b \cdot A_{ex} + Q_s}$$ where $$Q_s = \int_{L_{ck}} Q_{ck} \cdot dL_{ck}$$ and $$E_s = \int_{L_{ck}} Q_{ck} \cdot \frac{\left[\exp\left(\frac{Q_{ck}}{w_{ck} \cdot D_{ck}} d_{ck}\right) C_{ig} - C_{ig}^{indoor}\right]}{\left[\exp\left(\frac{Q_{ck}}{w_{ck} \cdot D_{ck}} d_{ck}\right) - 1\right]} \cdot dL_{ck}$$

Definition of Symbols Used in Table A-1

p: disturbance pressure (absolute atmospheric pressure minus absolute soil gas pressure at a point) [M/L/T^2]

t: time [T]

$\bar{P}$: mean soil gas pressure (approximated by the atmospheric pressure for the problems of interest here) [M/L/T^2]

ϕ_g: gas-filled porosity [L^3_{gas}/L^3_{soil}]

μ_g : soil gas dynamic viscosity [M/L/T]

$\vec{\nabla}$: vector del operator [L^{-1}]

K_g: soil permeability to soil gas flow [L^2]

$\vec{q}_g$: soil gas discharge vector [$L^3_{gas}/L^2_{area}/T$]

i: chemical-specific subscript

C_{ig}: gas-phase concentration of chemical i [M_i/L^3_{gas}]

$\vec{q}_w$: soil moisture specific discharge vector [$L^3_{fluid}/L^2_{area}/T$]

R_i : net loss rate of chemical i due to reaction [$M_i/L^3_{soil}/T$]

ϕ_w : moisture-filled porosity [L^3_{water}/L^3_{soil}]

ρ_b: soil bulk density [M_{soil}/L^3_{soil}]

f_{oc}: mass fraction of organic carbon in the soil [M_{oc}/M_{soil}]

$K_{oc,i}$: sorption coefficient of chemical i to organic carbon [$(M_i/M_{oc})/(M_i/L^3_{water})$]

H_i: Henry's law constant for chemical i [$(M_i/L^3_{gas})/(M_i/L^3_{water})$]

D_{ig}: effective porous media diffusion coefficients for chemical i in soil gas [L^2/T]

D_{iw}: effective porous media diffusion coefficients for chemical i in soil moisture [L^2/T]

d_i^a: molecular diffusion coefficient of chemical i in air [L^2/T]

d_i^w: molecular diffusion coefficient of chemical i in water [L^2/T]

ϕ_T : total soil porosity (= $\phi_g + \phi_w$) [L^3_{pores}/L^3_{soil}]

λ_i : first-order reaction rate [1/T]

C_{oxygen}: oxygen soil gas concentration [M/L^3-vapor]

rk_o : ratio of oxygen to hydrocarbon consumed [M_o/M_i]

m: total number of aerobically degrading chemicals

E_s: emission rate of chemical i to enclosed space [M/T]

A_{ex}: enclosed space air exchange rate [1/T]

V_b : enclosed space volume [L^3] where indoor air is assumed fully mixed

$C_{i,amb}$: concentration of chemical i in ambient air [M/L^3]

Q_s: soil gas flow rate to the enclosed space [L^3/T]

C_{og}^{min}: threshold oxygen concentration for aerobic biodegradation to occur.

Table A-2. Boundary Conditions

Boundaries	Boundary Condition(s)
All vertical plane-of-symmetry, all lateral boundaries, solid foundation sections, and the lower model domain boundary	$\vec{\nabla} p \cdot \vec{n} = 0$ $\vec{\nabla} C_{ig} \cdot \vec{n} = 0$ (except at the vapor source boundary)
Vapor source boundary	$C_{ig} = C_{i,g}^{source}$
Soil-atmosphere interface	$p^{atm}(t) = 0$ for steady atmospheric pressure, otherwise $p^{atm}(t) = A_1 \cdot \sin(\varphi_1 \cdot t + \theta_1) + A_2 \cdot \sin(\varphi_2 \cdot t + \theta_2)$ $C_{ig} = 0$ $C_{oxygen} = C_{og}^{atm}$ (0.28 mg/cm^3)
Disturbance pressure within the building	$p^{indoor}(t) = p^{atm}(t) + \Delta p_B(t)$
Foundation crack–soil interface.	$Q_{ck} = \left(-\frac{w_{ck}^3}{12\mu_g \cdot d_{ck}}\right)\left[p - p^{indoor}\right] = w_{ck}\left(\frac{K_g}{\mu_g}\right)\frac{\partial p}{\partial z}$ $Q_{ck} \cdot \frac{\left[\exp\left(\frac{Q_{ck}}{w_{ck} \cdot D_{ck}} d_{ck}\right)\right] C_{ig} - C_{ig}^{indoor}}{\left[\exp\left(\frac{Q_{ck}}{w_{ck} \cdot D_{ck}} d_{ck}\right) - 1\right]} =$ $= w_{ck} \cdot \left[C_{ig}\left(\frac{K_g}{\mu_g}\right)\left(\frac{\partial p}{\partial z}\right) - D\left(\frac{\partial C_{ig}}{\partial z}\right)\right]$

Definition of Symbols Used in Table A-2

$\vec{n}$: unit vector normal to the surface of interest

$p^{atm}(t)$: disturbance pressure at the soil-atmosphere interface [M/L/T^2]

$p^{indoor}(t)$: disturbance pressure within the building [M/L/T^2]

$\Delta p_B(t)$: pressure difference between the indoor air and the atmospheric air (or gauge pressure)

A: user-defined amplitudes [M/L/T^2]

φ: user-defined frequencies [radians/T]

θ: user-defined phases [radians]

Q_{ck}: soil gas flow rate per unit length of crack [(L^3_{gas}/T)/L]

w_{ck}: crack width [L]

d_{ck}: foundation thickness [L]

C_{og}^{atm}: oxygen atmospheric concentration [M/L^3-vapor]

D_{ck}: effective diffusion coefficient for transport in the crack [L^2/T].

A.2 Revision of the Indoor Air Mixing Equation Assumption

The indoor air concentration equation presented in Table A-1 was derived by assuming an instantaneous steady-state condition on the enclosed space mass balance. This assumption did not hold true for high frequency barometric pressure fluctuations; therefore, a revised indoor air mixing equation was derived to properly account for an accumulation term in simulations with transient pressure fluctuations. The revised equation is as follows:

$$C_{ig,m}^{indoor} = \frac{\left[C_{ig,m-1}^{indoor} \cdot V_b + \left(E_s + V_b \cdot A_{ex} \cdot C_{i,amb}\right) \cdot \left(t_m - t_{m-1}\right)\right]}{\left[V_b + \left(V_b \cdot A_{ex} + Q_s\right) \cdot \left(t_m - t_{m-1}\right)\right]}$$

where m is the time step index and all other variables are as defined for Table A-1.

[This page intentionally left blank.]

Appendix B

Model Inputs and Assumptions

[This page intentionally left blank.]

Table B-1. Model Inputs and Assumptions

Input/Assumption	Baseline Value	Alternative Values Modeled
Building and Foundation Assumptions		
Residential home	One home	Multiple homes
Building dimensions[a]	10 m x10 m (100 m^2 = 1,076 ft^2)	
Foundation type	Basement Slab-on-grade	
Foundation depth	2.0 m (basement) 0.2 m (slab-on-grade)	
Foundation thickness	0.15 m	
Enclosed space mixing volume	174 m^3	
Air exchange rate	0.5 h^{-1}	0.25, 1 h^{-1}
Building air flow rate	87 m^3/h	62.5, 75, 150, 200, 300 m^3/h
Building gauge pressure	5 Pa	−5, −2, 0, 1, 2, 5, 7, 20 Pa
Crack width	0.001 m	No cracks
Crack total length	39 m	No cracks
Crack location (illustrated in **Figure B-1**)	Perimeter	Center of foundation
Surrounding fill: soil gas intrinsic permeability	No fill (native soil)	5E-11 m^2
Surrounding fill: total porosity	No fill (native soil)	0.5
Surrounding fill: moisture content	No fill (native soil)	0.01
Source Assumptions		
Source location	Groundwater table: the vapors are on top of capillary fringe (vapors originating from either dissolved groundwater or NAPL plume sources)	Vadose zone (soil)
Source area	Infinite source	Finite source
Source depth	8 m bgs	3, 5, 12, 18 m bgs
Lateral distance from source to building	0 (directly under building)	5–30 m
Contaminant Assumptions		
Contaminant persistency	Recalcitrant	Aerobically biodegradable
Vapor concentration at source	NA (recalcitrant)	2–200 mg/L
Diffusion coefficient in air	3.17E-2 m^2/h	
Diffusion coefficient in water	3.53E-6 m^2/h	
Diffusion coefficient in the crack area	3.17E-2 m^2/h	
Henry's law constant	0.228 m^3_{water}/m^3_{vapor}	
Sorption coefficient to organic carbon	60 $(g/g_{oc})/(g/L^3_{water})$	600 $(g/g_{oc})/(g/L^3_{water})$
First-order biodegradation rate (λ)	NA (recalcitrant)	0.018, 0.18, 1.8 h^{-1}
Contaminant vapor transport type	Steady state	Transient

(continued)

Input/Assumption	Baseline Value	Alternative Values Modeled
Soil Properties		
Soil type/layers	Homogeneous, uniform sand	Sand with confining layers (see properties below)
Bulk density	1,700 kg/m^3	
Moisture saturation (water-filled porosity)	20% (0.07 m^3_{water}/m^3_{voids})	
Total soil porosity	0.35 m^3_{voids}/m^3_{soil}	
Mass fraction of organic carbon in the soil	0.001 (g_{oc}/g_{soil})	0.005 (g_{oc}/g_{soil})
Soil gas intrinsic permeability	10^{-11} m^2	
Input/Assumption	**High Moisture Layer**	**Barrier Layer**
Confining Layer Properties (alternative condition)		
Soil type	Silty sand	Silty clay
Bulk density	1,700 kg/m^3	1,700 kg/m^3
Pore water saturation	60% (0.21 m^3_{water}/m^3_{voids})	95% (0.38 m^3_{water}/m^3_{voids})
Soil gas intrinsic permeability	10^{-13} m^2	10^{-13} m^2
Total soil porosity	0.35 m^3_{voids}/m^3_{soil}	0.40 m^3_{voids}/m^3_{soil}

[a] The symmetrical scenarios domain includes only a quarter of the building footprint (5 m x 5 m footprint area) in the simulations.

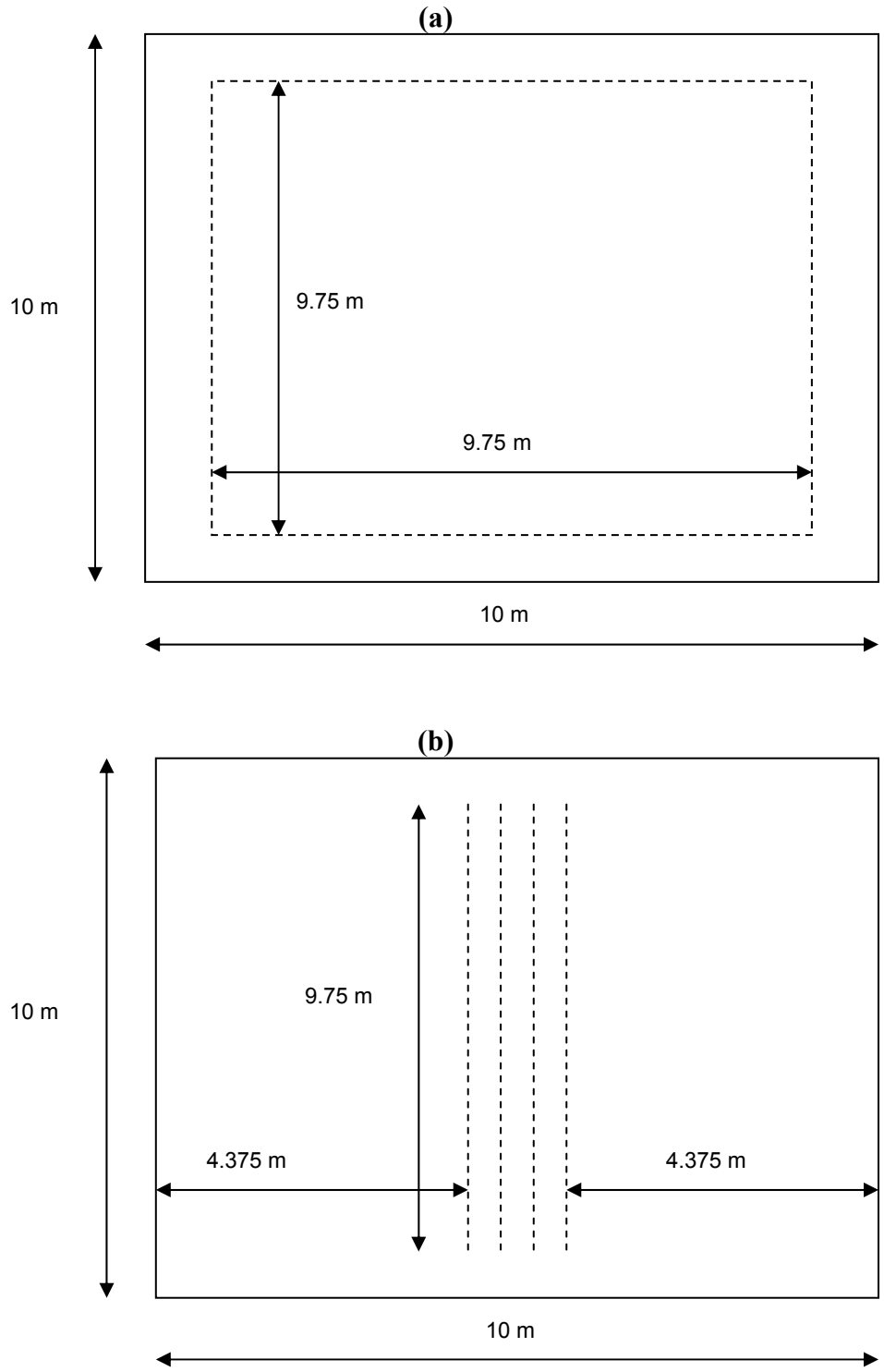

Figure B-1. Plan view of the foundation crack distribution (dashed lines) used in the simulations for perimeter cracks (a) and center-of-foundation cracks (b).

[This page intentionally left blank.]

Appendix C

Document Development and Peer Review

[This page intentionally left blank.]

Appendix C

Document Development and Peer Review

This appendix provides the history of the development and review process for EPA 530-R-10-003, *Conceptual Model Scenarios for the Vapor Intrusion Pathway*. The model simulations on which this document was based were conducted by Dr. Lilian D.V. Abreu of ARCADIS U.S., Inc., using a 3-D model of vapor intrusion processes that she originally developed as a graduate student of Dr. Paul Johnson at Arizona State University. Beginning in 2005, Dr. Abreu presented model simulations in a series of EPA-sponsored vapor intrusion workshops, where she demonstrated the power of her simulations in illustrating vapor intrusion processes. Based on the responses to these workshops, EPA contracted with Dr. Abreu to develop and document a comprehensive set of simulations to help vapor intrusion practitioners visualize vapor intrusion phenomena. From 2007 through the summer of 2009, Dr. Abreu worked through document development, editing, technical review, and response to comments with the vapor intrusion guidance development team, including representatives from the following organizations with experience and expertise in vapor intrusion and/or indoor air:

- **U.S. EPA**—13 staff from the Office of Solid Waste and Emergency Response, the Office of Superfund Remediation and Technology Innovation, the Office of Resource Conservation and Recovery, the Brownfields Office, four Office of Research and Development Laboratories, and two U.S. EPA Regions
- **Contractors-Consultants**—11 subject matter experts from Arizona State University, EnviroGroup Limited, GeoSyntec Consultants, Golder Associates, and RTI International
- **State Agencies—**4 expert practitioners/regulators from Kansas, New Jersey, and New York.

The remainder of this appendix describes the peer review of the model (including previous publications) conducted before the document was developed, internal EPA review of the document, and EPA's external peer review of the document and simulations it provides.

C.1 Prior Peer Review of the 3-D Model

The 3-D model, including its description and use, was the subject of Dr. Abreu's Ph.D. dissertation and was subject to all reviews for doctoral degrees at Arizona State University. The 3-D model was also peer reviewed and published in several journals, which are listed in **Section C.3**. In addition, the modeling results have been presented in several conferences and workshops, which are listed in **Section C.4**.

C.2 Internal EPA Review and EPA Peer Review

After initial review by the EPA members of the vapor intrusion guidance team, EPA's Vapor Intrusion Forum (VIF) reviewed the document in 2009. For this review, the document was sent to VIF, including members from EPA Regions, the Office of Solid Waste and Emergency Response, and the Office of Research and Development.

From June to August 2009, the document was subjected to EPA's External Peer Review process, where it was reviewed by four experts in the development and use of models for the vapor intrusion pathway (Dan Gallagher, California Environmental Protection Agency; John Menatti, Utah Department of Environmental Quality; Kelly Pennell, Brown University; and Frank Swartjes, National Institute of Public Health and the Environment [RIVM], The Netherlands). This peer review panel was selected to include the following expertise:

- Practical and theoretical understanding of the vapor intrusion pathway, including how volatile organic contaminants move and distribute in the subsurface (soil gas), indoor air, and outdoor air from dissolved and non-aqueous phase sources
- Experience in planning and interpreting site-specific vapor intrusion studies, including developing and refining conceptual site models of the migration and distribution of volatile contaminants
- Expertise in modeling the vapor intrusion pathway or other environmental media using numeric simulations and 1-D to 3-D models and in applying and calibrating models using site-specific data.

Once external peer review comments had been received, Dr. Abreu and the vapor intrusion guidance team developed responses to comments and made final revisions to the document to address them (from September to December 2009). From January through March 2010, the document received final EPA management and legal review prior to its finalization as of March 31, 2010.

C.3 3-D Model Peer-Reviewed Publications

Abreu, L.D.V. 2005. *A Transient Three-dimensional Numerical Model to Simulate Vapor Intrusion into Buildings*. UMI 3166060. Ph.D. Dissertation, Arizona State University, Tempe, AZ.

Abreu, L.D.V. and P.C. Johnson. 2005. Effect of vapor source-building separation and building construction on soil vapor intrusion as studied with a three-dimensional numerical model. *Environmental Science & Technology* 39(12)4550–4561.

Abreu, L.D.V. and P.C. Johnson. 2006. Simulating the effect of aerobic biodegradation on soil vapor intrusion into buildings: Influence of degradation rate, source concentration, and depth. *Environmental Science & Technology* 40(7):2304–2315.

Abreu, L.D.V., R.A. Ettinger, and T. McAlary. 2009. Simulated vapor intrusion attenuation factors including biodegradation for petroleum hydrocarbons. *Ground Water Monitoring and Remediation Journal* 29(1):105–117.

Abreu, L.D.V., R.A. Ettinger, and T. McAlary. 2009. Simulating the effect of aerobic biodegradation on soil vapor intrusion into buildings: Evaluation of low strength sources associated with dissolved gasoline plumes. API Publication 4775, April. API: Washington, DC.

C.4 3-D Model Work Presented at Conferences and Workshops

Abreu, L.D.V. 2010. *Conceptual Model Scenarios (CMS) for the Vapor Intrusion Pathway*. Final-Draft. Presented at the Twentieth Annual Association for Environmental Health and Sciences (AEHS) Meeting and West Coast Conference on Soils, Sediments, and Water, March 16, 2010. San Diego, CA.

Abreu, L.D.V., and R. Ettinger. 2009. *Understanding the Conceptual Site Model for Vapor Intrusion into Buildings.* Presented at the U.S.EPA National Forum on Vapor Intrusion, January 12–13, 2009. Philadelphia, PA.

Abreu, L.D.V., R. Ettinger, and T. McAlary. 2009. *Theoretical Overview of Vapor Intrusion Processes*. Presented at the Air and Waste Management Association (AWMA) Specialty Conference: Vapor Intrusion. January 27–30, 2009. San Diego, CA.

Abreu, L.D.V., R. Ettinger, and T. McAlary. 2007. *3D Numerical Modeling to Assess Vapor Intrusion Screening Criteria for Petroleum Hydrocarbon Sites*. Presented at the AWMA Specialty Conference—Vapor Intrusion: Learning from the Challenges. September 26–28, 2007. Providence, RI.

Abreu, L.D.V., R. Ettinger, and T. McAlary. 2007. *Application of 3D Numerical Modeling to Assess Vapor Intrusion Screening Criteria for Petroleum Hydrocarbon Sites.* Presented at the Seventeenth Annual AEHS Meeting and West Coast Conference on Soils, Sediments, and Water, March 19–22, 2007. San Diego, CA.

Abreu, L.D.V., P.C. Johnson, and T. McAlary. 2006. *3D Model Simulations and Implications to Near Building Sampling.* Presented at the EPA/AEHS Vapor Intrusion Workshop, March 16, 2006. San Diego, CA.

Abreu, L.D.V., and P.C. Johnson. 2005. *Modeling the Effect of Aerobic Biodegradation on Vapor Intrusion.* Presented at the National Ground Water Association/American Petroleum Institute (NGWA/API) Petroleum Vapor Intrusion Workshop, August 17, 2005. Costa Mesa, CA.

Abreu, L.D.V., and P.C. Johnson. 2005. *Vapor Intrusion: Lessons Learned Through Numerical Simulations.* Presented at the EPA/AEHS Vapor Intrusion Workshop, March 14–15, 2005. San Diego, CA.

Johnson, P.C., and L.D.V. Abreu. 2004. *Site-Specific Modeling in the Context of the OSWER Guidance?* Presented at the EPA/UMass Modeling Vapor Attenuation Workshop, October 18–19, 2004. Amherst, MA.

Abreu, L.D.V., and P.C. Johnson. 2004. *Learning Through the Simulations of Vapor Intrusion Scenarios.* Presented at the U.S Department of Energy/Petroleum Environmental Research Forum (DOE/PERF) Hydrocarbon Vapor Workshop, January 27–29, 2004. Brea, CA.

Johnson, P.C., and L.D.V. Abreu. 2003. *Confusion? Delusion? What Do We Really Know About Vapor Intrusion?* Presented at the Eighth Symposium in the Groundwater Resources Association's Series on Groundwater Contaminants: Subsurface Vapor Intrusion to Indoor Air: When is Soil and Groundwater Contamination an Indoor Air Issue? September 30, 2003. San Jose, CA.

Appendix D

Variables Index

[This page intentionally left blank.]

Variables Index

Note: This index includes only figures showing contour plots of the results of the 3-D model. The biodegradation rate is varied only in the figures that show x-y plots relating two variables (Figures 30, 31, 33, 34, and 36), which are not included in this index. Thus, biodegradation rate is not included as a variable in this index.

Baseline conditions are shown in **bold italics**. Biodegradable VOC scenarios are shown with open bullets (○).

Variable	Section Figure Number (page number)																																						
	3.1 Diffusive Transport		3.2 Advective Transport		4.1 Source Conc.	4.2 Source Depth and Lateral Distance				4.3 Other Conditions (Effect of Various Building Parameters, Multiple Sources)						4.4 Heterogeneous Subsurface										5.0 Biodegradable VOCs								6.0 Temporal and Spatial Variability					
	2 (13)	3 (14)	4 (16)	5 (18)	7a,b (22, 23)	8 (25)	9 (26)	10 (27)	12 (29)	13 (31)	14 (32)	15 (33)	16 (35)	17 (37)	18 (39)	19b (42)	19c (43)	20 (45)	21b (49)	22b (51)	23b (55)	24b (57)	25 (59)	26 (60)	27 (61)	28 (66)	29 (67)	32 (71)	35 (75)	37 (78)	38 (79)	39 (81)	40 (82)	42 (85)	43 (86)	44 (88)	45 (90)	46a (92)	46b (93)
SOURCE CONDITIONS																																							
Contaminant Persistence																																							
Recalcitrant	●	●	●	●	●	●	●	●	●	●	●	●	●	●	●	●	●	●	●	●	●	●	●	●	●									●	●	●	●	●	●
Biodegradable																										○	○	○	○	○	○	○	○						○
Number of Sources																																							
Single	●	●	●	●	●	●	●	●	●	●	●	●	●	●		●	●	●	●	●	●	●	●	●	●	○	○	○	○	○	○	○	○	●	●	●	●	●	●
Multiple														●	●																								
Source Depth																																							
Shallow (3 or 5 m)		●	●			●	●	●							●				●				●					○	○			○	○		●				
Deep (*8*, 12, or 18 m)	●		●	●	●	●	●	●	●	●	●	●	●	●	●	●	●	●		●	●	●		●	●	○	○	○	○	○	○			●		●	●	●	●
Source Location																																							
Groundwater (diss. or NAPL plume)	●		●	●	●	●	●	●	●	●	●	●	●	●	●	●	●	●	●	●	●	●	●	●	●	○	○	○	○	○	○	○	○	●	●	●	●	●	●
Vadose zone (residual or NAPL)		●													●																								
Source Extent																																							
Infinite	●	●	●	●	●	●	●	●	●	●	●	●	●	●	●	●	●	●					●	●	●	○	○	○	○	○	○	○	○	●	●	●	●	●	●
Finite														●					●	●	●	●																	
Vapor Concentration at Source																																							
Any	●	●	●	●		●	●	●	●	●	●	●	●	●	●	●	●	●	●	●	●	●	●	●	●									●	●	●	●	●	●
Low–Moderate (2–20 mg/L)					●																					○	○	○			○		○						
High (200 mg/L)					●																					○	○	○	○	○	○	○							
Lateral Distance from Source to Building																																							
Source under bldg.			●	●	●	●		●		●	●	●	●	●		●	●	●			●		●	●	●	○	○	○	○	○	○	○	○	●	●	●	●	●	●
Source laterally sep. from building	●	●					●		●						●				●	●		●																	

(continued)

Variable	Section Figure Number (page number)																																						
	3.1 Diffusive Transport		3.2 Advective Transport		4.1 Source Conc.	4.2 Source Depth and Lateral Distance				4.3 Other Conditions (Effect of Various Building Parameters, Multiple Sources)						4.4 Heterogeneous Subsurface										5.0 Biodegradable VOCs								6.0 Temporal and Spatial Variability					
	2 (13)	3 (14)	4 (16)	5 (18)	7a,b (22, 23)	8 (25)	9 (26)	10 (27)	12 (29)	13 (31)	14 (32)	15 (33)	16 (35)	17 (37)	18 (39)	19b (42)	19c (43)	20 (45)	21b (49)	22b (50)	23b (55)	24b (57)	25 (59)	26 (60)	27 (61)	28 (66)	29 (67)	32 (71)	35 (75)	37 (78)	38 (79)	39 (81)	40 (82)	42 (85)	43 (86)	44 (88)	45 (90)	46a (92)	46b (93)
SUBSURFACE CONDITIONS																																							
Soil Type/Layers																																							
Homogeneous	●	●	●	●	●	●	●	●	●	●	●	●	●	●	●											○	○	○	○					●	●		●	●	●
Heterogeneous																●	●	●	●	●	●	●	●	●	●					○	○	○	○			●			
Soil Moisture																																							
Low–Moderate	●	●	●	●	●	●	●	●	●	●	●	●	●	●	●	●	●	●	●	●	●	●	●	●	●	○	○	○	○	○	○	○	○	●	●	●	●	●	●
High																●	●	●	●	●	●	●	●							○	○	○	○	●	●	●			
Soil Permeability																																							
Low																●	●	●	●	●	●	●	●							○	○	○	○						
Moderate–High	●	●	●	●	●	●	●	●	●	●	●	●	●	●	●	●	●	●	●	●	●	●	●	●	●	○	○	○	○	○	○	○	○	●	●	●	●	●	●
Geologic Vapor Barrier																																							
None	●	●	●	●	●	●	●	●	●	●	●	●	●	●	●	●	●	●	●	●	●	●				○	○	○	○	○	○			●	●	●	●	●	●
Present																							●	●	●							○	○						
Transport Mechanism																																							
Diffusion	●	●			●	●	●	●	●	●	●	●	●	●	●	●	●	●	●	●	●	●	●	●	●	○	○	○	○	○	○	○	○	●	●	●	●	●	●
Advection			●	●	●	●	●	●	●	●	●	●	●	●	●	●	●	●	●	●	●	●	●	●	●	○	○	○	○	○	○	○	○	●	●	●		●	●
Transport Type																																							
Steady state	●	●	●	●	●	●	●	●	●	●	●	●	●	●	●	●	●	●	●	●	●	●	●	●	●	○	○	○	○	○	○	○	○					●	●
Transient																																		●	●	●	●		
BUILDING CHARACTERISTICS																																							
Buildings (Number)																																							
Single	●	●	●	●	●	●	●	●	●							●	●	●	●	●			●			○	○	○	○	○	○	○	○	●	●		●		
Multiple										●	●	●	●	●	●						●	●		●	●											●			
Building Pressurization																																							
Over-pressurized				●									●				●													○				●	●			●	●
Under-pressurized				●	●	●	●	●	●	●	●	●	●	●	●	●		●	●	●	●	●	●	●	●	○	○	○	○	○	○	○	○			●			
Foundation Cracks																																							
None	●	●												●																						●			
Perimeter			●	●	●	●	●	●	●	●	●	●	●	●	●	●	●	●	●	●	●	●	●	●	●	○	○	○	○	○	○	○	○	●	●	●	●	●	●
Center			●	●																																			
Foundation Type																																							
Basement	●	●	●	●	●	●	●	●	●	●	●	●	●		●	●	●	●	●	●	●	●	●	●	●	○			○	○	○	○	○	●	●		●	●	●
Slab on grade					●	●						●		●	●							●					○	○									●			
Permeable fill													●																										